

Catalyst speciation and deactivation in the ruthenium mediated transformation of ethynyl- β -lonol to α,β -Unsaturated esters for vitamin A synthesis

Asad Saib,^{a,b} Roman Goy,^c Jonathan Medlock,^c Bettina Wüstenberg,^c Gabriele Kociok-Köhn,^d
Catherine L. Lyall,^{a,b,d} John P. Lowe,^{a,b,d} Ulrich Hintermair^{a,b,e*}

Supplementary Information

^a Department of Chemistry, University of Bath, Claverton Down, BA2 7AY Bath, United Kingdom.

^b Dynamic Reaction Monitoring Facility, University of Bath, Claverton Down, BA2 7AY Bath, United Kingdom.

^c DSM-Firmenich AG, Wurmisweg 576, 4303 Kaiseraugst, Switzerland.

^d Materials and Chemical Characterisation Facility (MC²), University of Bath, Bath BA2 7AY, United Kingdom.

^e Institute for Sustainability, University of Bath, Bath BA2 7AY, United Kingdom.

* u.hintermair@bath.ac.uk

Table of Contents

1.0 General information.....	4
1.1 Materials	4
1.2 Analytical.....	4
2.0 Experimental Details	5
2.1 Preparation of $[Ru^{II}(\eta^3-CH_2C(Me)CH_2)_2(dppe)] [(dppe)Ru(MA)_2]^1$	5
2.2 Preparation of $[Ru^{II}(\eta^3-CH_2C(Me)CH_2)_2(dppm)]^1$	8
2.2 Purification of carboxylic acids	10
2.2.1 Pivalic acid.....	10
2.2.2 Adamantane carboxylic acid and benzoic acid	10
2.3 Preparation of ethynyl- β -ionol (2a) ²	11
2.4 Preparation of α,β -unsaturated carboxylates.....	14
2.4.1 3-hydroxy-3-methyl-5-(2,6,6-trimethylcyclohex-1-en-1-yl) penta-1,4-dien-1-yl pivalate (3ab).....	14
2.4.2 3-hydroxy-3-methyl-5-(2,6,6-trimethylcyclohex-1-en-1-yl)penta-1,4-dien-1-yl adamantane-1-carboxylate (3ae)	16
2.5 Synthetic procedure for generating compounds suitable for crystal structure determination .	18
2.5.1 A_p' $[(dppe)Ru^{II}(\eta^2-O_2CC^tBu)(\eta^1-O_2CC^tBu)(^tBuCCO_2H)]$	18
2.5.2 A_{ad}' $[(dppe)Ru^{II}(\eta^2-O_2CC(CH_2)_6(CH)_3C)(\eta^1-O_2CC(CH_2)_6(CH)_3C)((CH)_3(CH_2)_6CCCO_2H)]$	21
2.5.3 B_p' $[(dppe)Ru^{II}(\eta^1-O_2CC^tBu)_2(\mu-O_2CC^tBu)_2(\mu-H_2O)]$	24
2.5.4 B_{ad}' $[(dppe)Ru^{II}(\eta^1-O_2CC(CH_2)_6(CH)_3)_2(\mu-O_2CC(CH_2)_6(CH)_3)_2(\mu-H_2O)]$	27
2.5.5 B_{tr}' $[(dppe)Ru^{II}(\eta^1-O_2CCF_3)_2(\mu-O_2CCF_3)_2(\mu-OH_2)]$	29
2.5.6 B_b' $[(dppe)Ru^{II}(\eta^1-O_2CPh)_2(\mu-O_2CPh)_2(\mu-H_2O)]$	30
2.5.7 A_b $[(dppe)Ru^{II}(\eta^1-O_2CPh)_2]$	33
2.5.8 X_b²•H₂O $[(dppe)Ru^{II}(\eta^1-O_2CPh)_2(CO)(H_2O)]$	35
2.5.9 X_b² $[(dppe)Ru^{II}(\eta^1-O_2CPh)_2(CO)_2]$	37
2.6 Standard procedure for the ruthenium-mediated transformation of ethynyl- β -ionol into the α,β -unsaturated ester adduct.....	41
2.7 FlowNMR Apparatus	43
2.7.1 Data acquisition	44
2.7.2 FlowNMR reaction setup	44
3.0 X-Ray Crystallography	45
3.1 Crystal data for $[Ru^{II}(\eta^3-CH_2C(Me)CH_2)_2(dppe)]$	45
3.2 Crystal data for A_p' $[(dppe)Ru^{II}(\eta^2-O_2CC^tBu)(\eta^1-O_2CC^tBu)(^tBuCCO_2H)]$	47
3.3 Crystal data for B_p' $[(dppe)Ru^{II}(\eta^1-O_2CC^tBu)_2(\mu-O_2CC^tBu)_2(\mu-H_2O)]$	49

3.4 Crystal data for B_b' $[(dppe)Ru^{II}(\eta^1-O_2CPh)_2(\mu-O_2CPh)_2(\mu-H_2O)]$	51
3.5 Crystal data for A_{ad}' $[(dppe)Ru^{II}(\eta^2-O_2CC(CH_2)_6(CH)_3C)(\eta^1-O_2CC(CH_2)_6(CH)_3C)((CH)_3(CH_2)_6CCCO_2H)]$	53
3.6 Crystal data for B_{ad}' $[(dppe)Ru^{II}(\eta^1-O_2CC(CH_2)_6(CH)_3)_2(\mu-O_2CC(CH_2)_6(CH)_3)_2(\mu-H_2O)]$	55
3.7 Crystal data for B_{tf}' $[(dppe)Ru^{II}(\eta^1-O_2CCF_3)_2(\mu-O_2CCF_3)_2(\mu-OH_2)]$	57
3.8 Crystal data for X²_b•H₂O $[(dppe)Ru^{II}(\eta^1-O_2CPh)_2(CO)(H_2O)]$	59
3.9 Crystal data for X²_b $[(dppe)Ru^{II}(\eta^1-O_2CPh)_2(CO)_2]$	61
4.0 Supplementary data.....	63
4.1 Solvent effects.....	63
4.2 Influence of the carboxylic acid	63
4.3 Ligand effects	65
4.4 TON limitation.....	68
4.5 Substrate effects	68
4.6 Poisoning tests	71
4.7 <i>Operando</i> ¹ H FlowNMR analysis	72
4.8 Variable Time Normalisation Analysis	73
4.8.1 Change in catalyst loading	73
4.8.2 Change in pivalic acid loading	73
4.8.2 Change in ethynyl-β-ionol loading	74
4.8.3 Phenylacetylene concentration profile.....	75
4.9 Rate law derivation	77
4.9.1 Irreversible literature mechanism	77
4.9.2 Reversible literature mechanism	80
4.10 Identification of reaction intermediates by ³¹ P{ ¹ H} NMR	83
4.10.1 Precursor activation	83
4.10.2 Monitoring catalyst speciation under catalytic conditions using ³¹ P{ ¹ H} NMR	91
4.10.3 Deactivation pathways.....	93
4.11 Mechanistic relevance of $[(dppe)Ru^{II}(\eta^2-O_2CR)_2]$	100
4.12 Maximising catalyst productivity	104
5.0 References	106

1.0 General information

1.1 Materials

Unless otherwise stated, all manipulations were carried out under an inert atmosphere of argon using classical Schlenk and glovebox (MBraun UNIlab plus) techniques. Prior to use, all glassware were oven dried to 120 °C. All reactions were performed with anhydrous and degassed non-deuterated solvents; DCM (dried over CaH₂), Methanol (dried over magnesium), *n*-hexane (dried over potassium), THF (dried over potassium), and toluene (dried over sodium) were freshly distilled before use. Acetone, acetonitrile, chloroform, and ethyl acetate were purchased from commercial suppliers (Acro seal) and were used without further purification. All solvents were passed through 0.2 µm syringe filters (VWR 514-0070) prior to use.

All chemicals used were obtained either from Sigma Aldrich, Fisher chemicals or DSM, at reagent grade or higher, and used as received unless otherwise specified.

1.2 Analytical

NMR spectra were recorded on a Bruker Ultrashield 500 MHz Avance III HD equipped with a nitrogen cooled BBO Prodigy CryoProbe, Bruker AVIII 500 MHz and Bruker AVIII 400 MHz (BBO probe) at 25 °C, unless otherwise specified. Multiplicity of signals in the NMR data are represented by their peaks: s is singlet, d is doublet, t is triplet, q is quartet, qu is quintet, m is multiplet, dd is doublet of doublets, br is broad, etc. Coupling constants (*J*) were reported to the nearest 0.1 Hz. All NMR spectra were processed with the Bruker software TopSpin 4.0.6 or DynamicCentre 2.5.6. Further NMR processing and data plotting was carried on Microsoft Excel and/or Origin 2017.

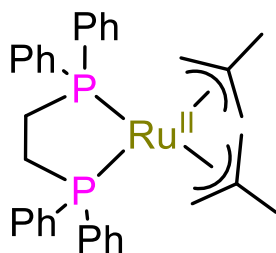
GC-FID/MS data was collected using a Shimadzu GCMS-QP2020 chromatograph equipped with a nitroterephthalic acid modified polyethylene glycol column of high polarity (DB-FFAP; 30 m x 0.25 mm x 0.25 µm) and a flame ionization detector (FID). Helium was used as a carrier gas with electron ionisation for mass spectrometry. Method details used are included when GC-FID/MS data is shown.

Column chromatographic separations were carried out on a BÜCHI Reveleris X2 Flash Chromatography System using a BÜCHI FlashPure Silica 24 g flash cartridge as a stationary phase silica. The mobile phase contained a gradient mixture of ethyl acetate and *n*-hexane.

IR spectrometric data was collected using a Bruker Alpha II FT-IR between 400 – 4,000 cm⁻¹ with 24 scans at 2 cm⁻¹ resolution. Multiplicity of signals in the IR data are represented by their peaks: s is sharp, m is medium, br is broad, w is wide etc.

2.0 Experimental Details

2.1 Preparation of $[\text{Ru}^{\text{II}}(\eta^3\text{-CH}_2\text{C}(\text{Me})\text{CH}_2)_2(\text{dppe})]$ $([(\text{dppe})\text{Ru}(\text{MA})_2])^1$



Synthesis: A 250 mL round bottom flask was charged with 1,2-bis(diphenyl-phosphino)ethane (5.33 g, 13.38 mmol) and $[(\text{methylallyl})_2\text{Ru}(\text{cod})]$ (4.11 g, 12.78 mmol). The flask was equipped with a reflux condenser and *n*-hexane (56 mL) was added. The reaction mixture was heated to reflux for 6 h with stirring, cooled to room temperature and then stored at 4 °C for 19 h. The resulting yellow suspension was filtered and the solid washed with *n*-hexane (2 x 40 mL). The solid was dried for 2 h at 30 °C (10 mbar) and 2 h under high vacuum at room temperature to obtain 6.49 g yellow crystals (89% yield).

Purification: A Schlenk flask was charged with $[\text{Ru}^{\text{II}}(\eta^3\text{-CH}_2\text{C}(\text{Me})\text{CH}_2)_2(\text{dppe})]$ (350 mg, 0.51 mmol) and dissolved in anhydrous acetone (35 mL). The yellow-grey solution was syringe-filtered through a 0.22 μm PTFE membrane (removing some fine, black solids) and then concentrated to half volume. *n*-hexane was added (18 mL) and the mixture stored at 4 °C overnight. The mixture was filtered and the solid dried under high vacuum leaving bright yellow, free-flowing micro crystals (280 mg, yield = 80%).

^1H NMR (500 MHz, $(\text{CD}_3)_2\text{CO}$), δ (ppm) = 7.89 (t, $^3J_{\text{HH}} = 8.1$ Hz, 4H, Ph_{ortho}), 7.45 (m, 6H, $\text{Ph}_{\text{meta and para}}$), 7.14 (m, 6H, $\text{Ph}_{\text{meta and para}}$), 6.80 (t, $^3J_{\text{HH}} = 7.3$ Hz, 4H, Ph_{ortho}), 3.57 (dd, $^3J_{\text{HH}} = 8.6$, 35.7 Hz, 2H, CH_2CH_2), 2.66 (br, 2H, CH_2CH_2), 2.05 (s, 6H, allylic $(\text{CH}_3)_2$), 1.71 (s, 2H, allylic CH_2), 1.37 (s, 2H, allylic CH_2), 0.83 (dd, $^3J_{\text{HH}} = 4.9$, 14.78 Hz, 2H, allylic CH_2), 0.00 (d, $^3J_{\text{HH}} = 14.6$ Hz, 2H, allylic CH_2).

$^{31}\text{P}\{^1\text{H}\}$ NMR (202 MHz, $(\text{CD}_3)_2\text{CO}$), δ (ppm) = 83.9 (s).

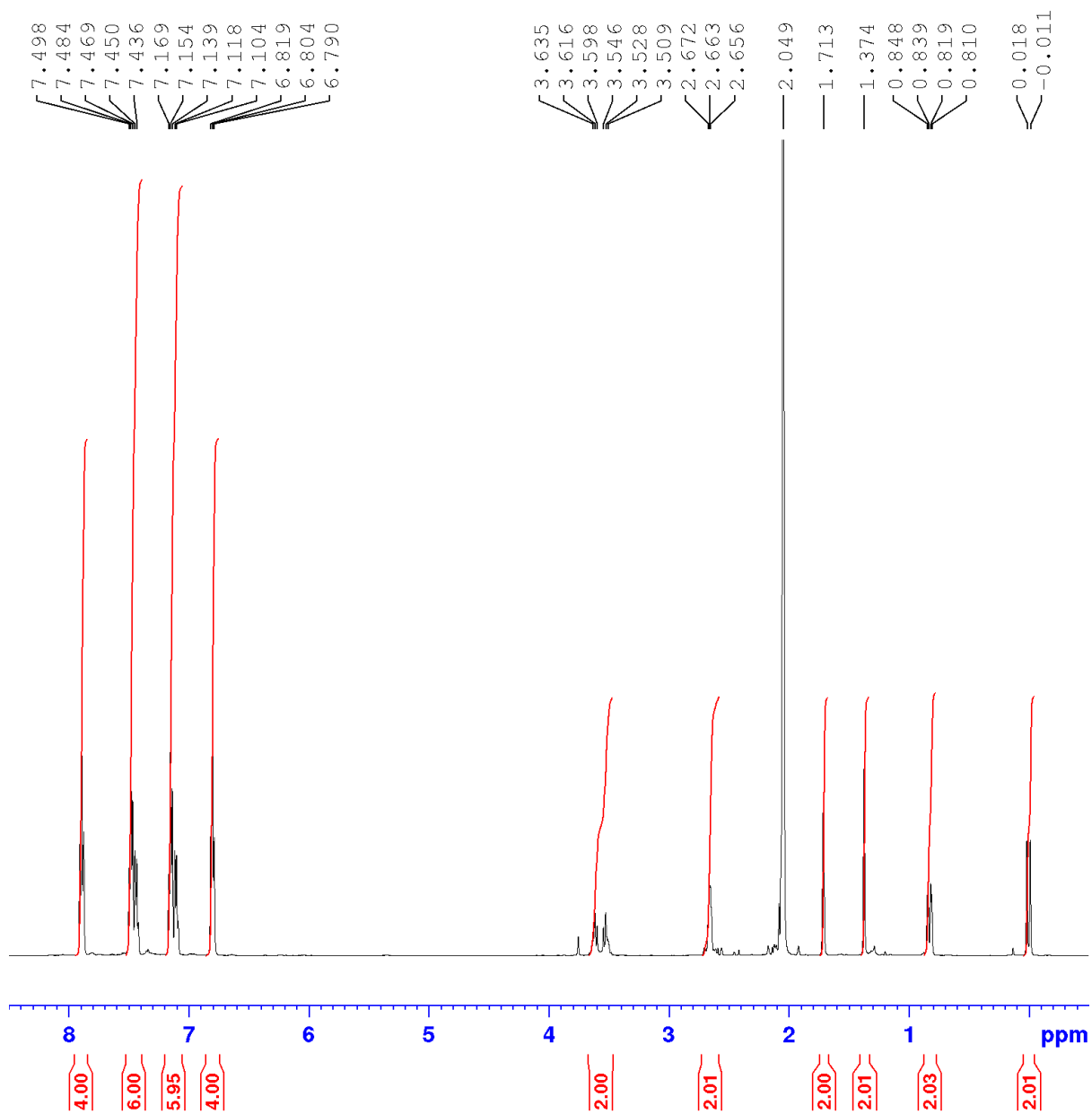


Figure S1. ^1H NMR of $[\text{Ru}^{\text{II}}(\eta^3\text{-CH}_2\text{C}(\text{Me})\text{CH}_2)_2(\text{dppe})]$ in $(\text{CD}_3)_2\text{CO}$.

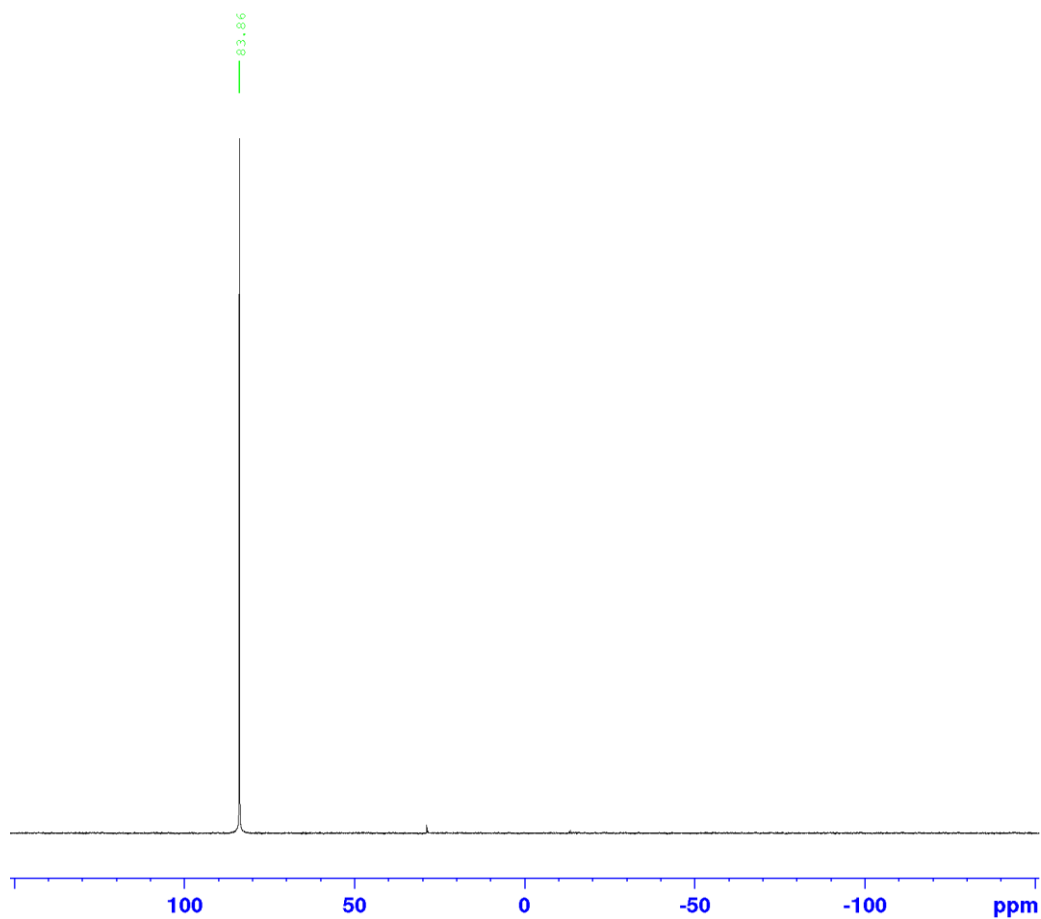


Figure S2. $^{31}\text{P}\{^1\text{H}\}$ NMR of $[\text{Ru}^{\text{II}}(\eta^3\text{-CH}_2\text{C}(\text{Me})\text{CH}_2)_2(\text{dppe})]$ in $(\text{CD}_3)_2\text{CO}$.

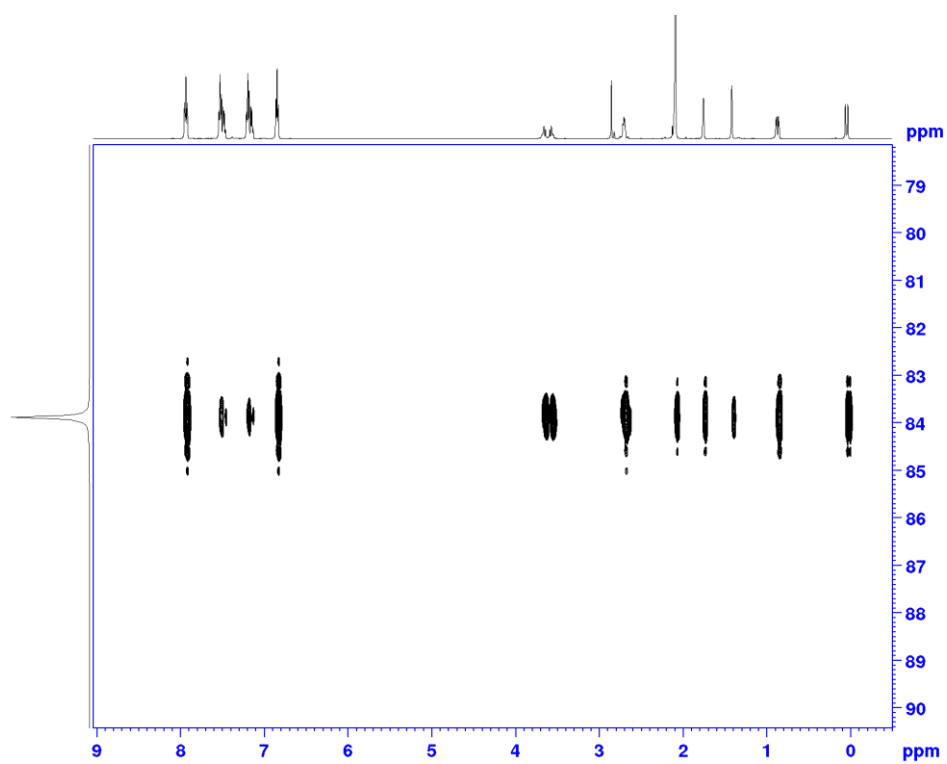
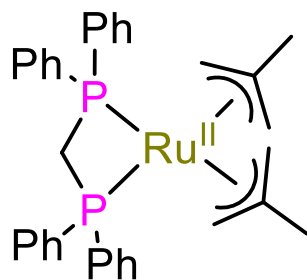


Figure S3. $^1\text{H}\text{-}^{31}\text{P}$ HMBC NMR of $[\text{Ru}^{\text{II}}(\eta^3\text{-CH}_2\text{C}(\text{Me})\text{CH}_2)_2(\text{dppe})]$ in $(\text{CD}_3)_2\text{CO}$.

2.2 Preparation of $[\text{Ru}^{\text{II}}(\eta^3\text{-CH}_2\text{C}(\text{Me})\text{CH}_2)_2(\text{dppm})]^1$



A flame dried Schlenk flask was charged with bis(diphenylphosphino)methane (821 mg, 0.7 mmol), $[(\text{methylallyl})_2\text{Ru}(\text{COD})]$ (399 mg, 1.25 mmol) and *n*-hexane (15.6 mL). The mixture was heated to reflux for 6 h with stirring, then cooled to room temperature and stored at 4 °C overnight. The resulting suspension was cannula filtered under argon, and the yellow solid was washed with cold *n*-hexane (2 x 5 mL). The residue was dried under high vacuum overnight giving free-flowing dark yellow micro crystals (yield = 368 mg, 92%).

^1H NMR (500 MHz, $(\text{CD}_3)_2\text{CO}$), δ (ppm) = 8.01 (t, $^3J_{\text{HH}} = 8.1$ Hz, 4H, Ph_{ortho}), 7.53 (m, $^3J_{\text{HH}} = 7.2$, 6H, Ph_{meta} and para), 7.16 (m, 6H, Ph_{meta} and para), 6.88 (t, $^3J_{\text{HH}} = 7.3$ Hz, 4H, Ph_{ortho}), 4.94 (t, $^3J_{\text{HH}} = 9.5$ Hz, 2H, PCH_2P), 2.65 (dd, 2H, allylic CH_2), 1.89 (s, 6H, allylic CH_3), 1.25 (s, 2H, allylic CH_2), 0.74 (d, $^3J_{\text{HH}} = 10.5$ Hz, 2H, allylic CH_2), 0.64 (br, 2H, allylic CH_2).

$^{31}\text{P}\{^1\text{H}\}$ NMR (202 MHz, $(\text{CD}_3)_2\text{CO}$), δ (ppm) = 12.7 (s).

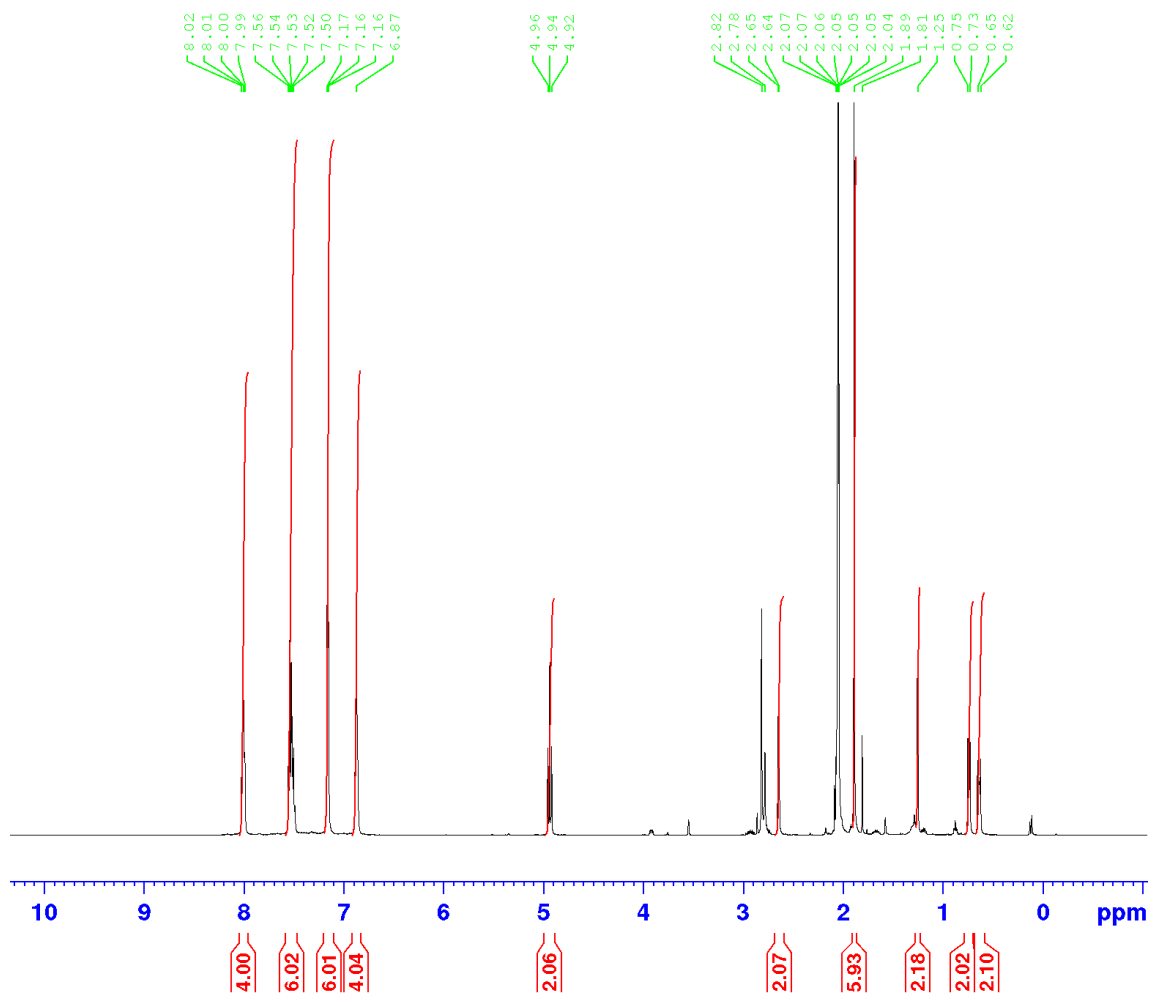


Figure S4. ^1H NMR of $[\text{Ru}^{\text{II}}(\eta^3\text{-CH}_2\text{C}(\text{Me})\text{CH}_2)_2(\text{dppm})]$ in $(\text{CD}_3)_2\text{CO}$.

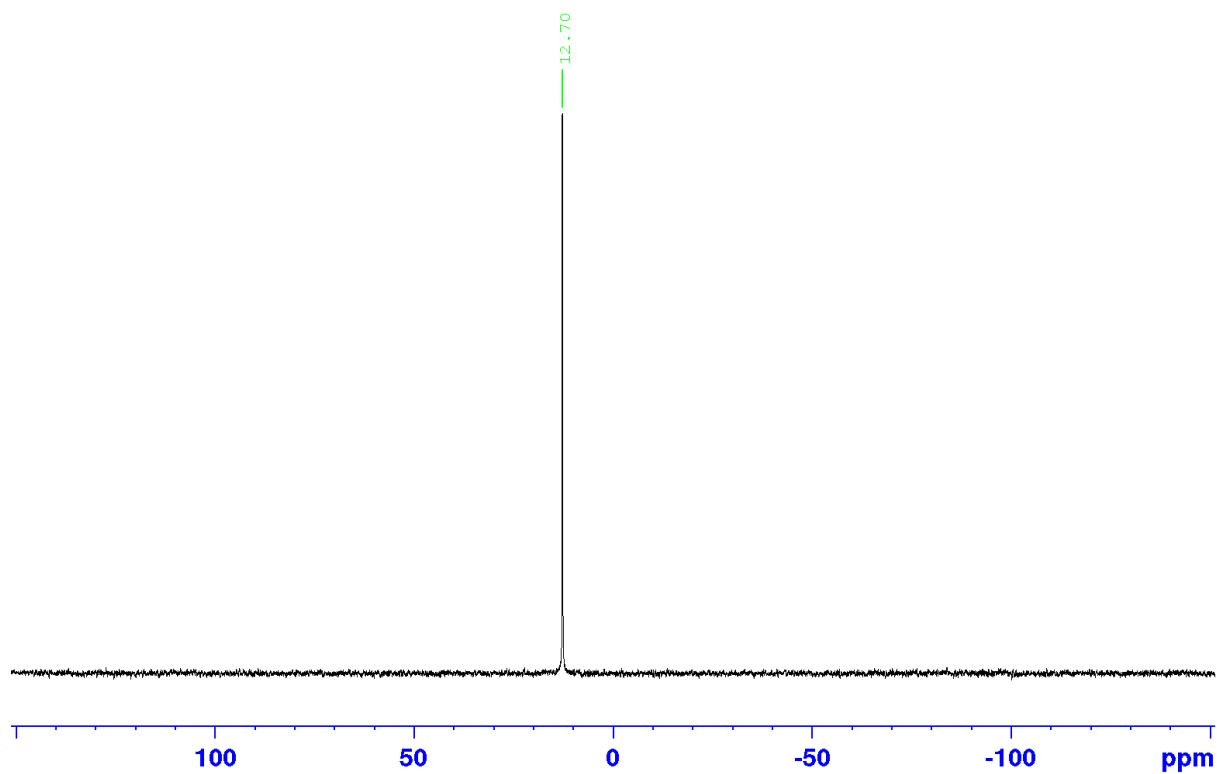


Figure S5. $^{31}\text{P}\{^1\text{H}\}$ NMR of $[\text{Ru}^{\text{II}}(\eta^3\text{-CH}_2\text{C}(\text{Me})\text{CH}_2)_2(\text{dppm})]$ in $(\text{CD}_3)_2\text{CO}$.

2.2 Purification of carboxylic acids

2.2.1 Pivalic acid

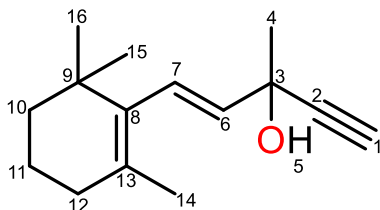
A Schlenk flask was charged with pivalic acid (30 g, 0.3 mol) and attached in a bulb-to-bulb distillation apparatus. The flask with crude pivalic acid was heated to 180 °C with an oil bath and the receiving flask was cooled to 0 °C. The head temperature of the distillation was 175 °C. The first 15% of distillate was discarded. Clear viscous liquid was distilled over 2 h into a Schlenk flask (yield = 24 g, 80%).

2.2.2 Adamantane carboxylic acid and benzoic acid

A Schlenk flask was charged with adamantane carboxylic acid (30 g, 0.167 mol) and recrystallised from anhydrous benzene (100 mL). The crystals were filtered and dried overnight under dynamic vacuum, with free-flowing white micro crystals isolated (yield = 24.2 g, 82%).

A Schlenk flask was charged with benzoic acid (30 g, 0.25 mol) and recrystallised from anhydrous ethanol. The crystals were filtered and dried overnight under dynamic vacuum, with free-flowing white micro crystals isolated (yield = 21.6 g, 72%).

2.3 Preparation of ethynyl- β -ionol (**2a**)²



Ethynyl- β -ionol was produced by DSM using a proprietary method. Crude ethynyl- β -ionol (30 g, 0.14 mol) and butylated hydroxytoluene (stabiliser; 150 mg, 0.68 mmol) were transferred into separate round bottom flasks in a Vigreux distillation apparatus. The round bottom flask with crude ethynyl- β -ionol was heated (120 °C / 0.5 mbar) with an oil bath. The receiving round bottom flask containing butylated hydroxytoluene (BHT) was cooled to 0 °C. The head temperature of the distillation was 122 °C at 0.4 mbar. Clear viscous liquid was distilled over the duration of a couple of hours. (Yield = 24 g, 80%).

¹H NMR (500 MHz, (CD₃)₂CO), δ (ppm) = 6.39 (d, 1H, ³J_{HH} = 16.2 Hz, H-7), 5.56 (d, 1H, ³J_{HH} = 15.9 Hz, H-6), 4.57 (s, 1H, H-5), 2.92 (s, 1H, H-1), 2.00 (t, 2H, ³J_{HH} = 6.3 Hz, H-12), 1.68 (s, 3H, H-14), 1.63 (m, 2H, H-11), 1.54 (s, 3H, H-4), 1.47 (m, 2H, H-10), 1.01 (s, 6H, H-15-16)

¹³C{¹H} NMR (125 MHz, (CD₃)₂CO), δ (ppm) = 205.5 (s, C-3), 138.3 (s, C-6), 136.5 (s, C-8), 128.1 (s, C-13), 125.7 (s, C-7), 87.7 (s, C-9), 72.3 (s, C-1), 66.9 (s, C-2), 39.3 (s, C-10), 32.4 (s, C-12), 30.7 (s, C-4), 28.2 (d, *J* = 4.08 Hz, C-15-16), 20.7 (s, C-14), 19.12 (s, C-11).

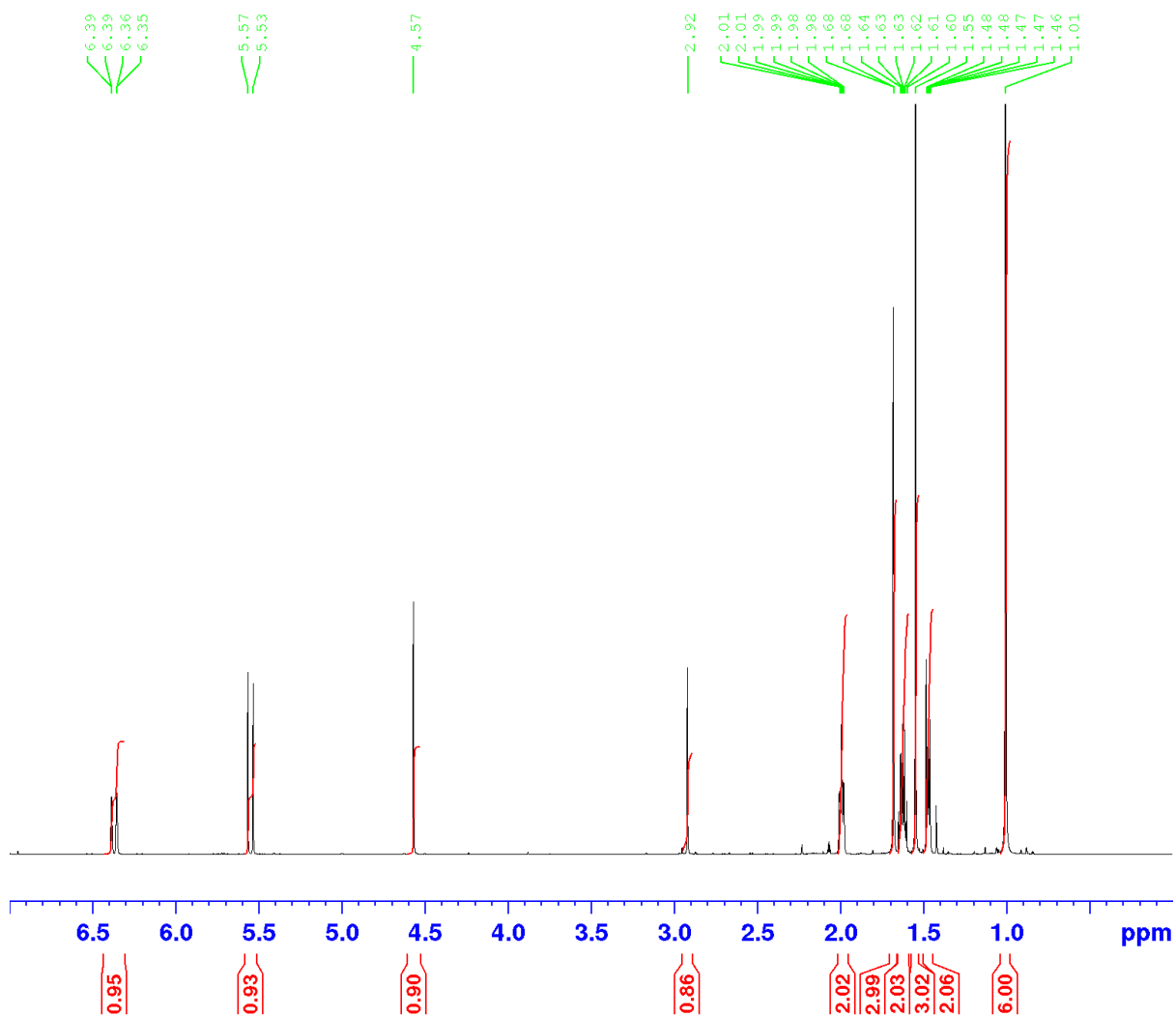


Figure S6. ^1H NMR of ethynyl- β -ionol in $(\text{CD}_3)_2\text{CO}$.

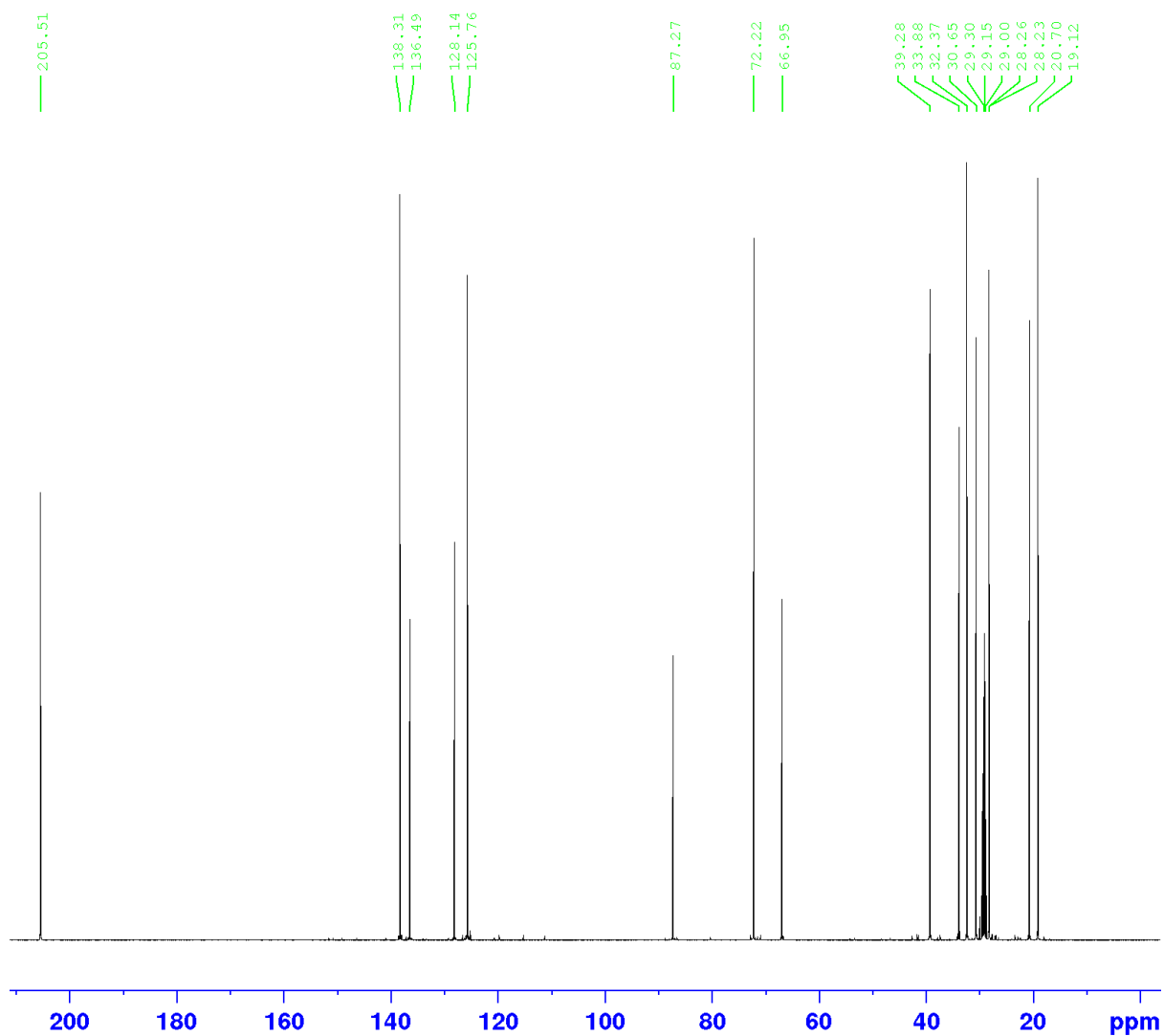
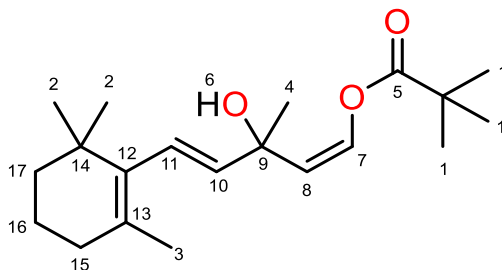


Figure S7. $^{13}\text{C}\{^1\text{H}\}$ NMR of ethynyl- β -ionol in $(\text{CD}_3)_2\text{CO}$.

2.4 Preparation of α,β -unsaturated carboxylates

2.4.1 3-hydroxy-3-methyl-5-(2,6,6-trimethylcyclohex-1-en-1-yl) penta-1,4-dien-1-yl pivalate (3ab)



Procedure adapted from literature for the isolation of the ester-adducts.² A Schlenk flask was charged with pivalic acid (1.32 g, 11 mmol), pivalic anhydride (0.4 ml, 2 mmol), ethynyl- β -ionol (2.18 g, 10 mmol), and ethyl acetate (10 mL). Subsequently, $[\text{Ru}^{\text{II}}(\eta^3\text{-CH}_2\text{C}(\text{Me})\text{CH}_2)_2(\text{dppe})]$ (61 mg, 0.1 mmol) was dissolved in ethyl acetate (5 mL) and syringed into the Schlenk flask and stirred for 40 hours for maximum conversion. The residue was purified by flash chromatography on a silica packed column with ethyl acetate as the eluent to give the product over several fractions. Fractions were poured into one Schlenk flask and concentrated under pressure to a brown oil (2.36 g, 72% yield).

^1H NMR (500 MHz, $(\text{CD}_3)_2\text{CO}$), δ (ppm) = 6.95 (d, $^3J_{\text{HH}} = 7.2$ Hz, 1H, H-7), 6.12 (d, $^3J_{\text{HH}} = 16.2$ Hz, 1H, H-11), 5.72 (d, $^3J_{\text{HH}} = 16.2$ Hz, 1H, H-10), 5.19 (d, $^3J_{\text{H-H}} = 8$ Hz, 1H, H-8), 1.96 (m, 2H, H-15), 1.65 (s, 3H, H-3), 1.61 (m, 2H, H-16), 1.58 (s, 3H, H-4), 1.44 (m, 2H, H-17), 1.25 (s, 9H, H-1), 0.94 (d, $^3J_{\text{HH}} = 6.3$ Hz, 6H, H-2)

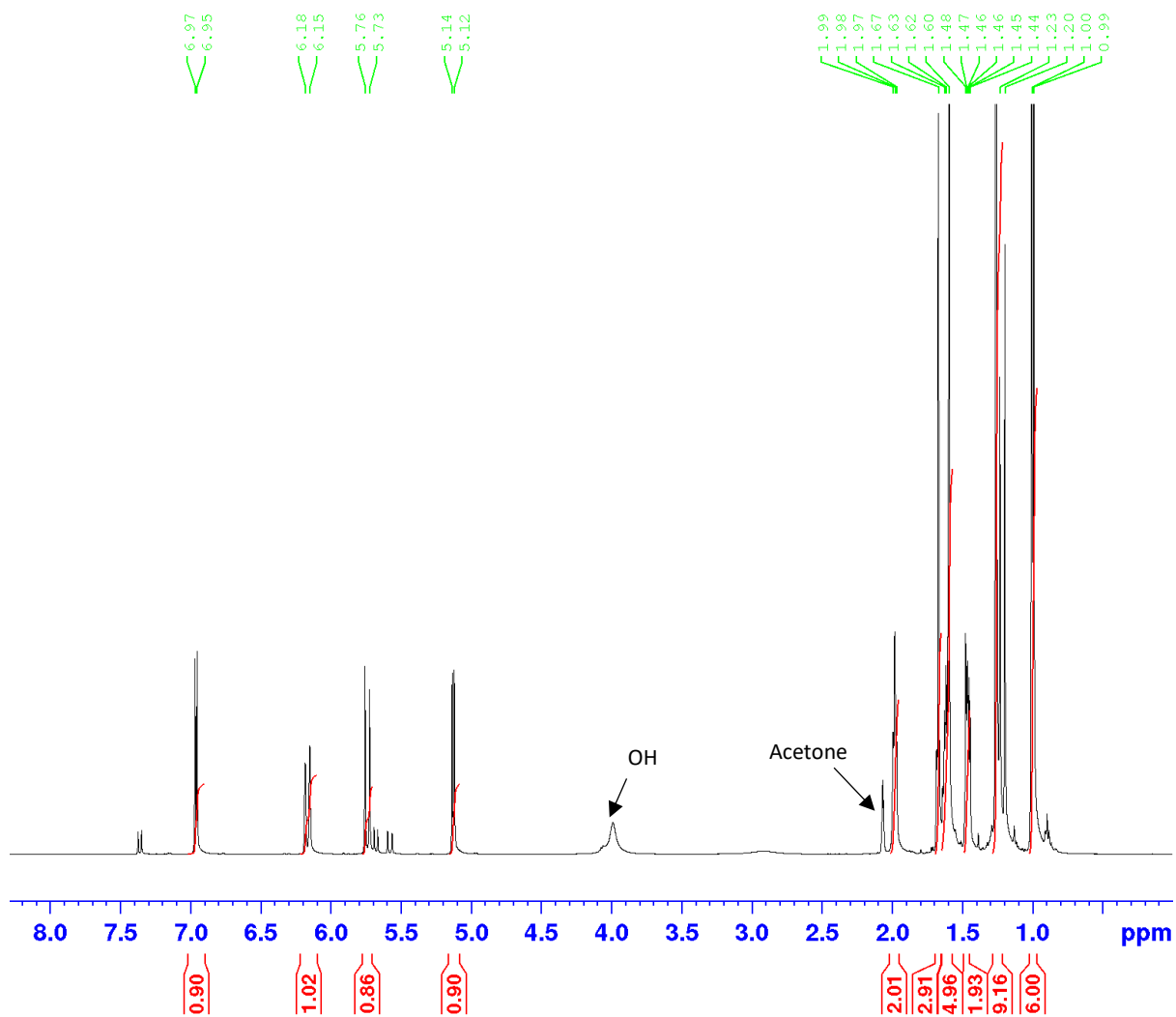
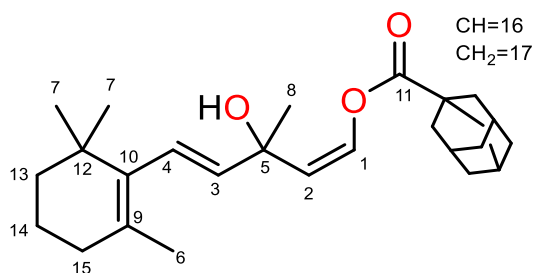


Figure S8. ^1H NMR of **3ab** in $(\text{CD}_3)_2\text{CO}$.

2.4.2 3-hydroxy-3-methyl-5-(2,6,6-trimethylcyclohex-1-en-1-yl)penta-1,4-dien-1-yl adamantane-1-carboxylate (**3ae**)



A Schlenk flask was charged with adamantane carboxylic acid (1.98 g, 11 mmol), pivalic anhydride (0.4 ml, 2 mmol), ethynyl- β -ionol (2.18 g, 10 mmol), and ethyl acetate (10 mL). Subsequently, $[\text{Ru}^{\text{II}}(\eta^3\text{-CH}_2\text{C}(\text{Me})\text{CH}_2)_2(\text{dppe})]$ (61 mg, 0.1 mmol) was dissolved in ethyl acetate (5 mL) and syringed into the Schlenk flask and stirred for 40 hours for maximum conversion. The residue was purified by flash chromatography on a silica packed column with ethyl acetate as the eluent to give the product over several fractions. Fractions were poured into one Schlenk flask and concentrated under pressure to a brown oil (68% yield).

^1H NMR (500 MHz, CDCl_3), δ (ppm) = 7.09 (d, $^3J_{\text{HH}} = 7.2$ Hz, 1H, H-1), 6.11 (d, $^3J_{\text{HH}} = 16.2$ Hz, 1H, H-4), 5.65 (d, $^3J_{\text{HH}} = 16.2$ Hz, 1H, H-3), 5.08 (d, $^3J_{\text{HH}} = 7.2$ Hz, 1H, H-2), 2.04 (s, 3H, H-16), 2.00 (s, 1H, H-18), 1.97 (m, 2H, H-15), 1.92 (m, 10H, H-17), 1.65 (s, 3H, H-6), 1.6 (m, 2H, H-14), 1.53 (s, 3H, H-8), 1.45 (m, 2H, H-13), 0.98 (d, 6H, H-7)

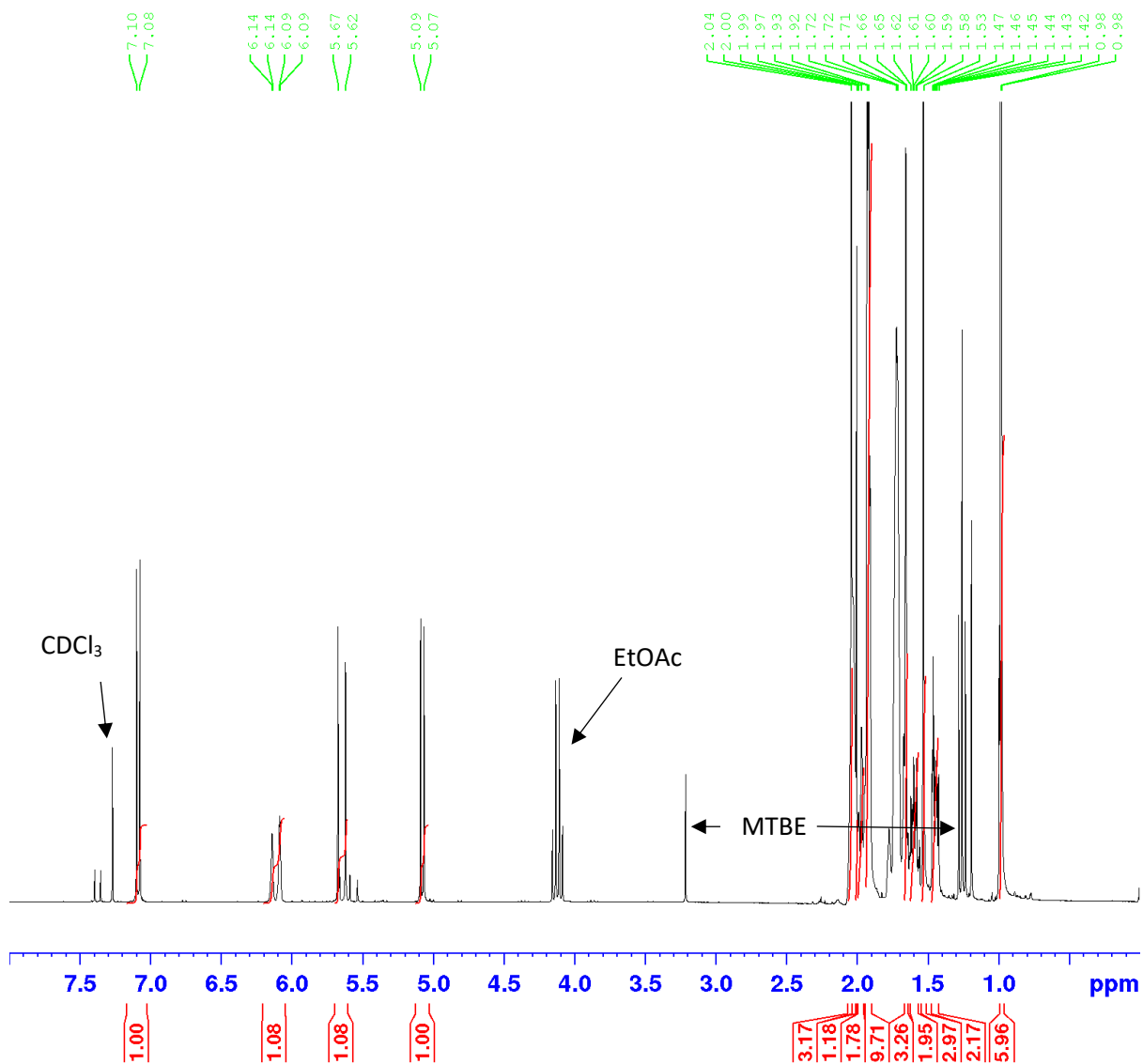
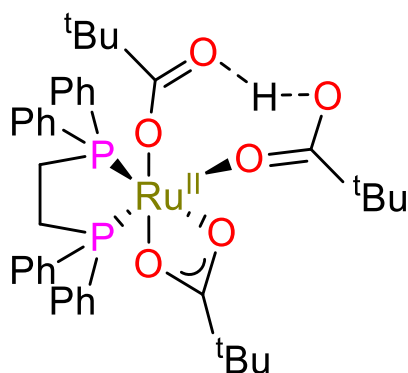


Figure S9. ¹H NMR of **3ae** in CDCl₃ containing methyl tert-butyl ether (MTBE) and EtOAc.

2.5 Synthetic procedure for generating compounds suitable for crystal structure determination

2.5.1 A_p' [(dppe)Ru^{II}(η^2 -O₂CC^tBu)(η^1 -O₂CC^tBu)(^tBuCCO₂H)]



A Schlenk flask was charged with ~100 eq. of pivalic acid (1 g, 9.8 mmol) and [Ru^{II}(η^3 -CH₂C(Me)CH₂)₂(dppe)] (60 mg, 0.1 mmol), which were dissolved in anhydrous ethyl acetate (15 mL) and stirred for 1 hour. The solvent was concentrated at 40 °C for 2 hours. The remaining solid was dissolved into dry n-hexane at first signs of boiling and allowed to cool gradually from +60 °C to -20 °C for the formation of yellow microcrystalline crystals (yield = 32 mg, 48.4%).

¹H NMR (500 MHz, (CD₃)₂CO), δ (ppm) = 7.57 (br, 8H, Ph), 7.36 (m, 12H, Ph), 2.72 (s, 4H, CH₂-CH₂), 0.58 (s, 18H, (CH₃)₃)₂

³¹P{¹H} NMR (202 MHz, (CD₃)₂CO), δ (ppm) = 89.5 (s)

¹³C{¹H} NMR (125 MHz, (CD₃)₂CO), δ (ppm) = 193.4 (s, COO), 136.7 (s, Ph), 133.5 (t, J_{CH} = 4.7 Hz, Ph), 130.3 (s, Ph), 128.7 (t, J_{CH} = 4.7 Hz, Ph), 39.8 (s, CH₂-CH₂), 38.9 (s, CH₂-CH₂), 27.6 (s), 27.14 (s, (CH₃)₃)₂

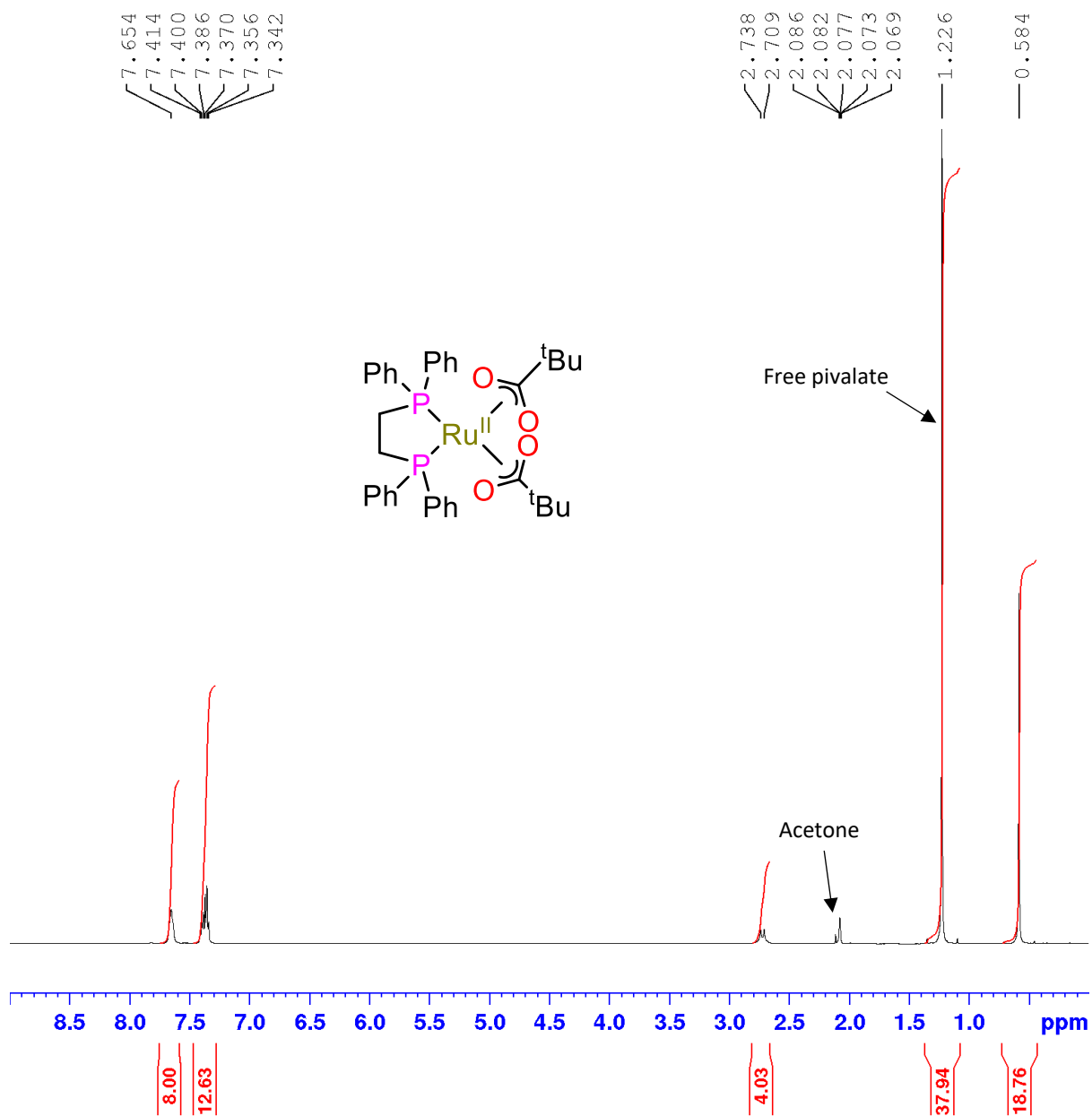


Figure S10. ¹H NMR of [(dppf)Ru^{II}(η²-O₂CC^tBu)(η¹-O₂CC^tBu)(^tBuCCO₂H)] (**A_p**) crystals dissolved in (CD₃)₂CO

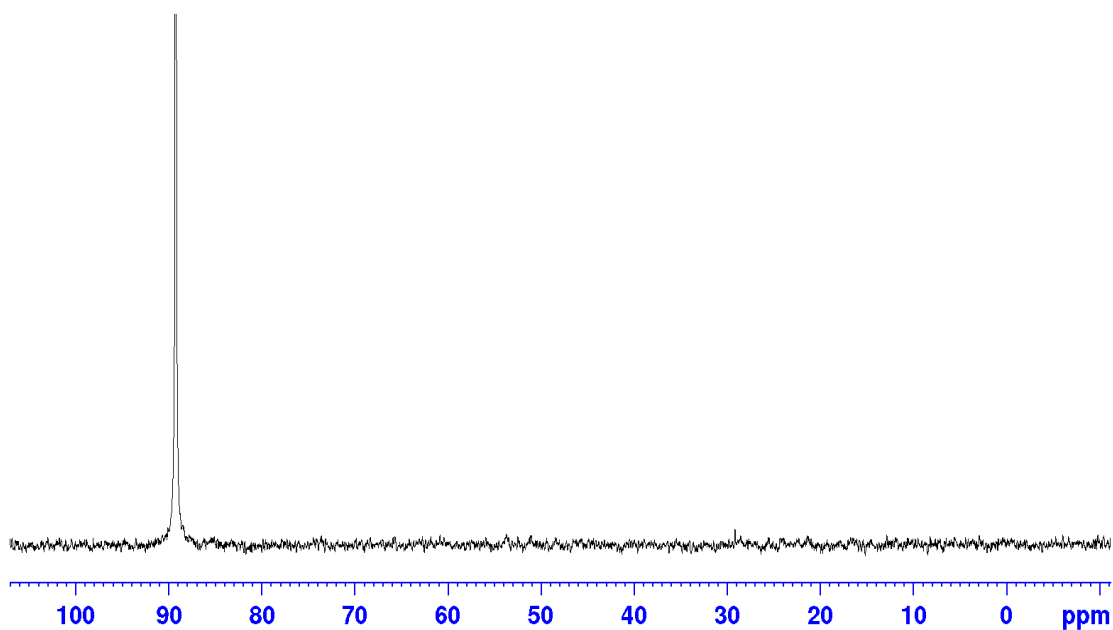


Figure S11. $^{31}\text{P}\{^1\text{H}\}$ NMR of $[(\text{dppe})\text{Ru}^{\text{II}}(\eta^2\text{-O}_2\text{CC}^t\text{Bu})(\eta^1\text{-O}_2\text{CC}^t\text{Bu})(^t\text{BuCCO}_2\text{H})]$ (**A_p**) crystals dissolved in $(\text{CD}_3)_2\text{CO}$

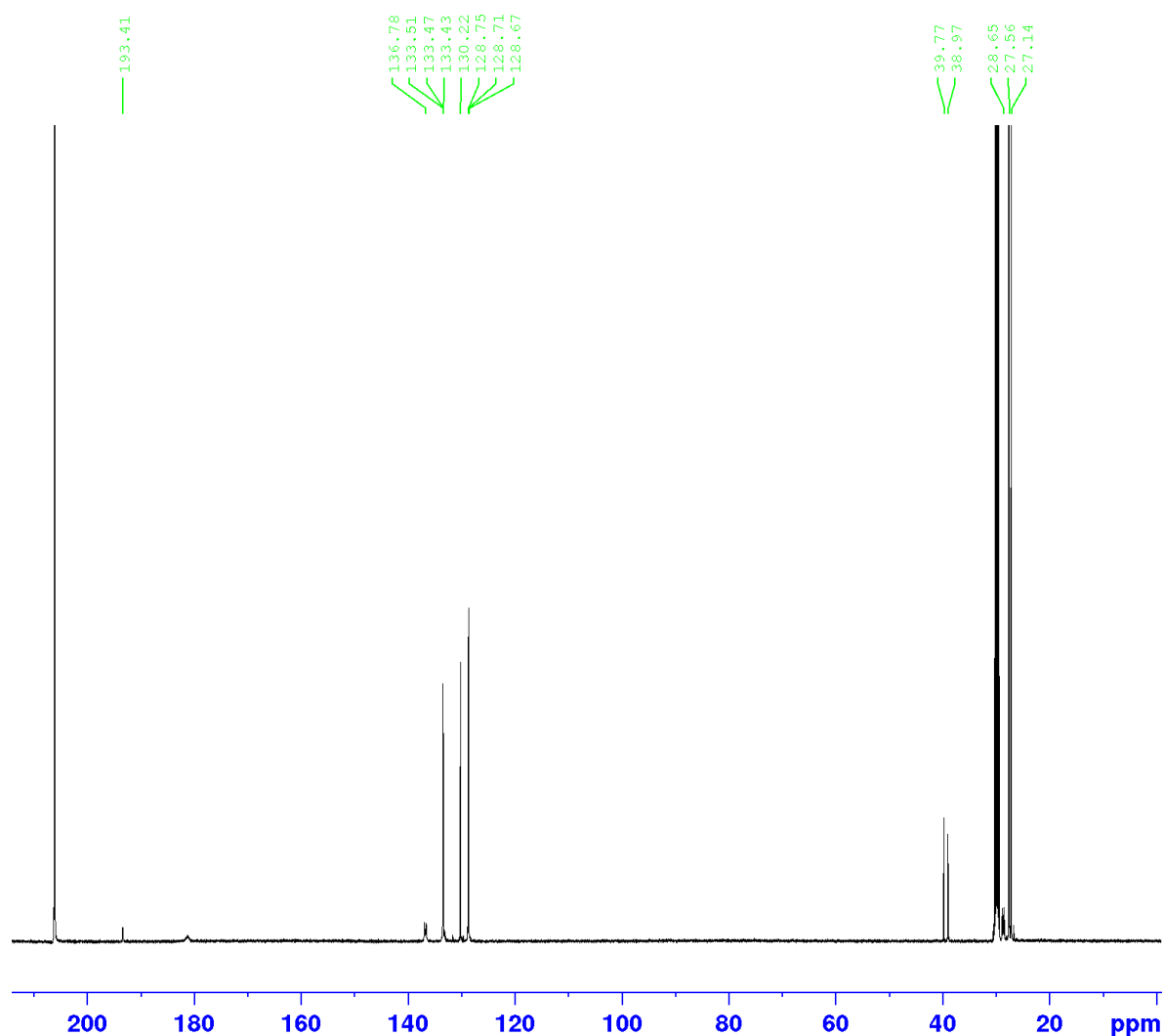
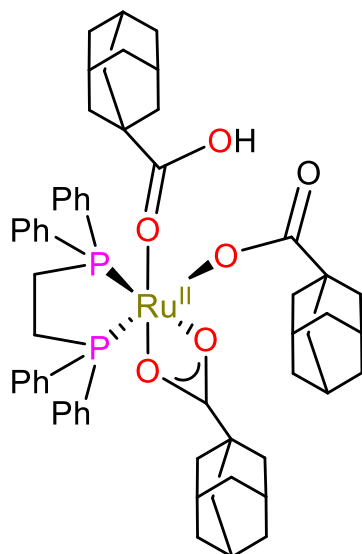


Figure S12. $^{13}\text{C}\{^1\text{H}\}$ NMR of $[(\text{dppe})\text{Ru}^{\text{II}}(\eta^2\text{-O}_2\text{CC}^t\text{Bu})(\eta^1\text{-O}_2\text{CC}^t\text{Bu})(^t\text{BuCCO}_2\text{H})]$ crystals dissolved in $(\text{CD}_3)_2\text{CO}$.

2.5.2 **A_{ad}'** [(dppe)Ru^{II}(η²-O₂CC(CH₂)₆(CH)₃C)(η¹-O₂CC(CH₂)₆(CH)₃C)((CH)₃(CH₂)₆CCCO₂H)]



A Schlenk flask was charged with adamantane carboxylic acid (0.25 g, 1.4 mmol) and [Ru^{II}(η³-CH₂C(Me)CH₂)₂(dppe)] (60 mg, 0.1 mmol) which were dissolved in anhydrous acetone (10 mL). After 0.5 h the solvent was evaporated for 2 hours (40 °C). The remaining solid was dissolved in a supersaturated solution with anhydrous acetone and set up for slow diffusion with *n*-hexane to obtain sharp yellow crystals in the glovebox (yield = 28 mg, 45%).

¹H NMR (500 MHz, CDCl₃), δ (ppm) = 7.50 (br, 8H, Ph), 7.31 (m, 12H, Ph), 2.63 (br, 4H, CH₂-CH₂), 1.71 (br, 6H, (CH)₆), 1.50 (d, *J*_{HH} = 11.93 Hz, 6H, (CH₂)₃), 1.41 (d, *J*_{HH} = 11.93 Hz, 6H, (CH₂)₃), 1.23 (s, 12H, (CH₂)₆).

³¹P{¹H} NMR (202 MHz, CDCl₃), δ (ppm) = 90.7 (s)

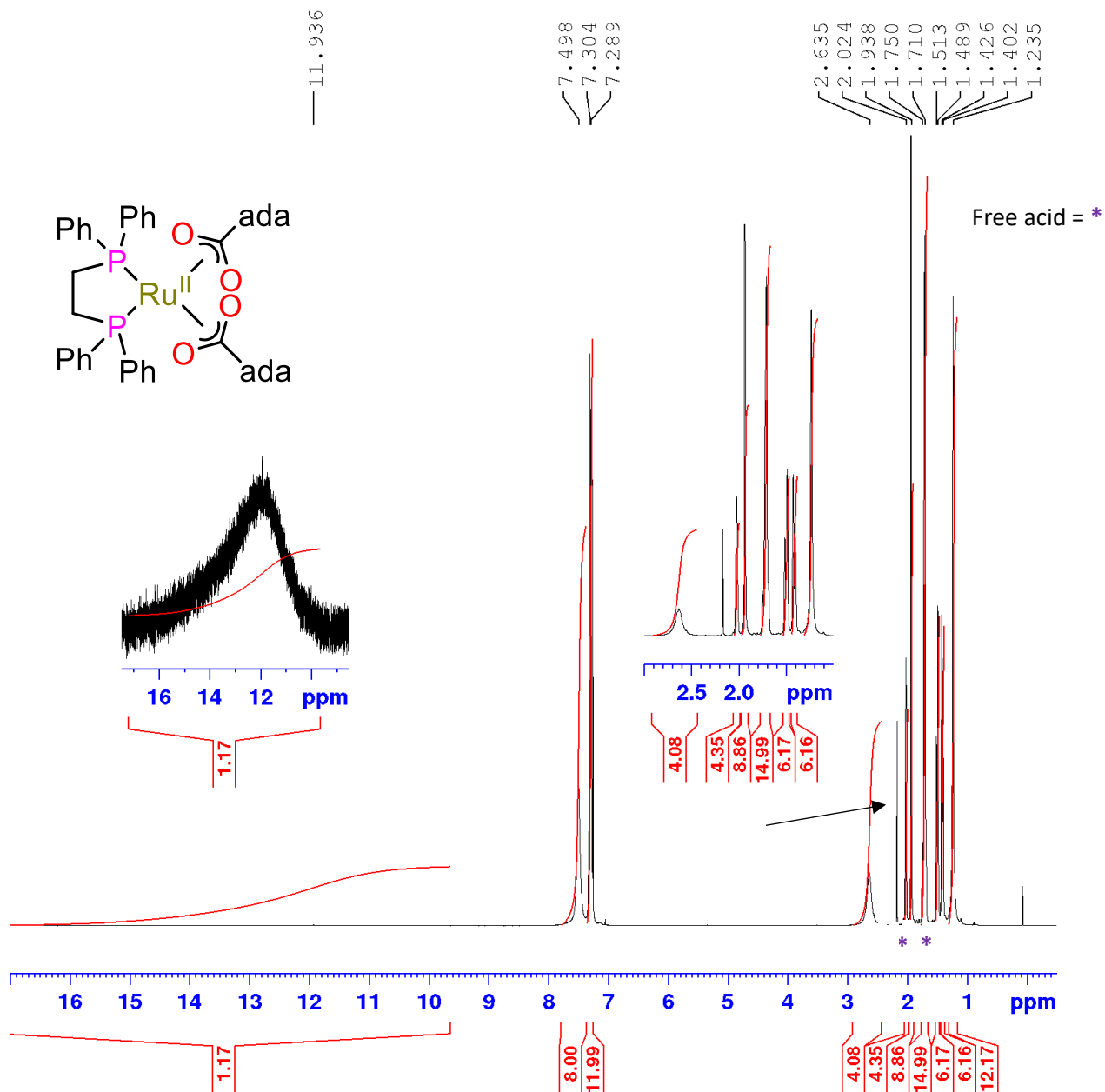


Figure S13. ¹H NMR of $[(dppe)Ru^{II}(\eta^2-O_2CC(CH_2)_6(CH)_3C)(\eta^1-O_2CC(CH_2)_6(CH)_3C)((CH)_3(CH_2)_6CCCO_2H)]$ (**A'**_{ad}) crystals dissolved in CDCl₃.

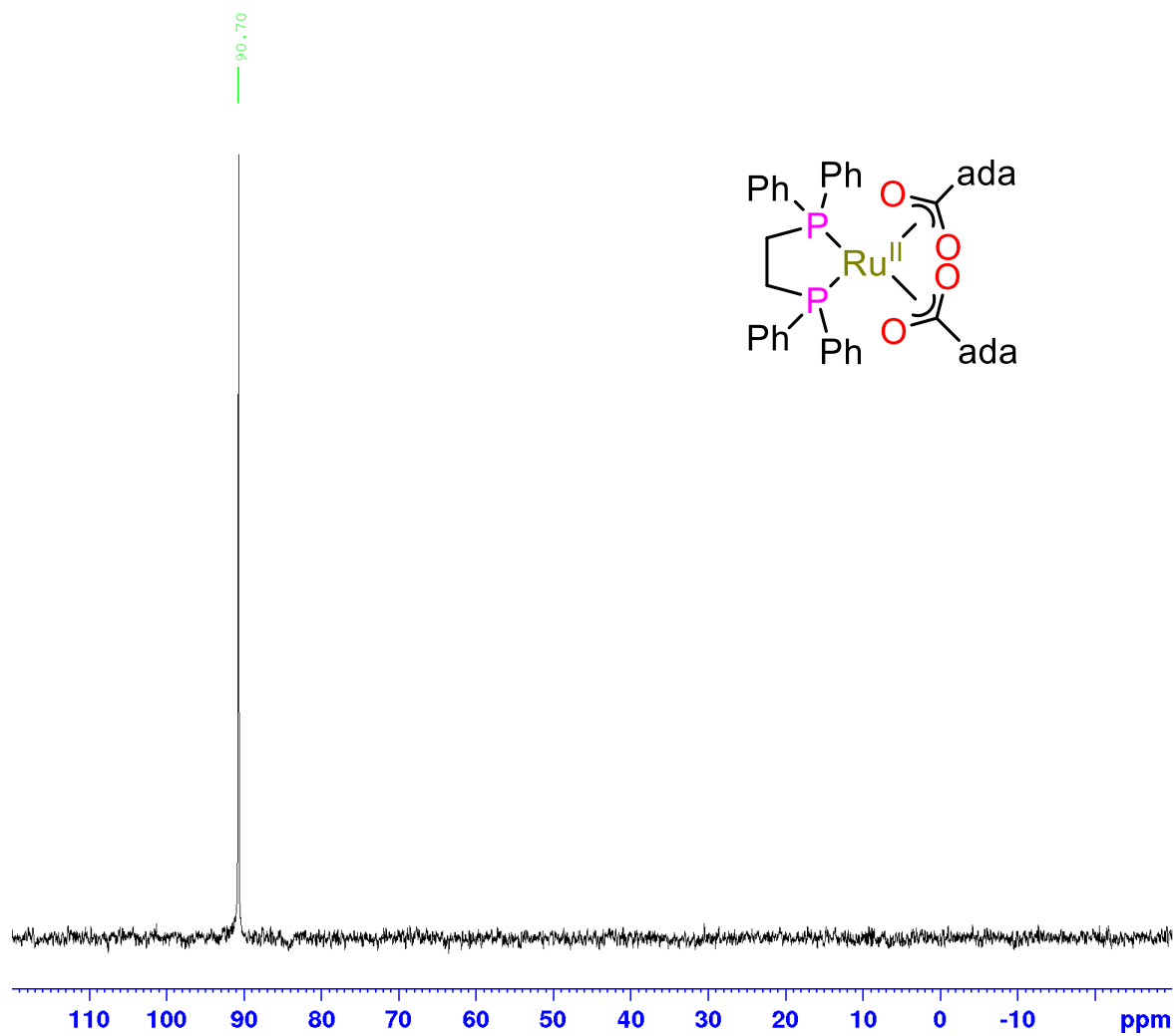
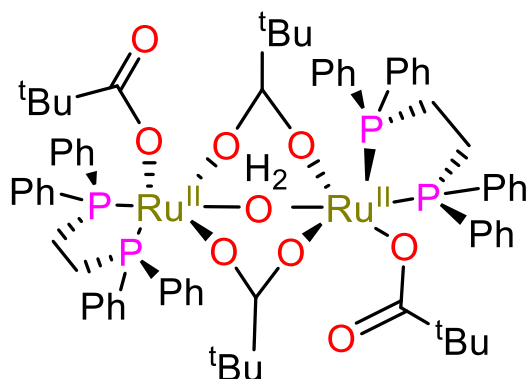


Figure S14. $^{31}\text{P}\{^1\text{H}\}$ NMR of $[(\text{dppe})\text{Ru}^{\text{II}}(\eta^2\text{-O}_2\text{CC}(\text{CH}_2)_6(\text{CH})_3\text{C})(\eta^1\text{-O}_2\text{CC}(\text{CH}_2)_6(\text{CH})_3\text{C})((\text{CH})_3(\text{CH}_2)_6\text{CCCO}_2\text{H})]$ (A'_{ad}) crystals dissolved in CDCl_3

2.5.3 B_p' [$\{(dppe)Ru^{II}(\eta^1-O_2CC^tBu)\}_2(\mu-O_2CC^tBu)_2(\mu-H_2O)$]



A Schlenk flask was charged with pivalic acid (0.5 g, 4.9 mmol) and $[Ru^{II}(\eta^3-CH_2C(Me)CH_2)_2(dppe)]$ (60 mg, 0.1 mmol) which were dissolved in anhydrous ethyl acetate (10 mL). After 0.5 h the solvent was evaporated for 2 hours (40 °C). The remaining solid was dissolved in $(CD_3)_2CO$ and set up for slow diffusion with *n*-hexane to obtain sharp yellow crystal formation in the glovebox (yield = 0.33 mg, 26.6%).

1H NMR (500 MHz, $(CD_3)_2CO$), δ (ppm) = 7.58 (br, 8H, Ph), 7.37 (m, 12H, Ph), 2.86 (br, 4H, CH_2-CH_2), 0.7 (s, 18H, $(CH_3)_3$)

$^{31}P\{^1H\}$ NMR (202 MHz, $(CD_3)_2CO$), δ (ppm) = 89.5 (s), 29.3 (s)

$^{13}C\{^1H\}$ NMR (125 MHz, $(CD_3)_2CO$), δ (ppm) = 205.22 (s), 132.7 (t, $J_{CH} = 5.1$ Hz), 129.49 (s), 127.9 (t, $J_{CH} = 5.1$ Hz), 26.62 (s), 26.1 (s)

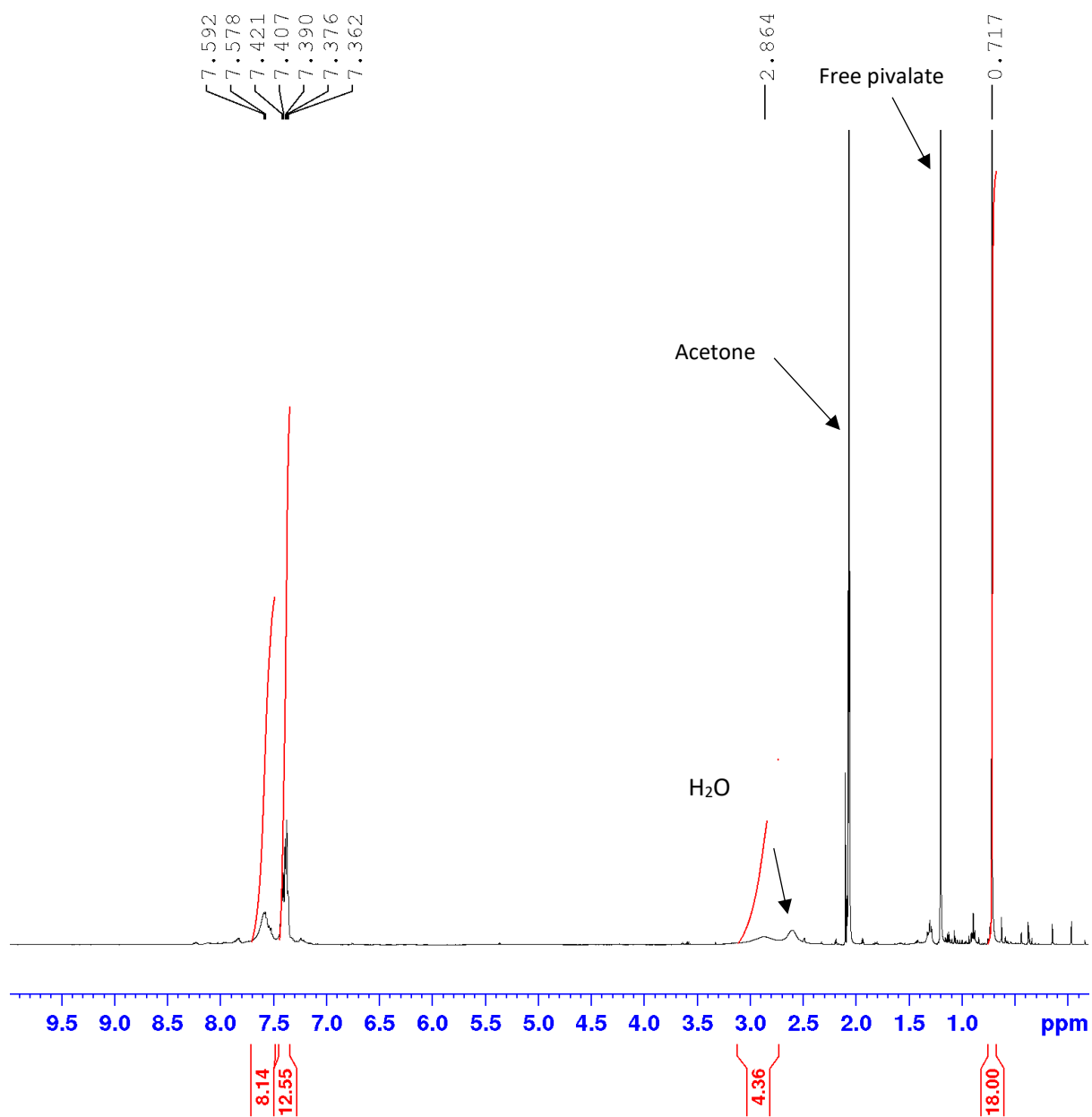


Figure S15. ^1H NMR of B_p' $\{[(\text{dppe})\text{Ru}^{\text{II}}(\eta^1\text{-O}_2\text{CC}^t\text{Bu})_2(\mu\text{-O}_2\text{CC}^t\text{Bu})_2(\mu\text{-H}_2\text{O})]\}$ in $(\text{CD}_3)_2\text{CO}$.

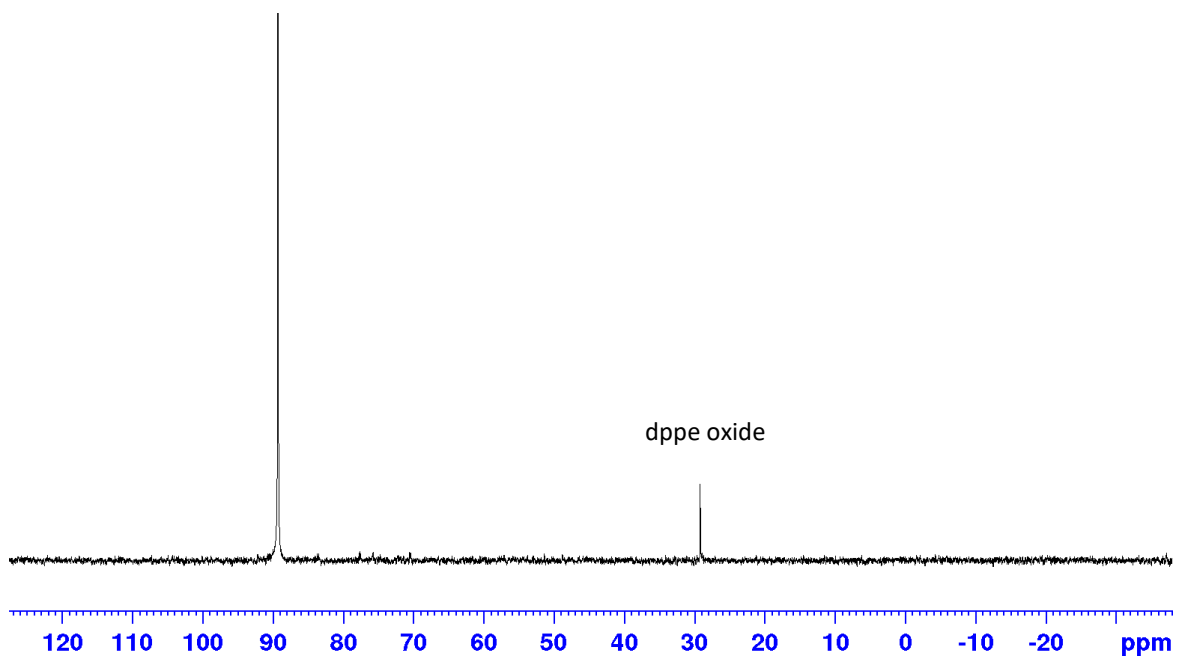


Figure S16. $^{31}\text{P}\{^1\text{H}\}$ NMR of B_p' [$\{(\text{dppe})\text{Ru}^{\text{II}}(\eta^1\text{-O}_2\text{CC}^t\text{Bu})_2\}(\mu\text{-O}_2\text{CC}^t\text{Bu})_2(\mu\text{-H}_2\text{O})$] dissolved in $(\text{CD}_3)_2\text{CO}$.

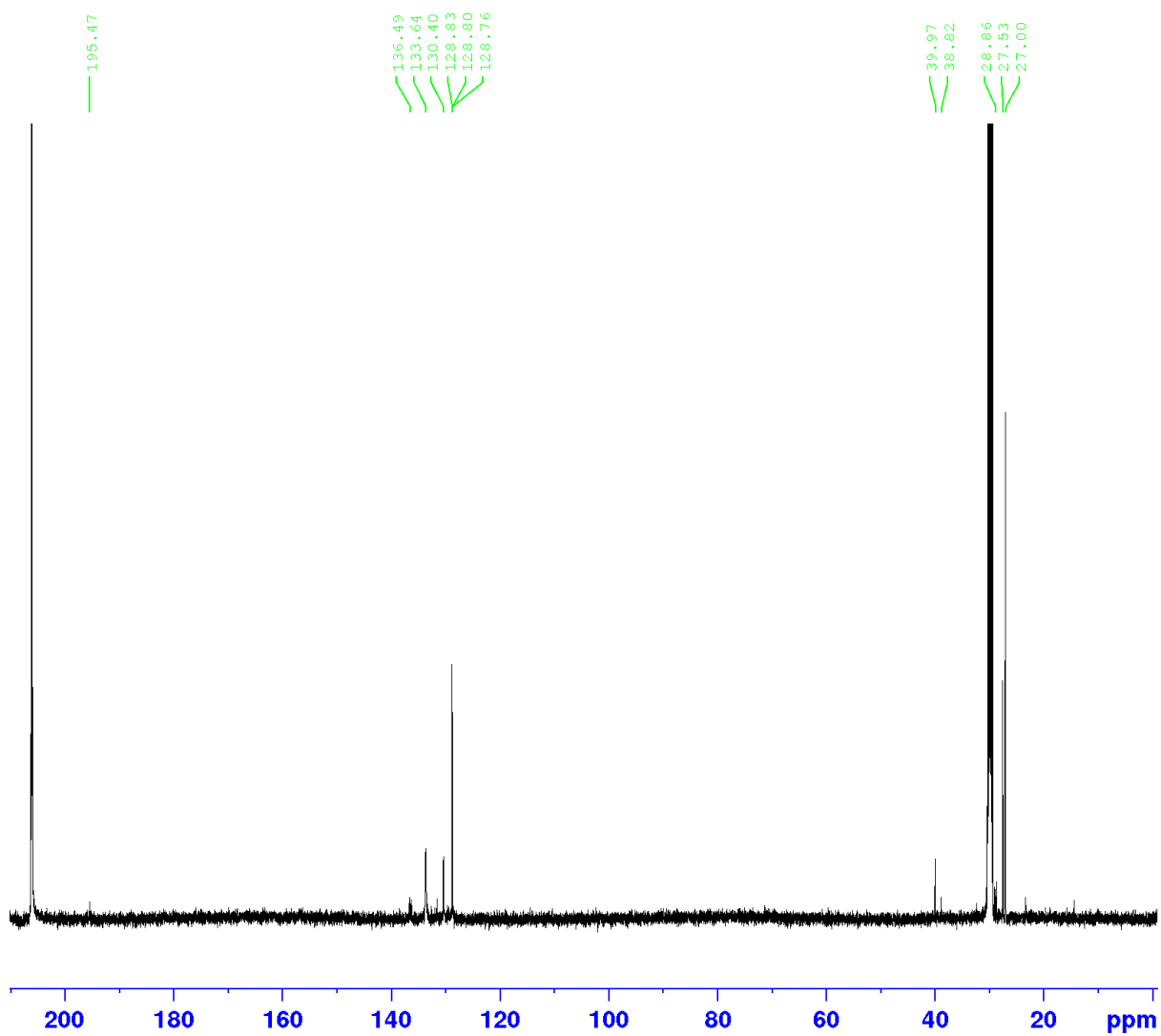
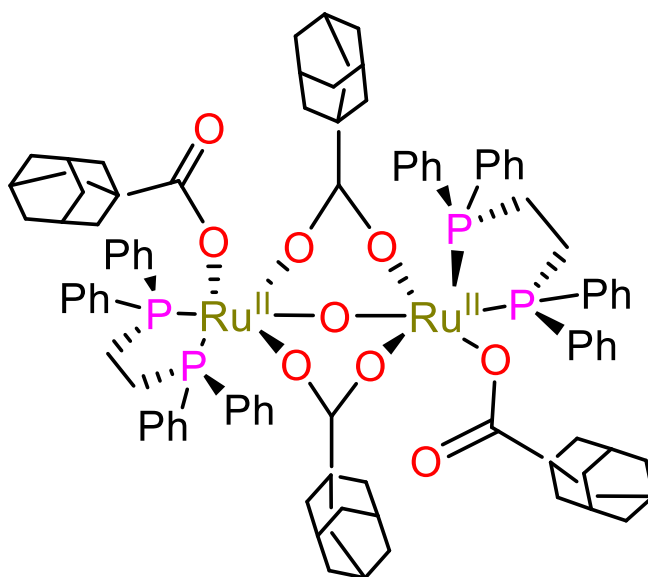


Figure S17. $^{13}\text{C}\{^1\text{H}\}$ NMR of B_p' [$\{(\text{dppe})\text{Ru}^{\text{II}}(\eta^1\text{-O}_2\text{CC}^t\text{Bu})_2\}(\mu\text{-O}_2\text{CC}^t\text{Bu})_2(\mu\text{-H}_2\text{O})$] dissolved in $(\text{CD}_3)_2\text{CO}$.

2.5.4 **B_{ad}'** [$\{(\text{dppe})\text{Ru}^{\text{II}}(\eta^1\text{-O}_2\text{CC}(\text{CH}_2)_6(\text{CH}_3))\}_2(\mu\text{-O}_2\text{CC}(\text{CH}_2)_6(\text{CH}_3))_2(\mu\text{-H}_2\text{O})$]



A Schlenk flask was charged with adamantane carboxylic acid (0.25 g, 1.4 mmol) and $[\text{Ru}^{\text{II}}(\eta^3\text{-CH}_2\text{C}(\text{Me})\text{CH}_2)_2(\text{dppe})]$ (60 mg, 0.1 mmol) which were dissolved in anhydrous acetone (10 mL). After 0.5 h the solvent was evaporated for 2 hours (40 °C). The remaining solid was dissolved in a supersaturated solution with anhydrous toluene and slow diffusion of *n*-hexane were set up for yellow sharp crystal formation in the glovebox. The crystals were collected and washed with cold hexane before being concentrated. The residue was in CDCl_3 for analysis.

^1H NMR (500 MHz, $(\text{CD}_3)_2\text{CO}$, 298 K) δ (ppm) = 7.50 (br, 8H, Ph), 7.31 (m, 12H, Ph), 2.63 (br, 4H, $\text{CH}_2\text{-CH}_2$), 1.73 (br, 6H, $(\text{CH})_6$), 1.51(d, $J_{\text{H-H}} = 11.93$ Hz, 6H, $(\text{CH}_2)_3$), 1.41 (d, $J_{\text{H-H}} = 11.93$ Hz, 6H, $(\text{CH}_2)_3$), 1.23 (s, 12H, $(\text{CH}_2)_6$)

$^{31}\text{P}\{^1\text{H}\}$ NMR (202 MHz, $(\text{CD}_3)_2\text{CO}$, 298 K) δ (ppm) = 90.4 (s)

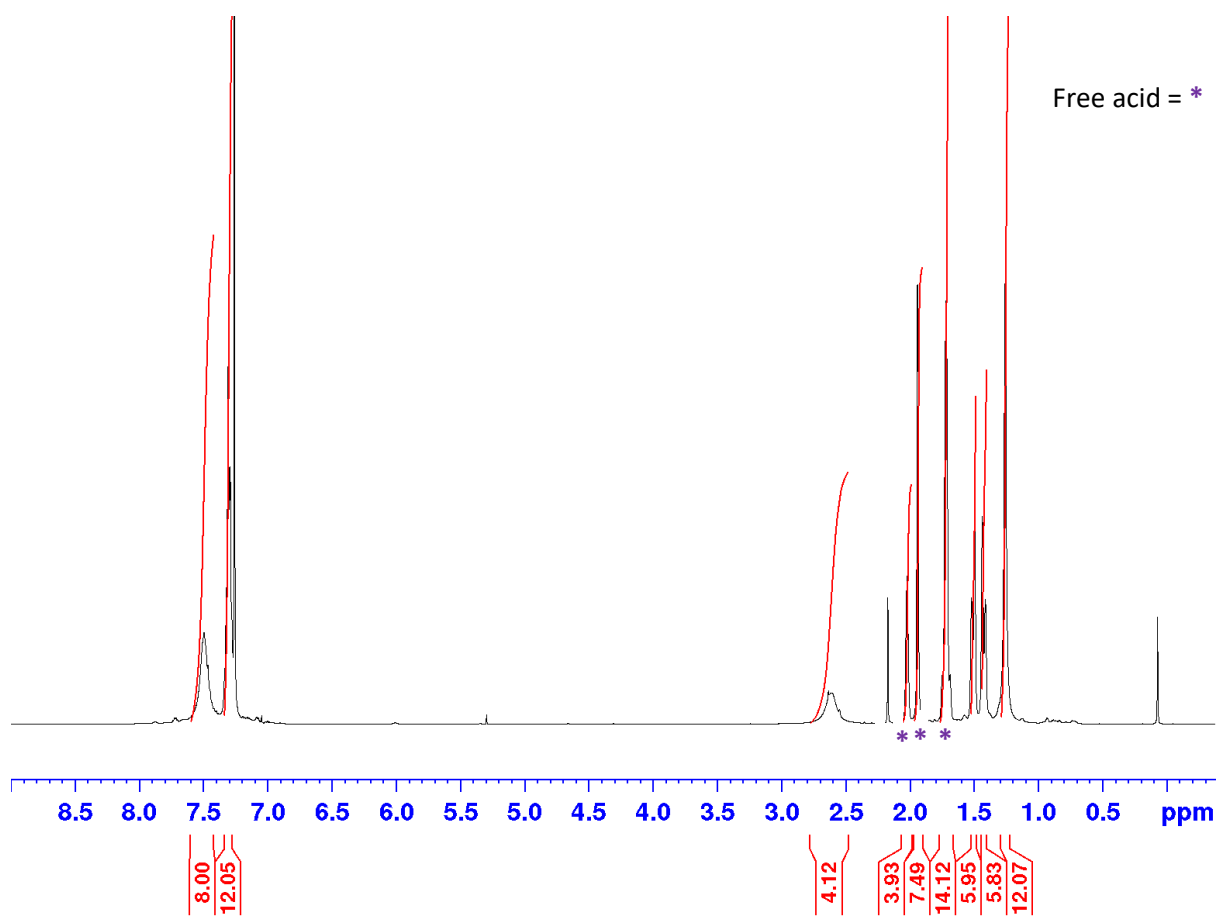


Figure S18. ^1H NMR of $\text{B}_{ad'}$ [$\{(\text{dppe})\text{Ru}^{\text{II}}(\eta^1\text{-O}_2\text{CC}(\text{CH}_2)_6(\text{CH}_3)_2)\}_2(\mu\text{-O}_2\text{CC}(\text{CH}_2)_6(\text{CH}_3)_2(\mu\text{-H}_2\text{O}))$] in CDCl_3 .

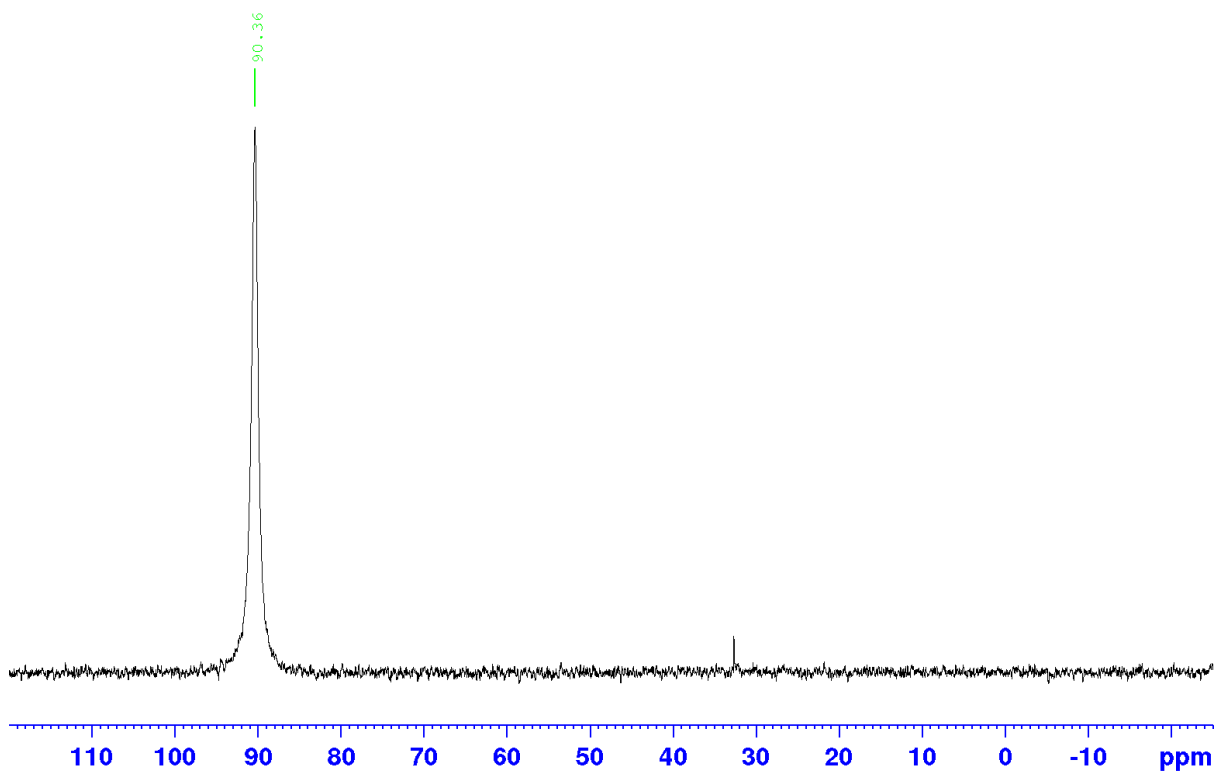
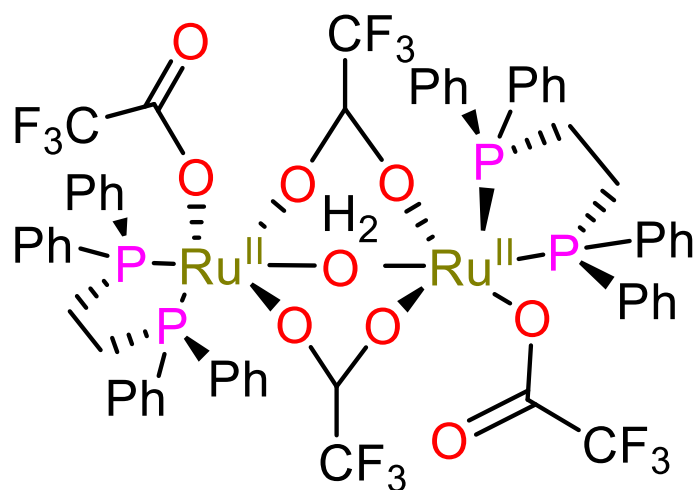


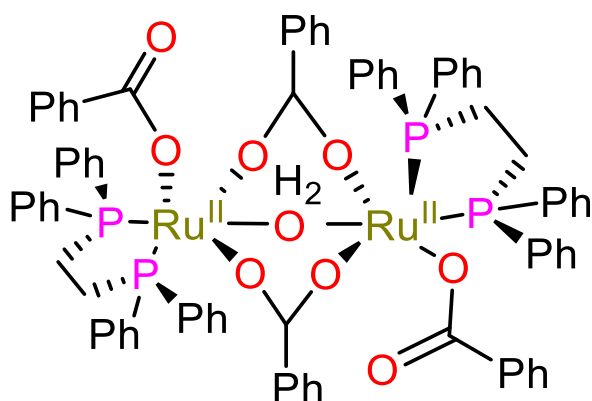
Figure S19. $^{31}\text{P}\{^1\text{H}\}$ NMR of $\text{B}_{ad'}$ [$\{(\text{dppe})\text{Ru}^{\text{II}}(\eta^1\text{-O}_2\text{CC}(\text{CH}_2)_6(\text{CH}_3)_2)\}_2(\mu\text{-O}_2\text{CC}(\text{CH}_2)_6(\text{CH}_3)_2(\mu\text{-H}_2\text{O}))$] dissolved in CDCl_3 .

2.5.5 **B_{tr}'** [{(dppe)Ru^{II}(η¹-O₂CCF₃)₂(μ-O₂CCF₃)₂(μ-OH₂)}]



A Schlenk flask was charged with trifluoroacetic acid (0.55 mL, 0.5 mmol) and [Ru^{II}(η³-CH₂C(Me)CH₂)₂(dppe)] (30 mg, 0.05 mmol) which were dissolved in anhydrous acetone (10 mL). After 0.5 h the solvent was evaporated for 2 hours (40 °C). The remaining solid was dissolved in a supersaturated solution with anhydrous acetone and slow diffusion of *n*-hexane were set up for yellow sharp crystal formation in the glovebox.

2.5.6 **B₆'** [$\{(\text{dppe})\text{Ru}^{\text{II}}(\eta^1\text{-O}_2\text{CPh})_2(\mu\text{-O}_2\text{CPh})_2(\mu\text{-H}_2\text{O})\}$]



A Schlenk flask was charged with benzoic acid (0.25 g, 2.1 mmol) and $[\text{Ru}^{\text{II}}(\eta^3\text{-CH}_2\text{C}(\text{Me})\text{CH}_2)_2(\text{dppe})]$ (60 mg, 0.1 mmol) which were dissolved in anhydrous acetone (10 mL). After 0.5 h the solvent was evaporated for 2 hours (40 °C). The remaining solid was dissolved to make a supersaturated solution with anhydrous acetone and set up for slow diffusion with *n*-hexane in the glovebox. This resulted in the formation of yellow crystals.

^1H NMR (500 MHz, $(\text{CD}_3)_2\text{CO}$), δ (ppm) = 8.07 (d, $J_{\text{HH}} = 8.0$ Hz 1H, Ph), 7.61 (d, $J_{\text{HH}} = 7.4$ Hz, 3H, Ph), 7.52 (t, $J_{\text{HH}} = 7.4$ Hz and 15.2 Hz, 1H, Ph), 7.4 (t, $J_{\text{HH}} = 7.4$ Hz and 14.9 Hz, 2H, Ph), 7.26 (m, 3H, Ph), 7.64 (br, 8H, Ph), 7.27 (m, 12H, Ph), 2.74 (m, 4H, CH_2CH_2)

$^{31}\text{P}\{^1\text{H}\}$ NMR (202 MHz, $(\text{CD}_3)_2\text{CO}$), δ (ppm) = 89.9 (s), 78.2 (s)

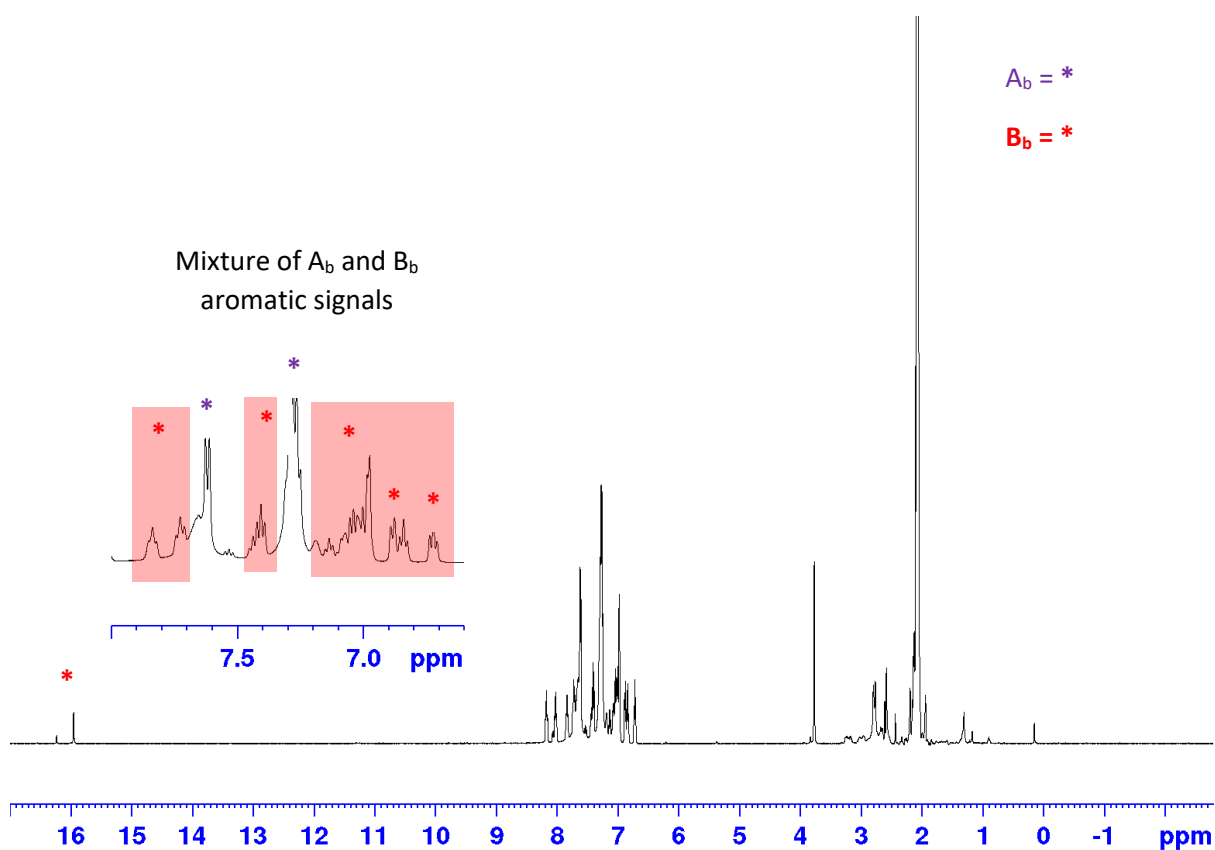


Figure S20. ^1H NMR of B_b' [$\{(dppe)Ru^{II}(\eta^1-O_2CPh)_2(\mu-O_2CPh)_2(\mu-H_2O)\}$] dissolved in $(CD_3)_2CO$ showing a mixture of A_b and B_b shifts.

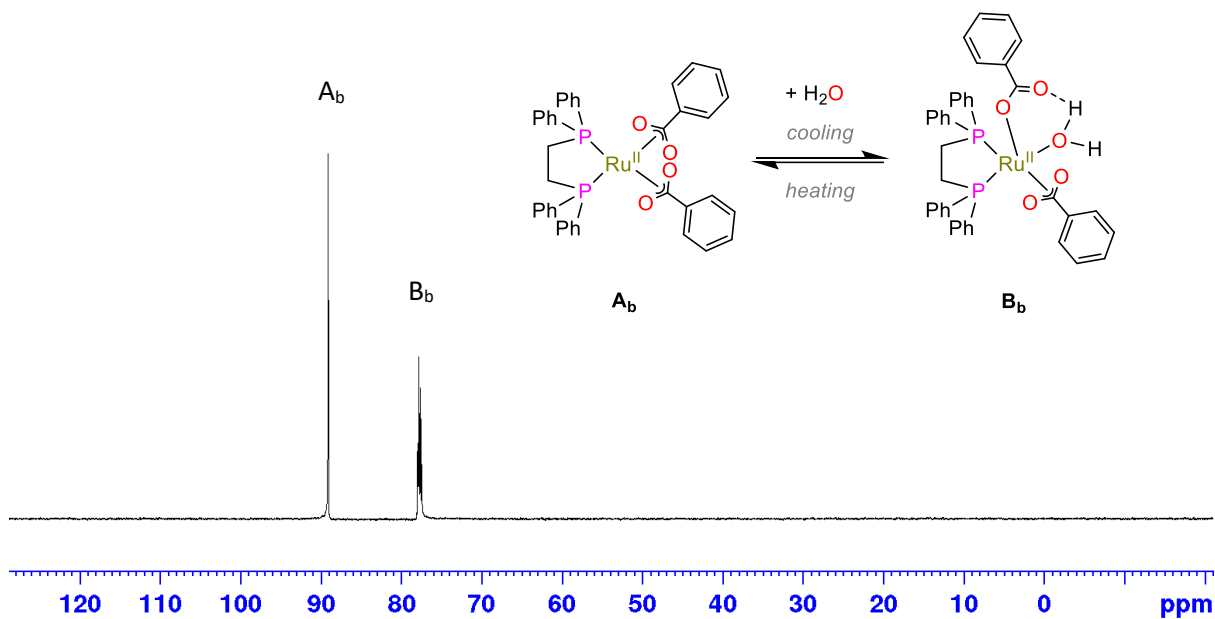


Figure S21. $^{31}\text{P}\{^1\text{H}\}$ NMR of B_b' [$\{(dppe)Ru^{II}(\eta^1-O_2CPh)_2(\mu-O_2CPh)_2(\mu-H_2O)\}$] dissolved in $(CD_3)_2CO$.

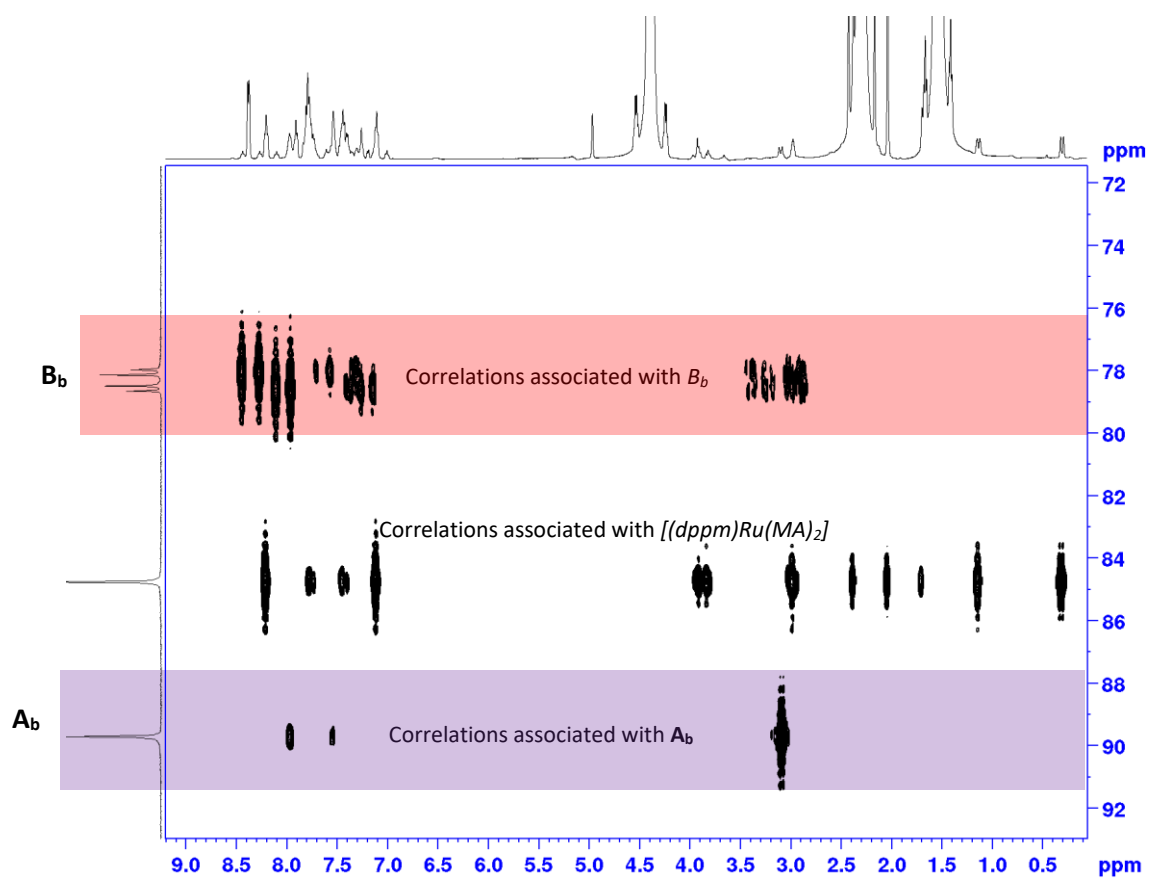


Figure S22. ^1H - ^{31}P HMBC NMR of a mixture of $[\text{Ru}^{\text{II}}(\eta^3\text{-CH}_2\text{C}(\text{Me})\text{CH}_2)_2(\text{dppe})]$ A_b and B_b in EtOAc

2.5.7 A_b [(dppe)Ru^{II}(η¹-O₂CPh)₂]

The formation of B_b was found to form due to the presence of moisture in the system. Here an experiment was performed with all reagents prepared as anhydrously as possible to yield only A_b. A Schlenk flask was charged with anhydrous benzoic acid (20 mg, 0.16 mmol) and [Ru^{II}(η³-CH₂C(Me)CH₂)₂(dppe)] (30 mg, 0.05 mmol) which were dissolved in anhydrous (CD₃)₂CO (1 mL).

¹H NMR (500 MHz, (CD₃)₂CO), δ (ppm) = 7.64 (br, 8H, Ph), 7.61 (d, J_{HH} = 7.4 Hz, 4H, Ph), 7.38 (t, J_{HH} = 7.4 Hz, 2H, Ph), 7.27 (m, 12H, Ph), 7.24 (m, 4H, Ph), 2.76 (m, 4H, J_{HH} = 14.3 Hz, CH₂CH₂)

³¹P{¹H} NMR (202 MHz, (CD₃)₂CO), δ (ppm) = 89.9 (s)

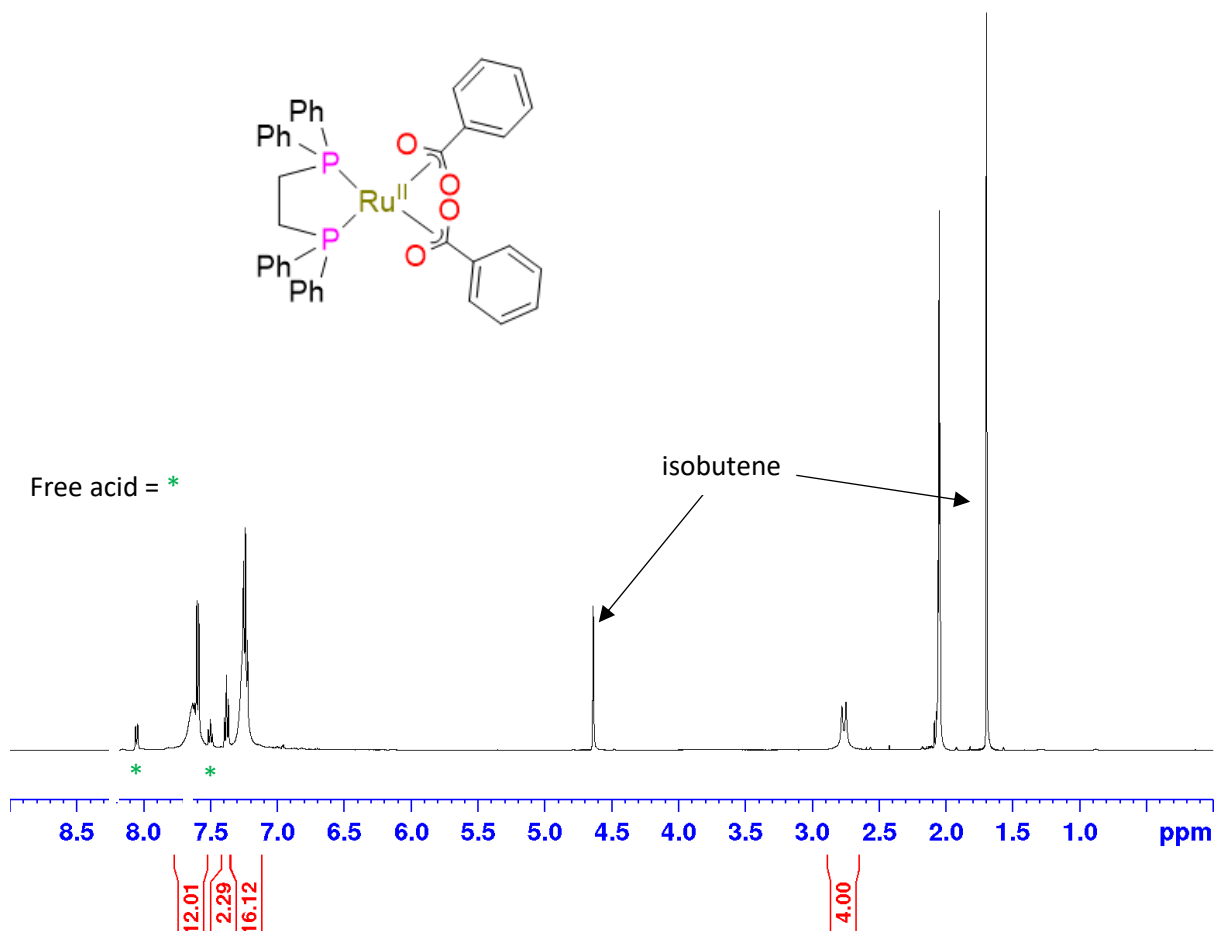


Figure S23. 1H NMR of A_b [(dppe)Ru^{II}(η¹-O₂CPh)₂] in (CD₃)₂CO without the presence of moisture and the formation of isobutene in (CD₃)₂CO.

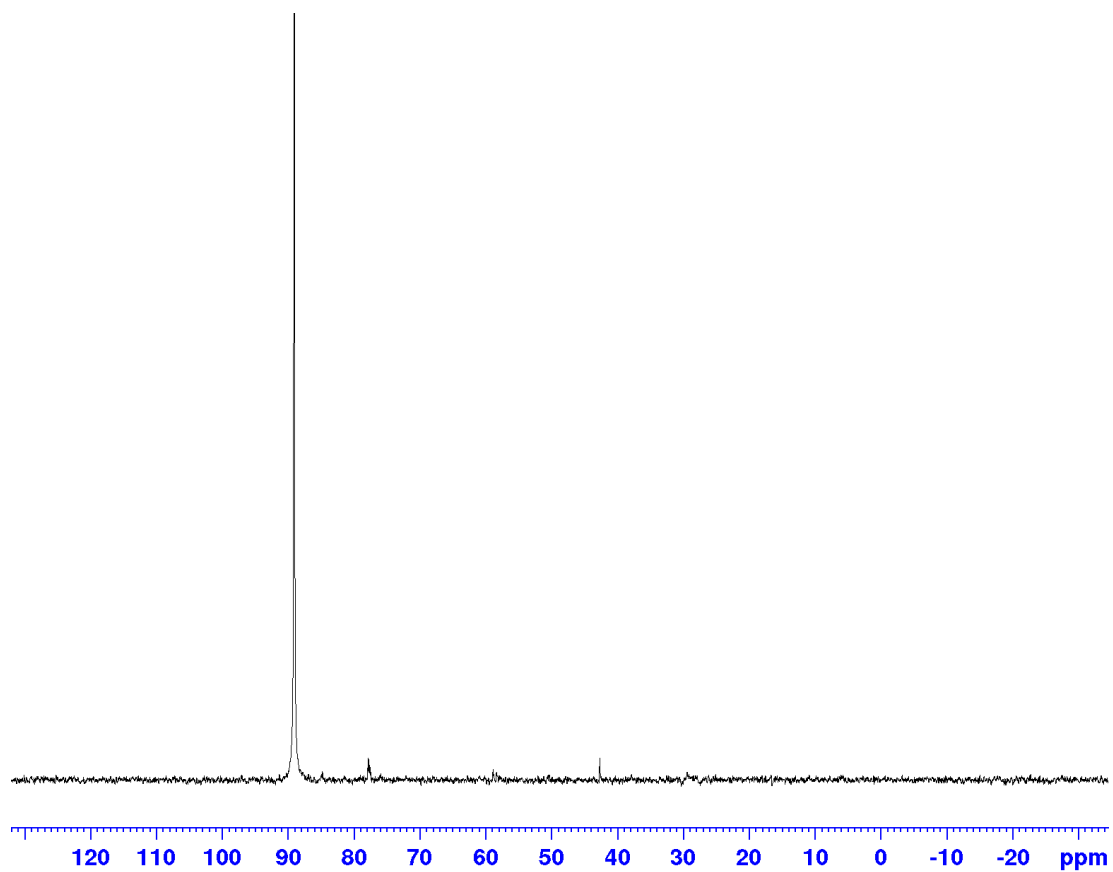
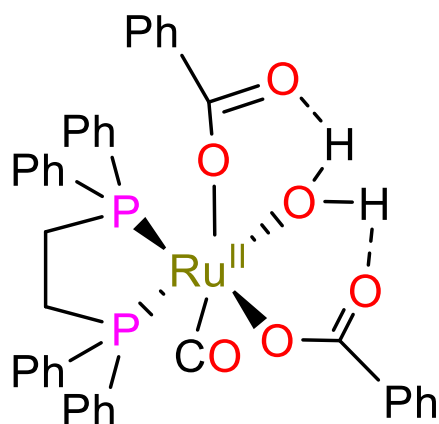


Figure S24. $^{31}\text{P}\{^1\text{H}\}$ NMR of \mathbf{A}_b [$(\text{dppe})\text{Ru}^{\text{II}}(\eta^1\text{-O}_2\text{CPh})_2$] in $(\text{CD}_3)_2\text{CO}$.

2.5.8 $X^2_b \cdot H_2O$ [(dppe)Ru^{II}(η^1-O_2CPh)₂(CO)(H₂O)]



A Schlenk flask was charged with benzoic acid (1.81 g, 15 mmol), ethynyl- β -ionol (2.18 g, 10 mmol), tri-*o*-tolyl phosphate (461 mg, 1.25 mmol) (internal standard) and anhydrous acetone (10 mL). In a second flask, [Ru^{II}($\eta^3-CH_2C(Me)CH_2$)₂(dppe)] (61 mg, 0.1 mmol, 1 mol%) was dissolved in anhydrous acetone (5 mL) and syringed into the first Schlenk flask to trigger the reaction. After reaction completion a ³¹P{¹H} NMR was recorded (Figure S25) and the sample was then concentrated and layered with *n*-hexane (20 mL). Yellow crystals were observed at the bottom of the vial.

³¹P{¹H} NMR (202 MHz, (CH₃)₂CO), δ (ppm) = 53.3

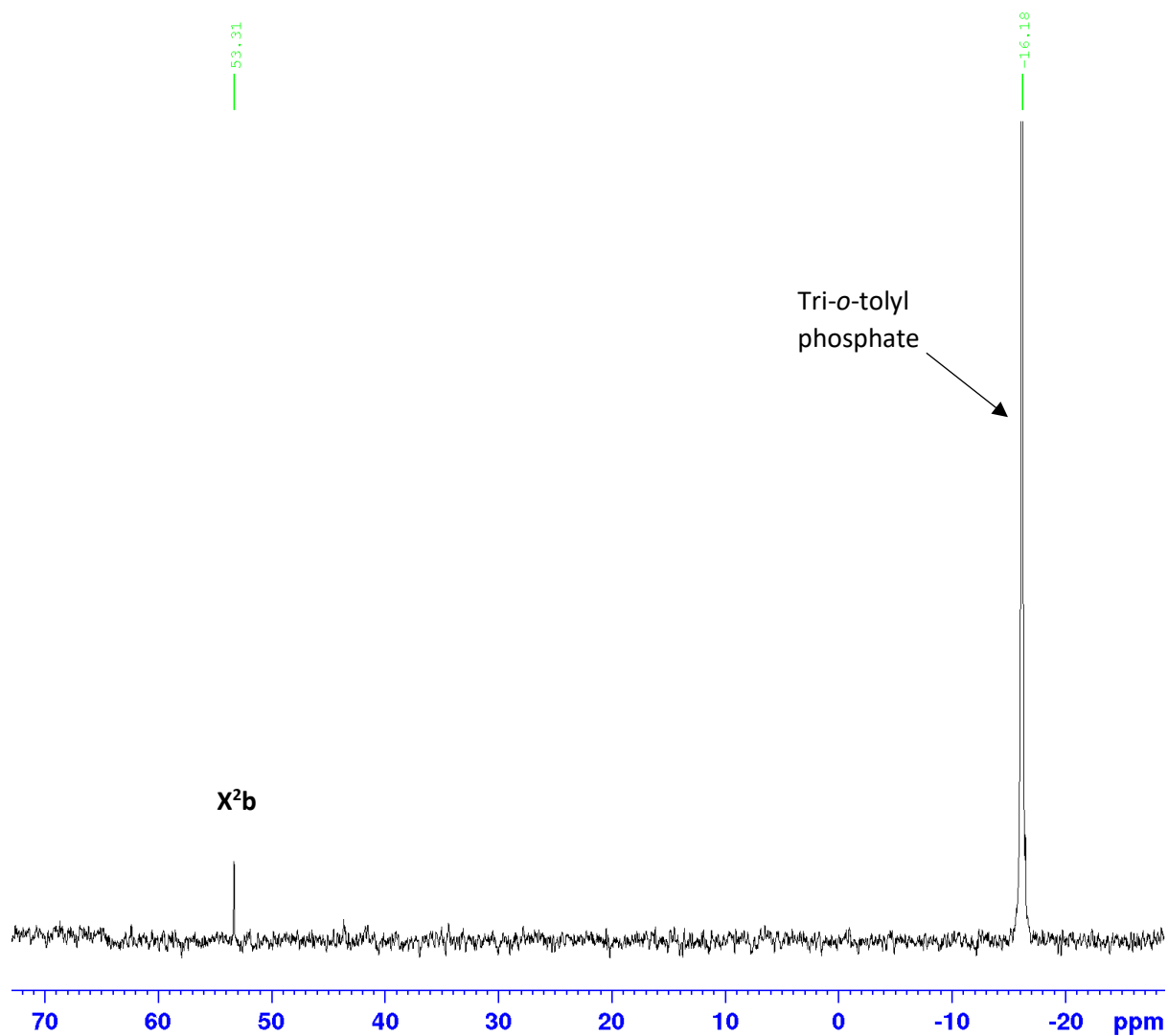
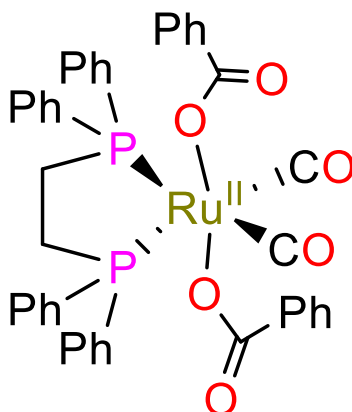


Figure S25. $^{31}\text{P}\{^1\text{H}\}$ NMR of X^2b , obtained after the reaction of ethynyl- β -ionol (0.66 M) with benzoic acid (1 M) catalysed by $[\text{Ru}^{\text{II}}(\eta^3\text{-CH}_2\text{C}(\text{Me})\text{CH}_2)_2(\text{dppe})]$ (0.5 mol%) in acetone.

2.5.9 X²_b [(dppe)Ru^{II}(η¹-O₂CPh)₂(CO)₂]



A Schlenk flask was charged with benzoic acid (1.81 g, 15 mmol), [Ru^{II}(η³-CH₂C(Me)CH₂)₂(dppe)] (61 mg, 0.1 mmol), and anhydrous acetone (10 mL) under inert conditions and stirred for 3 hours producing a 50:50 mixture of [(dppe)Ru^{II}(η²-OOCPh)₂] and [(dppe)Ru^{II}(η²-OOCPh)(η¹-OOCPh)(H₂O)] in solution. CO was bubbled in the reaction flask *via* PEEK tubing for 10 seconds. The flask was left overnight, and the solution slowly changed from yellow to white with some precipitate visible. The solution was concentrated under vacuum and washed with cold hexane (2 x ~5 mL). The white crystals were redissolved in acetone and layered with *n*-hexane (20 mL). White crystals were observed at the bottom of the vial. The crystals were separated and redissolved in CDCl₃ for characterisation.

¹H NMR (500 MHz, (CDCl₃), δ (ppm) = 7.5 (m, 8H, Ph), 7.2 (m, 4H, Ph), 7.2 (m, 6H, Ph_{acid}), 7.14 (m, 8H, Ph), 7.04 (m, 4H, Ph_{acid}), 3.03 (d, *J*_{PH} = 17.8 Hz, 4H)

³¹P{¹H} NMR (202 MHz, CDCl₃), δ (ppm) = 52.0 (s)

³¹P{¹H} NMR (202 MHz, (CD₃)₂CO), δ (ppm) = 53.7 (s)

¹³C{¹H} NMR (125 MHz, (CD₃)₂CO, 298 K) δ (ppm) = 195.7 (dd, *J*_{CH} = 106.7 Hz, 18.9 Hz, C=O), 172.2 (s, COO), 134.1 (s, Ph_{acid}), 132.4 (t, *J*_{CH} = 5.4 Hz, Ph), 130.8 (s, Ph_{acid}), 129.9 (s, Ph), 129.3 (s, Ph), 129.0 (t, *J*_{CH} = 5.4 Hz, Ph), 128.5 (s, Ph_{acid}), 127.0 (s, Ph_{acid}), 25.8 (dd, *J*_{CH} = 22.3 Hz, 20.0 Hz, (CH₂)₂)

T-IR (cm⁻¹): 3061 (w) ν_{CH-benzoic}, 2043 (s) ν_{C=O}, 1996 (s) ν_{C=O}, 1611 (s) ν_{CO-benzoic}, 1433 (w) ν_{Ph(P-Ph)}, 1333 (s) ν_{C-O-benzoic (coordinated)}, 1102 (w) δ_(C-CH in the plane), 742 (m) δ_(C-C out of the plane), 688 (s) δ_(C-C in the plane), 521 (s) ν_{Ru-P}

Ru-P

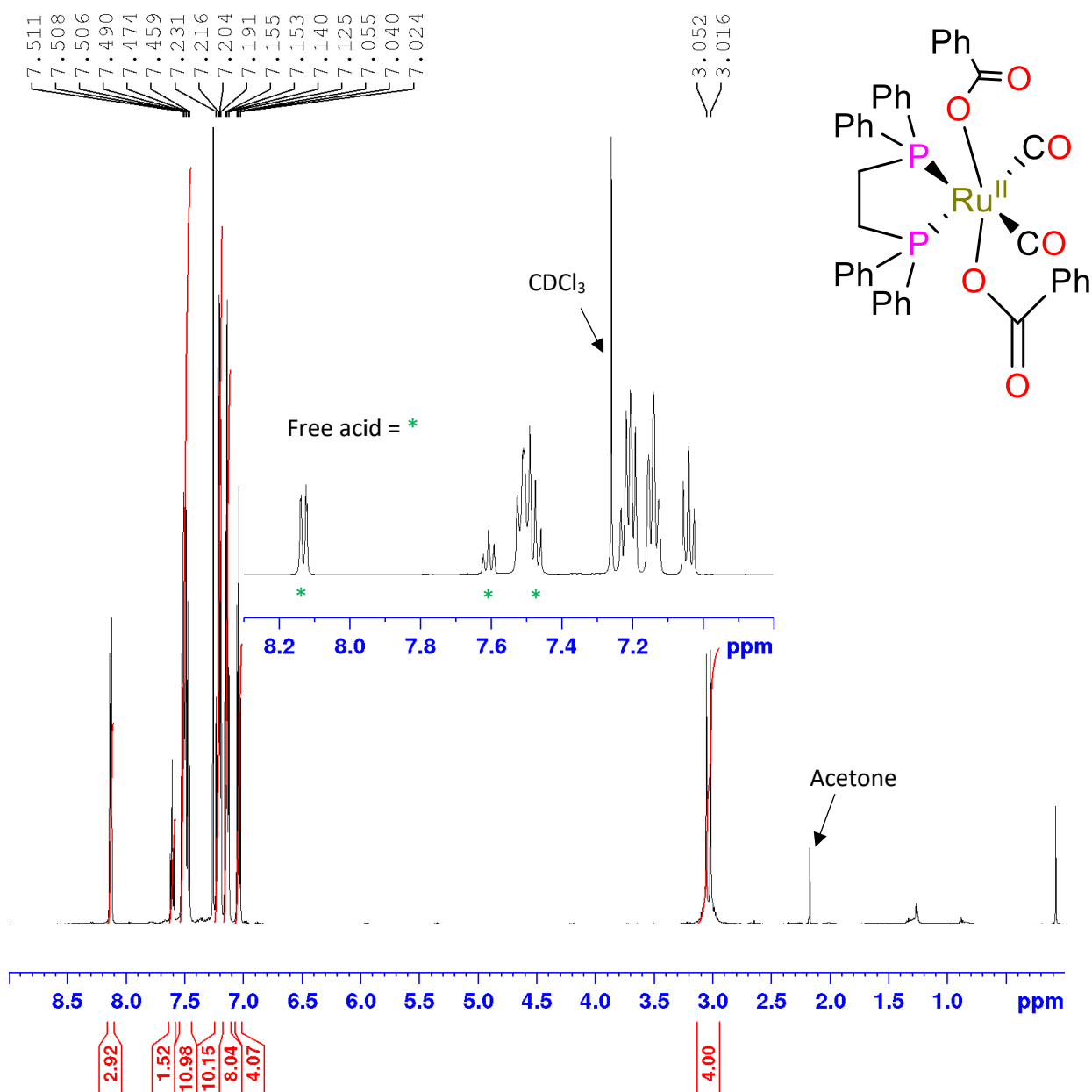


Figure S26. 1H NMR spectrum of the isolated $[(dppe)Ru^{II}(CO)_2(\eta^1-O_2CPh)_2]$ (X^2b) in $CDCl_3$.

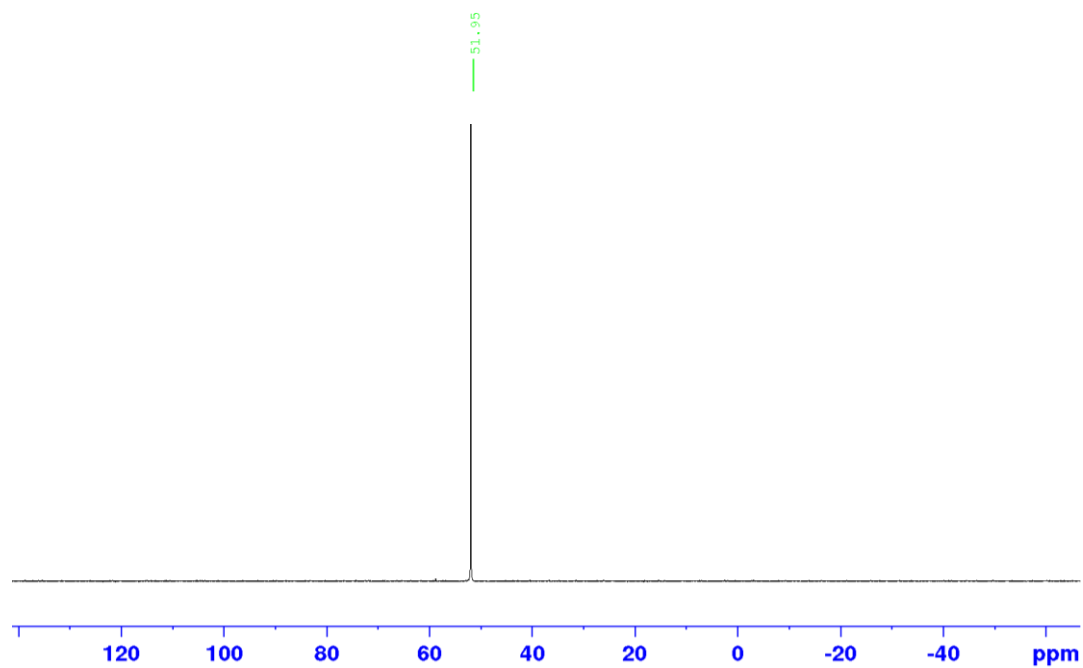


Figure S27. $^{31}\text{P}\{^1\text{H}\}$ NMR spectrum of the isolated $[(\text{dppe})\text{Ru}^{\text{II}}(\text{CO})_2(\eta^1\text{-O}_2\text{CPh})_2]$ ($\mathbf{X}^2\mathbf{b}$) in CDCl_3

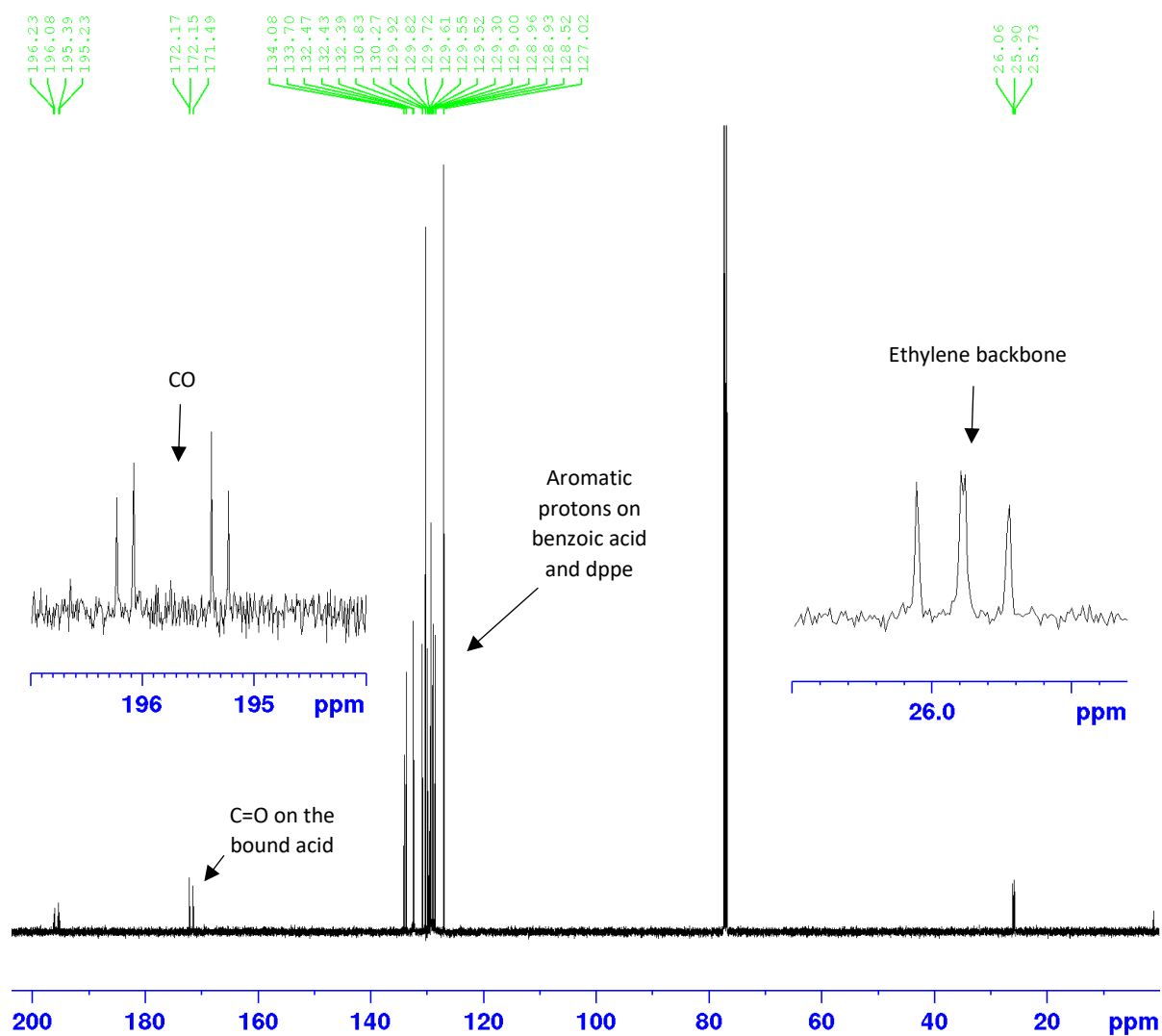


Figure S28. $^{13}\text{C}\{^1\text{H}\}$ NMR of $[(\text{dppe})\text{Ru}^{\text{II}}(\text{CO})_2(\eta^1\text{-O}_2\text{CPh})_2]$ in CDCl_3 .

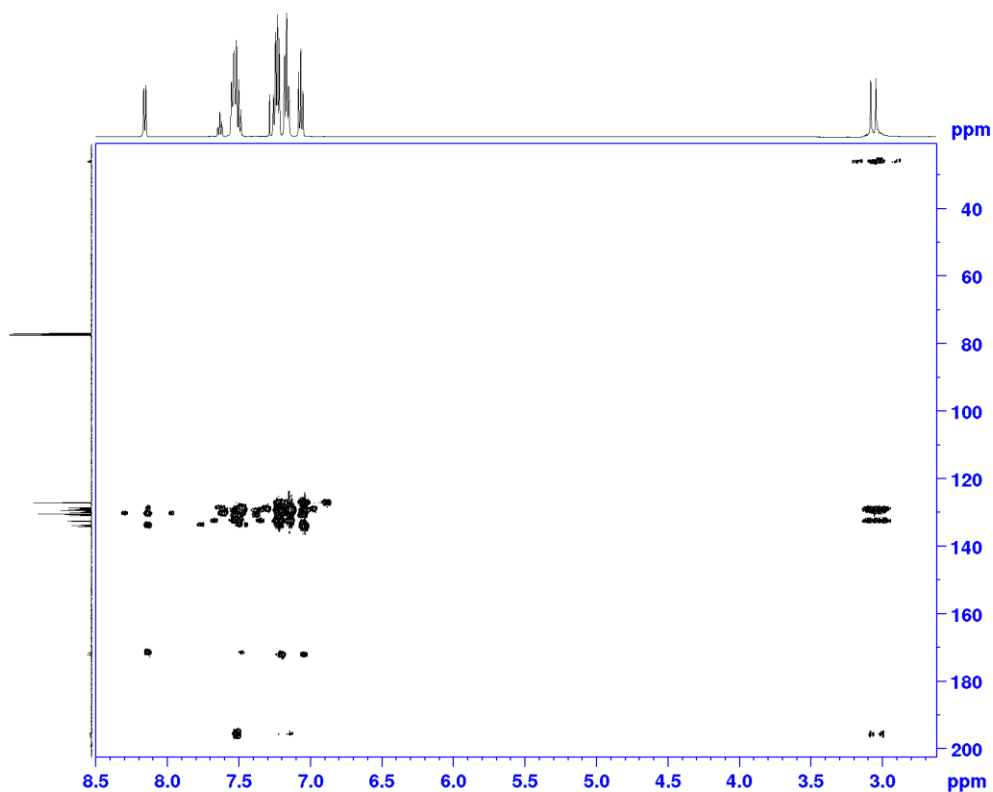


Figure S29. ^1H - ^{13}C HMBC NMR of $[(\text{dppe})\text{Ru}^{\text{II}}(\text{CO})_2(\eta^1\text{-O}_2\text{CPh})_2]$ in CDCl_3 .

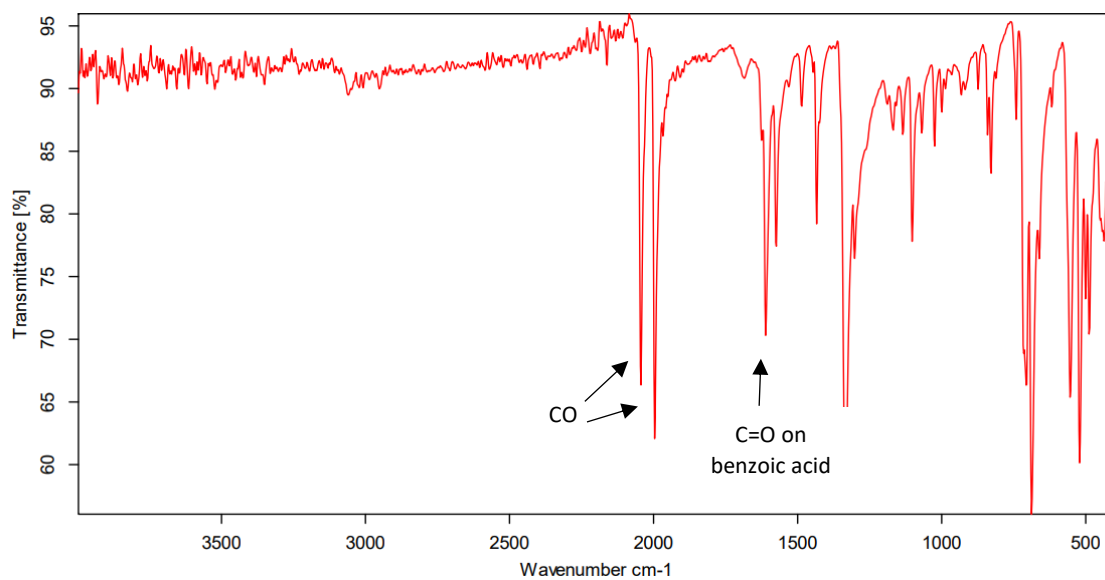


Figure S30. FTIR ATR dry spectrum of the isolated $[(\text{dppe})\text{Ru}^{\text{II}}(\text{CO})_2(\eta^1\text{-O}_2\text{CPh})_2]$, recorded under Ar atmosphere.

The IR spectrum of $[(\text{dppe})\text{Ru}^{\text{II}}(\text{CO})_2(\eta^1\text{-O}_2\text{CPh})_2]$ shows two distinct shifts at 2043 cm^{-1} and 1996 cm^{-1} corresponding to the terminal carbonyl stretching modes of the Z-carbonyl structure.^{3,4}

2.6 Standard procedure for the ruthenium-mediated transformation of ethynyl- β -ionol into the α,β -unsaturated ester adduct

A Schlenk flask was charged with pivalic acid (1.32 g, 11 mmol), pivalic anhydride (0.4 mL, 2 mmol), ethynyl- β -ionol (2.18 g, 10 mmol), 1,3,5-trimethoxybenzene (420 mg, 2.5 mmol) and anhydrous acetone (10 mL). In a second flask, $[\text{Ru}^{\text{II}}(\eta^3\text{-CH}_2\text{C}(\text{Me})\text{CH}_2)_2(\text{dppe})]$ (61 mg, 0.1 mmol, 1 mol%) was dissolved in anhydrous acetone (5 mL) and syringed into the first Schlenk flask to start the reaction. The reaction was periodically monitored with quantitative ^1H NMR and $^{31}\text{P}\{^1\text{H}\}$ NMR spectroscopy by integration relative to the internal standard 1,3,5-trimethoxybenzene.

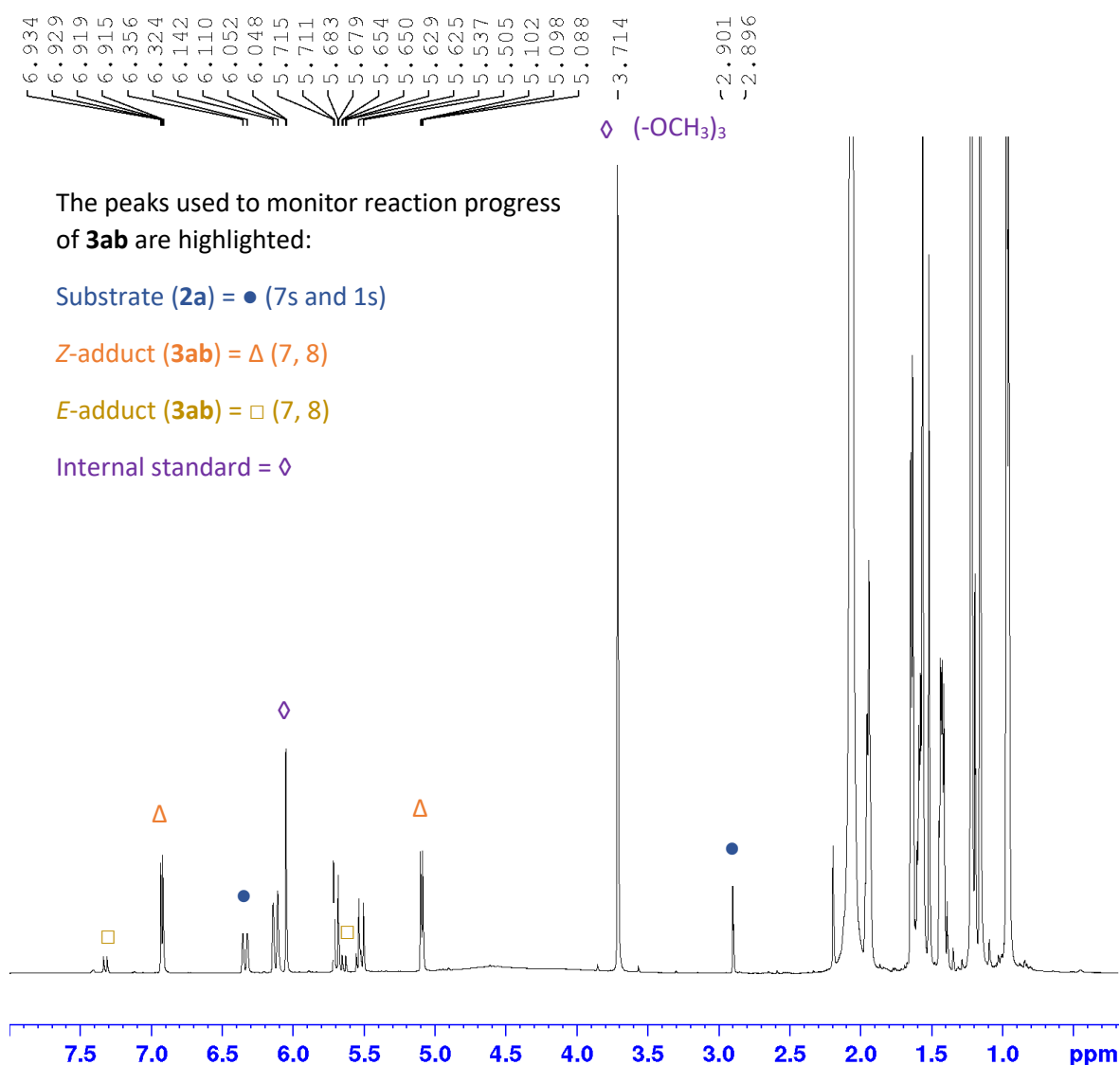


Figure S31. Exemplary ^1H NMR spectrum recorded during a Ru-mediated transformation of ethynyl- β -ionol (0.66 M) with pivalic acid (0.73 M) and pivalic anhydride (0.13 M) catalysed by $[(\text{dppe})\text{Ru}(\text{MA})_2]$ in anhydrous acetone (15 mL) at 20 °C. Product yields obtained from quantitative ex-situ ^1H NMR spectroscopy against trimethoxybenzene (167 mM) as internal standard. Spectrum taken after 12 hours of reaction initiation, intentionally showing both substrate and product peaks.

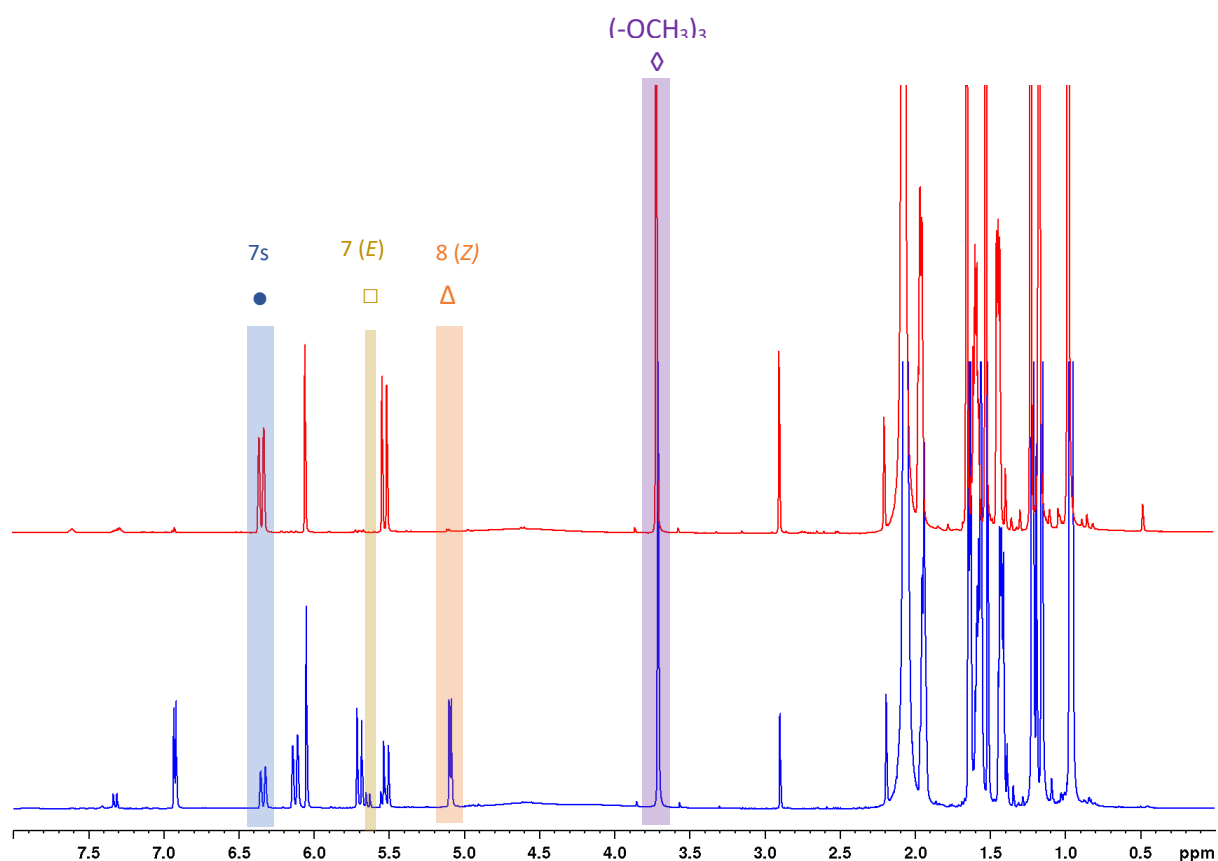


Figure S32. ^1H NMR spectra showing the Ru-mediated transformation of ethynyl- β -ionol (0.66 M) with pivalic acid (0.73 M) and pivalic anhydride (0.13 M) into **3ab** catalysed by $[(\text{dppe})\text{Ru}(\text{MA})_2]$ in anhydrous acetone (15 mL) at 20 °C from quantitative ^1H FlowNMR monitoring, at 4 mL/min, at two different time points, red: start of the reaction (5 minutes), blue: after 12 hours. The purpose is to clearly provide an example to visually illustrate the best peaks to use for quantification of all FlowNMR data.

Table S1. T_1 times for all peaks of interest in the catalytic transformation of ethynyl- β -ionol (0.66 M) with pivalic acid (0.73 M) and pivalic anhydride (0.13 M) into **3ab** catalysed by $[(\text{dppe})\text{Ru}(\text{MA})_2]$ in anhydrous acetone, determined via inversion recovery NMR experiment.

Compound	Peak name	F2 (ppm)	T_1 (s)
Ethynyl- β -ionol	H-7	6.39	3.7(3)
Ethynyl- β -ionol	H-1	2.84	8.9(9)
3ab	H-7	6.95	4.6(3)
3ab	H-8	5.19	4.2(4)
Internal standard	TMB (aliphatic)	3.75	2.4(1)
Internal Standard	TMB (aromatic)	6.03	6.5(10)

2.7 FlowNMR Apparatus

The FlowNMR apparatus (Figure S33) consisted of 3 main components: the reaction vessel (highlighted in red by heat exchanger 3), the flow path (highlighted in yellow by heat exchanger 1) and the flow tube (highlighted in blue by heat exchanger 2). The flow path was composed of PEEK tubing (PEEK, OD 1/16", ID 0.76 mm, Upchurch Scientific) which connected the reaction vessel to the UV-Visible flow cell (PEEK SMA-Z, Ocean Optics) and InsightMR flow tube (Bruker). The InsightMR flow tube consisted of PEEK (OD 1/32", ID 0.51 mm, Upchurch Scientific) transfer lines housed within concentrically aligned Teflon tubing that connects to the flow tip (Figure S33). A Vapourtec SF-10 peristaltic pump was connected to the FlowNMR apparatus *via* PEEK tubing (O.D 1/16", I.D 0.76 mm, Upchurch Scientific). Connections to reaction vessels were secured *via* rubber septa, HPLC-type (1/16") or Swagelok (1/16") fittings. Thermal regulation of the flow path and flow tube was maintained by 2 heat exchangers (Julabo CORIO CD-300F, thermofluid 50:50 ethylene glycol/water). Thermal regulation of the reaction vessel was controlled by either a heat exchanger (Julabo CORIO CD-300F, thermofluid 50:50 ethylene glycol/water) connected to a reactor jacket (DrySyn Snowstorm ONE) or a hotplate (IKA RCT B S002) with a reactor jacket (paraffin oil bath).

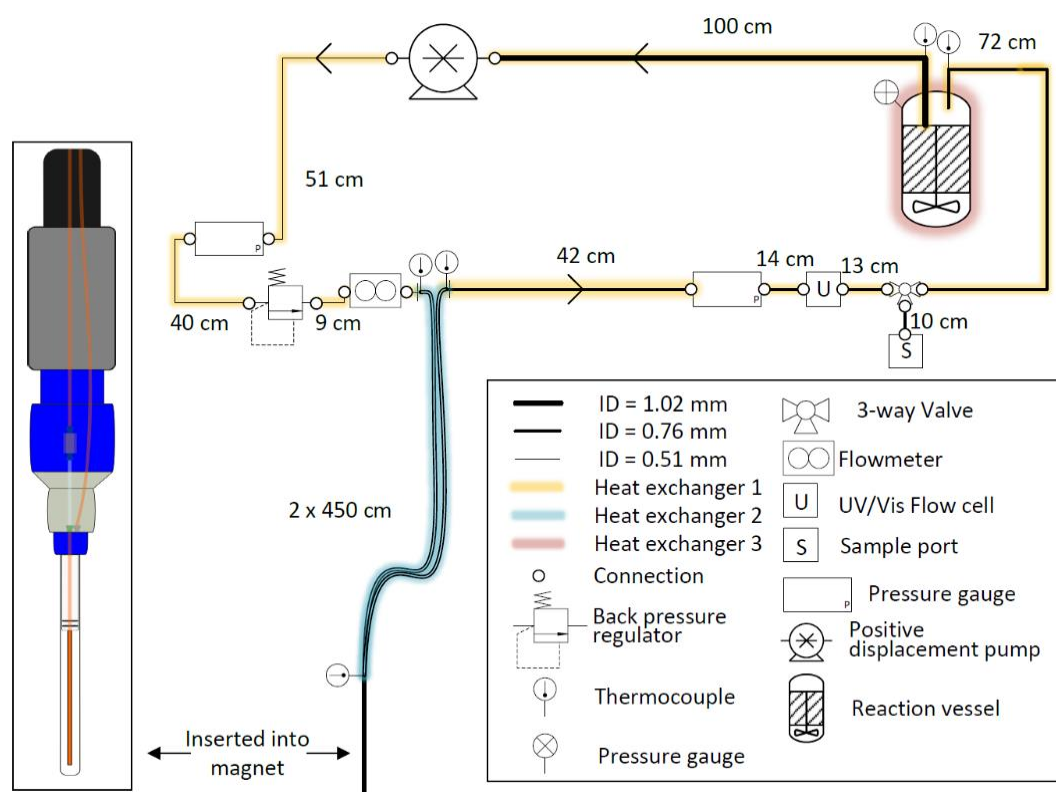


Figure S33. Piping and instrumentation schematic of the closed-loop recirculating FlowNMR setup, with exemplary length scales, tubing ID (indicated by the line thickness), and showing sequential temperature control by use of independent heat exchangers (colour coded for clarity).

2.7.1 Data acquisition

For all FlowNMR reactions, non-deuterated solvents were used, and the frequency lock was switched off. Automated shimming and tuning were performed whilst the flow was turned off. Accurate quantification of spectra acquired during flow is complicated by flow effects which effect the observed relaxation times and the equilibrium magnetisation of the sample. To account for these flow effects, a correction factor was needed for each peak of interest in the spectra that were quantified, as has been described previously.⁵ Briefly, spectra of starting materials, products, internal standards and (where possible) intermediates were recorded under static conditions (0 mL min⁻¹) with a long relaxation delay (60 seconds) to ensure they were fully quantitative. A spectrum was also recorded with flowrate of the reaction (4 mL min⁻¹) to calculate the comparison of the integral area of peaks. For each peak of interest, a correction factor (CF) could be calculated (Equation 1; *I* = peak integral), which could then be applied to subsequent spectra acquired under flowing conditions (Equation 2).

$$\text{Equation 1: } CF = \frac{I_{Static}}{I_{Flow}}$$

$$\text{Equation 2: } I_{Corrected} = CF \times I$$

Data acquisition was started using InsightMR software (Bruker) queuing up interleaved ¹H NMR and ³¹P{¹H} NMR experiments every 4 minutes with the following acquisition parameters:

¹H NMR (Number of scans (NS) = 8, Receiver gain (RG) = 4, Dummy scans (DS) = 0 s, Acquisition time (AQ) = 1.6 s, Relaxation delay (D₁) = 1 s)

³¹P{¹H} NMR (NS = 48, RG = 203, DS= 0 s, AQ = 0.4, D₁ = 0.5 s)

2.7.2 FlowNMR reaction setup

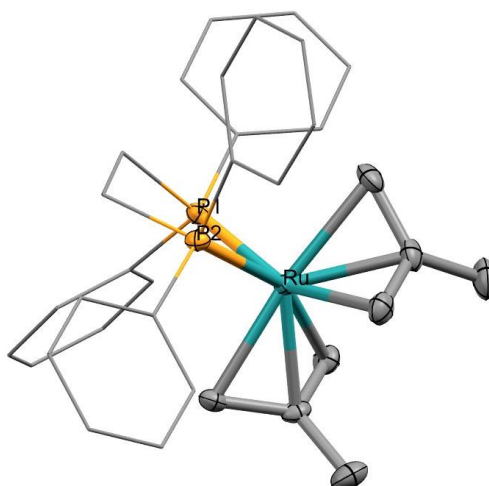
The FlowNMR apparatus was purged for 15 minutes with argon to remove traces of air and moisture. Anhydrous acetone (25 mL) was pumped through the flow apparatus, which was then further purged with argon for 15 minutes. In a typical reaction, a Schlenk flask charged with pivalic acid (1.13 g, 11 mmol), pivalic anhydride (0.4 mL, 2 mmol), ethynyl-β-ionol (2.18 g, 10 mmol), 1,3,5-trimethoxybenzene (420 mg, 2.5 mmol) and anhydrous acetone (10 mL) was connected to the system and the homogeneous mixture circulated around the flow apparatus. After the data acquisition had been started, [Ru^{II}(η³-CH₂C(Me)CH₂)₂(dppe)] (61 mg, 0.1 mmol, 1mol%) was dissolved in anhydrous acetone (5 mL) and syringed into the Schlenk flask containing all other reagents to initiate the reaction. Variations of catalytic runs consisting of different starting reagents were added in same amounts unless stated otherwise.

3.0 X-Ray Crystallography

Crystals were selected using the oil drop technique, in perfluoropolyether oil and mounted at 150(2) K with an Oxford Cryostream N₂ cooling device. Intensity data were collected on a Rigaku SuperNova Dual EosS2 single crystal diffractometer using monochromated Cu-K α radiation ($\lambda = 1.54184 \text{ \AA}$) or on a Rigaku Xcalibur, EosS2 single crystal diffractometer using graphite monochromated Mo-K α radiation ($\lambda = 0.71073 \text{ \AA}$). Unit cell determination, data collection, data reduction and absorption correction were performed using the CrysAlisPro software.⁶ The structures were solved with SHELXT⁷ and refined by a full-matrix least-squares procedure based on F² (SHELXL-2018-19).⁷ All non-hydrogen atoms were refined anisotropically. Hydrogen atoms were placed onto calculated positions and refined using a riding model.

Data analysis and graph display were carried out using the SHELXle⁸ and Mercury⁹ software packages.

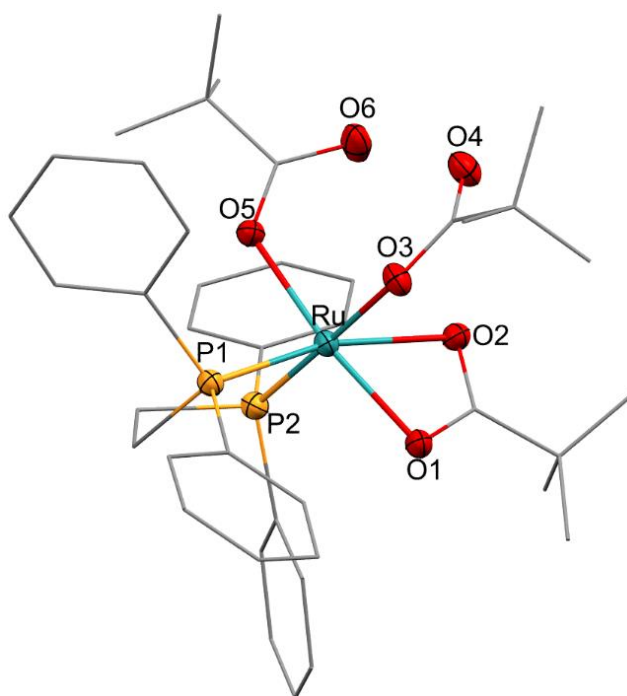
3.1 Crystal data for $[Ru^{II}(\eta^3\text{-CH}_2\text{C(Me)CH}_2)_2(\text{dppe})]$



CCDC	2296244
Identification code	e22uh2
Empirical formula	C ₃₄ H ₃₈ P ₂ Ru
Formula weight	609.65
Temperature	149.9(6) K
Wavelength	0.71073 \AA
Crystal system	Monoclinic
Space group	I2/a

Unit cell dimensions	a = 20.4141(3) Å	$\alpha = 90^\circ$
	b = 13.33648(14) Å	$\beta = 104.7984(12)^\circ$
	c = 22.5810(3) Å	$\gamma = 90^\circ$
Volume	5943.81(14) Å ³	
Z	8	
Density (calculated)	1.363 Mg/m ³	
Absorption coefficient	0.656 mm ⁻¹	
F(000)	2528	
Crystal size	0.761 x 0.643 x 0.397 mm ³	
Theta range for data collection	3.055 to 30.275°	
Index ranges	-28<=h<=28, -18<=k<=18, -31<=l<=31	
Reflections collected	85135	
Independent reflections	8371 [R(int) = 0.0266]	
Completeness to theta = 25.242°	99.8 %	
Absorption correction	Semi-empirical from equivalents	
Max. and min. transmission	1.00000 and 0.89179	
Refinement method	Full-matrix least-squares on F ²	
Data / restraints / parameters	8371 / 0 / 368	
Goodness-of-fit on F ²	1.101	
Final R indices [I>2sigma(I)]	R1 = 0.0210, wR2 = 0.0473	
R indices (all data)	R1 = 0.0266, wR2 = 0.0502	
Extinction coefficient	n/a	
Largest diff. peak and hole	0.382 and -0.450 e.Å ⁻³	

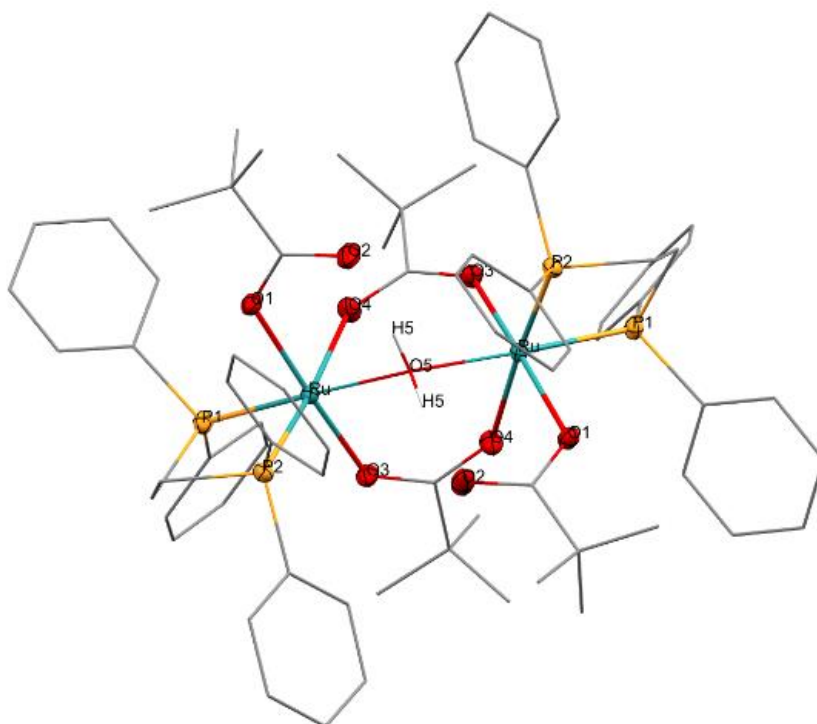
3.2 Crystal data for $A_p' [(dppe)Ru^{II}(\eta^2-O_2CC^tBu)(\eta^1-O_2CC^tBu)(^tBuCCO_2H)]$



CCDC:	2296250	
Identification code	e18uh6	
Empirical formula	C ₄₁ H ₅₂ O ₆ P ₂ Ru	
Formula weight	803.83	
Temperature	150.00(10) K	
Wavelength	0.71073 Å	
Crystal system	Monoclinic	
Space group	P2 ₁ /n	
Unit cell dimensions	a = 11.0204(3) Å	α = 90°
	b = 20.0420(5) Å	β = 97.977(3)°
	c = 18.3864(5) Å	γ = 90°
Volume	4021.72(19) Å ³	
Z	4	
Density (calculated)	1.328 Mg/m ³	
Absorption coefficient	0.513 mm ⁻¹	
F(000)	1680	
Crystal size	0.258 x 0.133 x 0.131 mm ³	

Theta range for data collection	3.248 to 26.400°.
Index ranges	-13<=h<=13, -24<=k<=25, -22<=l<=22
Reflections collected	65193
Independent reflections	8217 [R(int) = 0.0689]
Completeness to theta = 25.242°	99.8 %
Absorption correction	Semi-empirical from equivalents
Max. and min. transmission	1.00000 and 0.96294
Refinement method	Full-matrix least-squares on F ²
Data / restraints / parameters	8217 / 2 / 520
Goodness-of-fit on F ²	1.011
Final R indices [I>2sigma(I)]	R1 = 0.0351, wR2 = 0.0647
R indices (all data)	R1 = 0.0587, wR2 = 0.0715
Extinction coefficient	n/a
Largest diff. peak and hole	0.418 and -0.373 e.Å ⁻³

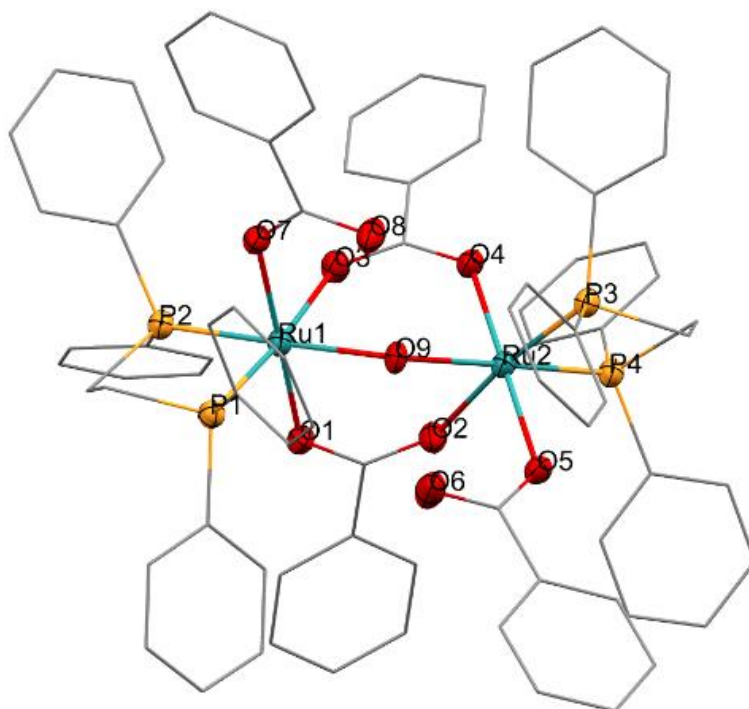
3.3 Crystal data for **B_p'** [$\{(dppe)Ru^{II}(\eta^1-O_2CC^tBu)\}_2(\mu-O_2CC^tBu)_2(\mu-H_2O)$]



CCDC:	2296242	
Identification code	s19uh4	
Empirical formula	C ₇₂ H ₈₆ O ₉ P ₄ Ru ₂	
Formula weight	1421.42	
Temperature	150.00(10) K	
Wavelength	1.54184 Å	
Crystal system	Monoclinic	
Space group	C2/c	
Unit cell dimensions	a = 13.34263(10) Å	α = 90°
	b = 22.71892(16) Å	β = 98.2700(6)°
	c = 22.67074(14) Å	γ = 90°
Volume	6800.72(8) Å ³	
Z	4	
Density (calculated)	1.388 Mg/m ³	
Absorption coefficient	4.928 mm ⁻¹	
F(000)	2952	
Crystal size	0.219 x 0.160 x 0.072 mm ³	

Theta range for data collection	3.872 to 73.134°.
Index ranges	-16<=h<=16, -27<=k<=28, -28<=l<=24
Reflections collected	38898
Independent reflections	6807 [R(int) = 0.0338]
Completeness to theta = 67.684°	100.0 %
Absorption correction	Semi-empirical from equivalents
Max. and min. transmission	1.00000 and 0.59470
Refinement method	Full-matrix least-squares on F ²
Data / restraints / parameters	6807 / 0 / 403
Goodness-of-fit on F ²	1.037
Final R indices [I>2sigma(I)]	R1 = 0.0213, wR2 = 0.0522
R indices (all data)	R1 = 0.0220, wR2 = 0.0527
Extinction coefficient	n/a
Largest diff. peak and hole	0.385 and -0.569 e.Å ⁻³

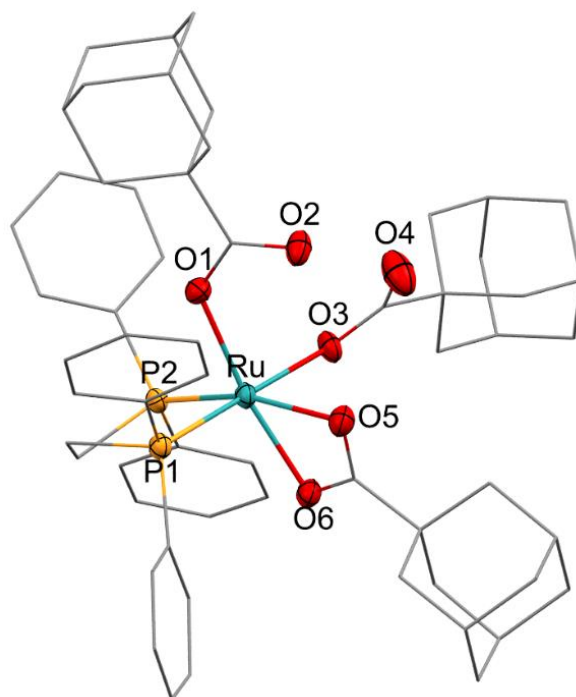
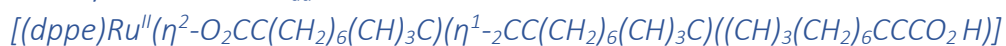
3.4 Crystal data for **B_b'** [$\{(dppe)Ru^{II}(\eta^1-O_2CPh)_2(\mu-O_2CPh)_2(\mu-H_2O)\}$]



CCDC:	2296245	
Identification code	s22uh21	
Empirical formula	C ₃₃₈ H ₃₀₉ O ₄₁ P ₁₆ Ru ₈	
Formula weight	6330.91	
Temperature	150.00(10) K	
Wavelength	1.54184 Å	
Crystal system	Triclinic	
Space group	P-1	
Unit cell dimensions	a = 14.1251(4) Å	α = 88.9659(18)°
	b = 23.5850(6) Å	β = 76.443(2)°
	c = 23.8891(5) Å	γ = 76.138(2)°
Volume	7505.2(3) Å ³	
Z	1	
Density (calculated)	1.401 Mg/m ³	
Absorption coefficient	4.545 mm ⁻¹	
F(000)	3257	

Crystal size	0.060 x 0.060 x 0.040 mm ³
Theta range for data collection	3.864 to 72.905°.
Index ranges	-17<=h<=17, -29<=k<=21, -28<=l<=29
Reflections collected	88483
Independent reflections	29616 [R(int) = 0.0523]
Completeness to theta = 67.684°	99.9 %
Absorption correction	Semi-empirical from equivalents
Max. and min. transmission	1.00000 and 0.85447
Refinement method	Full-matrix least-squares on F ²
Data / restraints / parameters	29616 / 192 / 1900
Goodness-of-fit on F ²	1.030
Final R indices [I>2sigma(I)]	R1 = 0.0432, wR2 = 0.1021
R indices (all data)	R1 = 0.0625, wR2 = 0.1130
Extinction coefficient	n/a
Largest diff. peak and hole	1.113 and -0.783 e.Å ⁻³

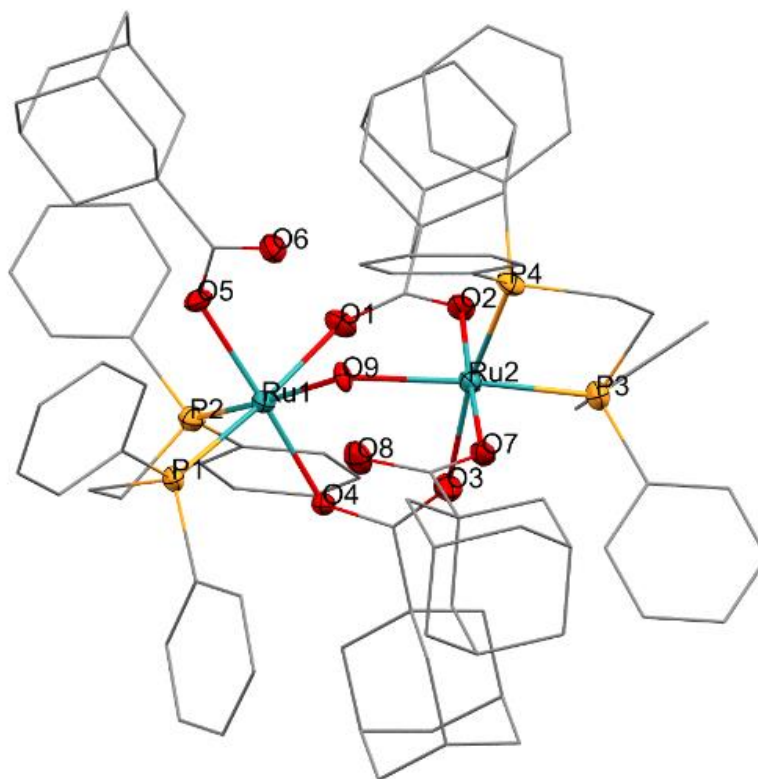
3.5 Crystal data for A_{ad}'



CCDC:	2296243	
Identification code	s22uh25	
Empirical formula	C ₅₉ H ₆₉ O ₆ P ₂ Ru	
Formula weight	1037.15	
Temperature	150.00(10) K	
Wavelength	1.54184 Å	
Crystal system	Triclinic	
Space group	P-1	
Unit cell dimensions	a = 13.32259(17) Å	α = 103.4974(10)°
	b = 13.34539(17) Å	β = 94.3216(10)°
	c = 17.15744(18) Å	γ = 118.4367(13)°
Volume	2545.56(6) Å ³	
Z	2	
Density (calculated)	1.353 Mg/m ³	
Absorption coefficient	3.491 mm ⁻¹	
F(000)	1090	

Crystal size	0.348 x 0.253 x 0.214 mm ³
Theta range for data collection	3.866 to 73.021°.
Index ranges	-16<=h<=16, -16<=k<=16, -21<=l<=19
Reflections collected	49074
Independent reflections	10098 [R(int) = 0.0213]
Completeness to theta = 67.684°	99.9 %
Absorption correction	Gaussian
Max. and min. transmission	1.000 and 0.400
Refinement method	Full-matrix least-squares on F ²
Data / restraints / parameters	10098 / 705 / 796
Goodness-of-fit on F ²	1.062
Final R indices [I>2sigma(I)]	R1 = 0.0310, wR2 = 0.0786
R indices (all data)	R1 = 0.0313, wR2 = 0.0788
Extinction coefficient	n/a
Largest diff. peak and hole	1.562 and -0.713 e.Å ⁻³

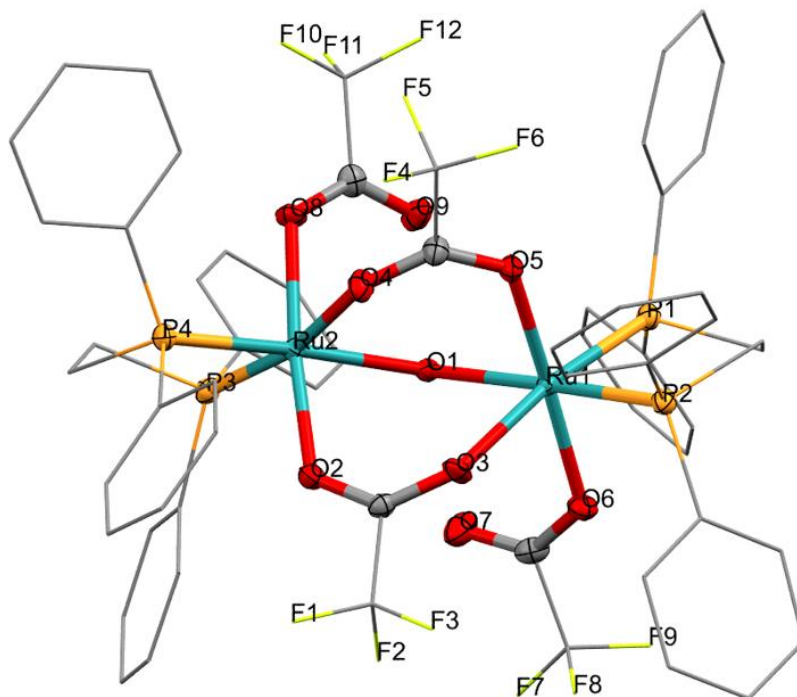
3.6 Crystal data for **B_{ad}'** [$\{(dppe)Ru^{II}(\eta^1-O_2CC(CH_2)_6(CH_3)_2)\}_2(\mu-O_2CC(CH_2)_6(CH_3)_2)(\mu-H_2O)$]



CCDC:	2296246	
Identification code	s22uh10_sq	
Empirical formula	C ₉₉ H ₁₁₄ O ₁₀ P ₄ Ru ₂	
Formula weight	1789.92	
Temperature	150.01(10) K	
Wavelength	1.54184 Å	
Crystal system	Monoclinic	
Space group	P2 ₁ /n	
Unit cell dimensions	a = 13.8453(3) Å	α = 90°
	b = 24.5721(4) Å	β = 101.926(2)°
	c = 29.3748(6) Å	γ = 90°
Volume	9777.8(3) Å ³	
Z	4	
Density (calculated)	1.216 Mg/m ³	
Absorption coefficient	3.540 mm ⁻¹	
F(000)	3744	

Crystal size	0.339 x 0.059 x 0.033 mm ³
Theta range for data collection	3.598 to 73.247°.
Index ranges	-17<=h<=16, -30<=k<=30, -36<=l<=36
Reflections collected	197376
Independent reflections	197376 [R(int) = ?]
Completeness to theta = 67.684°	100.0 %
Absorption correction	Gaussian
Max. and min. transmission	1.000 and 0.442
Refinement method	Full-matrix least-squares on F ²
Data / restraints / parameters	197376 / 102 / 1065
Goodness-of-fit on F ²	1.131
Final R indices [I>2sigma(I)]	R1 = 0.1016, wR2 = 0.2199
R indices (all data)	R1 = 0.1223, wR2 = 0.2299
Extinction coefficient	n/a
Largest diff. peak and hole	1.639 and -2.019 e.Å ⁻³

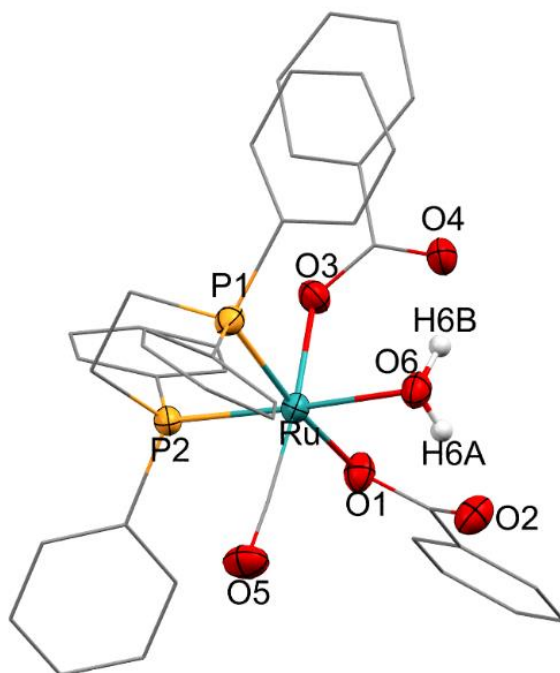
3.7 Crystal data for $\text{B}_{\text{tr}}' [\{ (\text{dppe})\text{Ru}^{\text{II}}(\eta^1\text{-O}_2\text{CCF}_3)_2(\mu\text{-O}_2\text{CCF}_3)_2(\mu\text{-OH}_2) \}]$



CCDC:	2296248	
Identification code	e23uh8	
Empirical formula	$\text{C}_{61} \text{H}_{52} \text{Cl}_2 \text{F}_{12} \text{O}_9 \text{P}_4 \text{Ru}_2$	
Formula weight	1553.94	
Temperature	149.9(7) K	
Wavelength	0.71073 Å	
Crystal system	Monoclinic	
Space group	$P2_1/c$	
Unit cell dimensions	$a = 19.9752(7)$ Å	$\alpha = 90^\circ$
	$b = 19.5957(8)$ Å	$\beta = 96.739(5)^\circ$
	$c = 16.0602(5)$ Å	$\gamma = 90^\circ$
Volume	$6243.0(4)$ Å ³	
Z	4	
Density (calculated)	1.653 Mg/m ³	
Absorption coefficient	0.764 mm ⁻¹	
F(000)	3120	

Crystal size	0.210 x 0.190 x 0.150 mm ³
Theta range for data collection	2.863 to 26.373°.
Index ranges	-24<=h<=24, -24<=k<=24, -20<=l<=20
Reflections collected	58880
Independent reflections	12695 [R(int) = 0.0835]
Completeness to theta = 25.242°	99.5 %
Absorption correction	Semi-empirical from equivalent
Max. and min. transmission	1.00000 and 0.91027
Refinement method	Full-matrix least-squares on F ²
Data / restraints / parameters	12695 / 2 / 819
Goodness-of-fit on F ²	1.092
Final R indices [I>2sigma(I)]	R1 = 0.0643, wR2 = 0.1170
R indices (all data)	R1 = 0.1003, wR2 = 0.1287
Extinction coefficient	n/a
Largest diff. peak and hole	1.183 and -0.968 e.Å ⁻³

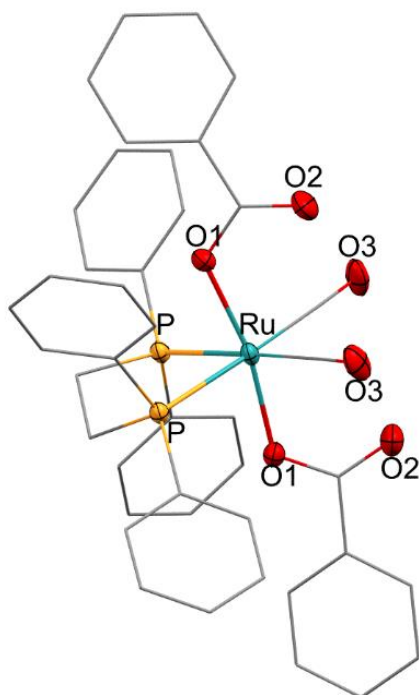
3.8 Crystal data for $X^2_b \cdot H_2O$ $[(dppe)Ru^{II}(\eta^1-O_2CPh)_2(CO)(H_2O)]$



CCDC:	2296247	
Identification code	s23uh8	
Empirical formula	C ₄₁ H ₃₆ O ₆ P ₂ Ru	
Formula weight	787.71	
Temperature	150.00(10) K	
Wavelength	1.54184 Å	
Crystal system	Orthorhombic	
Space group	Pbca	
Unit cell dimensions	a = 17.38650(12) Å	α = 90°
	b = 18.59091(14) Å	β = 90°
	c = 22.10176(13) Å	γ = 90°
Volume	7143.97(8) Å ³	
Z	8	
Density (calculated)	1.465 Mg/m ³	
Absorption coefficient	4.792 mm ⁻¹	
F(000)	3232	
Crystal size	0.367 x 0.220 x 0.170 mm ³	
Theta range for data collection	4.000 to 72.948°.	

Index ranges	-21<=h<=21, -22<=k<=22, -17<=l<=27
Reflections collected	97666
Independent reflections	7121 [R(int) = 0.0509]
Completeness to theta = 67.684°	100.0 %
Absorption correction	Semi-empirical from equivalents
Max. and min. transmission	1.00000 and 0.65840
Refinement method	Full-matrix least-squares on F ²
Data / restraints / parameters	7121 / 0 / 459
Goodness-of-fit on F ²	1.106
Final R indices [I>2sigma(I)]	R1 = 0.0358, wR2 = 0.0863
R indices (all data)	R1 = 0.0393, wR2 = 0.0887
Extinction coefficient	n/a
Largest diff. peak and hole	0.861 and -0.532 e.Å ⁻³

3.9 Crystal data for $X^2_b[(dppe)Ru^{II}(\eta^1-O_2CPh)_2(CO)_2]$



CCDC:	2296249	
Identification code	s23uh24	
Empirical formula	C ₄₂ H ₃₄ O ₆ P ₂ Ru	
Formula weight	797.70	
Temperature	150.01(10) K	
Wavelength	1.54184 Å	
Crystal system	Tetragonal	
Space group	P-42 ₁ c	
Unit cell dimensions	a = 14.82724(7) Å	α = 90°
	b = 14.82724(7) Å	β = 90°
	c = 16.45463(14) Å	γ = 90°
Volume	3617.50(5) Å ³	
Z	4	
Density (calculated)	1.465 Mg/m ³	
Absorption coefficient	4.742 mm ⁻¹	
F(000)	1632	
Crystal size	0.100 x 0.050 x 0.030 mm ³	
Theta range for data collection	4.013 to 72.919°.	

Index ranges	-18<=h<=18, -18<=k<=18, -19<=l<=20
Reflections collected	62561
Independent reflections	3612 [R(int) = 0.0434]
Completeness to theta = 67.684°	100.0 %
Absorption correction	Semi-empirical from equivalents
Max. and min. transmission	1.00000 and 0.66237
Refinement method	Full-matrix least-squares on F ²
Data / restraints / parameters	3612 / 0 / 262
Goodness-of-fit on F ²	1.034
Final R indices [I>2sigma(I)]	R1 = 0.0193, wR2 = 0.0451
R indices (all data)	R1 = 0.0207, wR2 = 0.0457
Absolute structure parameter	-0.012(4)
Extinction coefficient	n/a
Largest diff. peak and hole	0.183 and -0.389 e.Å ⁻³

4.0 Supplementary data

4.1 Solvent effects

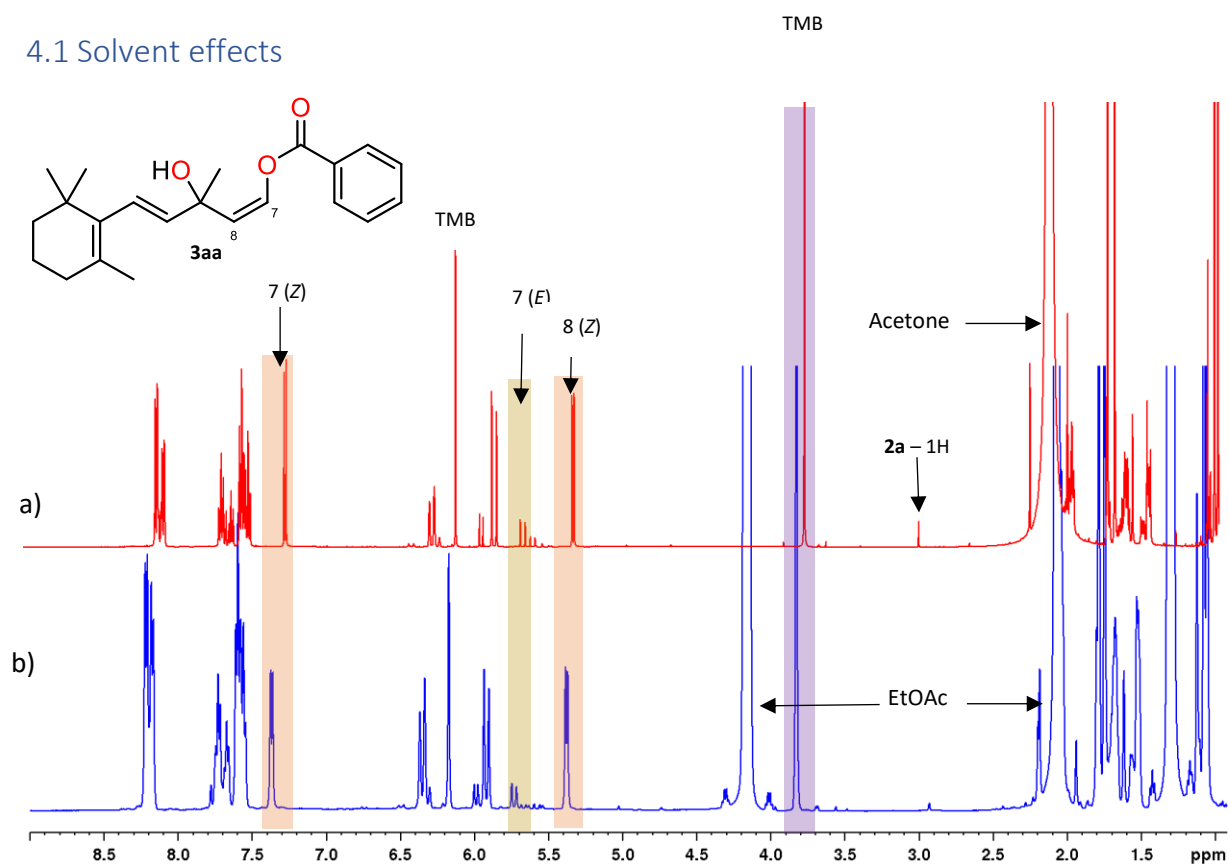


Figure S34. ^1H NMR spectra of the crude product (3aa) mixture of the Ru-mediated transformation (sum of Z and E adduct) of ethynyl- β -ionol (0.667 M), benzoic acid (1 M) and $[(\text{dppe})\text{Ru}(\text{MA})_2]$ (1 mol%) at room temperature after 38 hours under inert atmosphere in a) acetone – 93% product yield and b) ethyl acetate – 96% product yield. Illustrating clean ^1H spectrum with a small amount of substrate still observed in both spectra. The E-isomer also highlighted.

4.2 Influence of the carboxylic acid

Table S2. Screening of different carboxylic acids used in the Ru-mediated transformation of ethynyl- β -ionol into their respective ester-adducts under inert atmosphere with anhydrous ethyl acetate at different temperatures, reaction times and volumes.

Entry	Carboxylic acid	Temperature ($^{\circ}\text{C}$)	Time (h)	EtOAc (mL)	Yield (%)
1	Benzoic acid	20	24	10	85
2		10	24	10	89
3	Acetic acid	20	24	10	12
4	Cyclohexane carboxylic acid	20	24	10	95
5		0	24	10	97
6		20	24	10	97
7		10	24	0	>99
8		30	4	0	>99

9	Pivalic acid	20	6	0	>99
10		40	2	0	95
12	1-Adamantane	10	21	10*	97
13	carboxylic acid	20	3	10	98

*Sample was not homogeneous

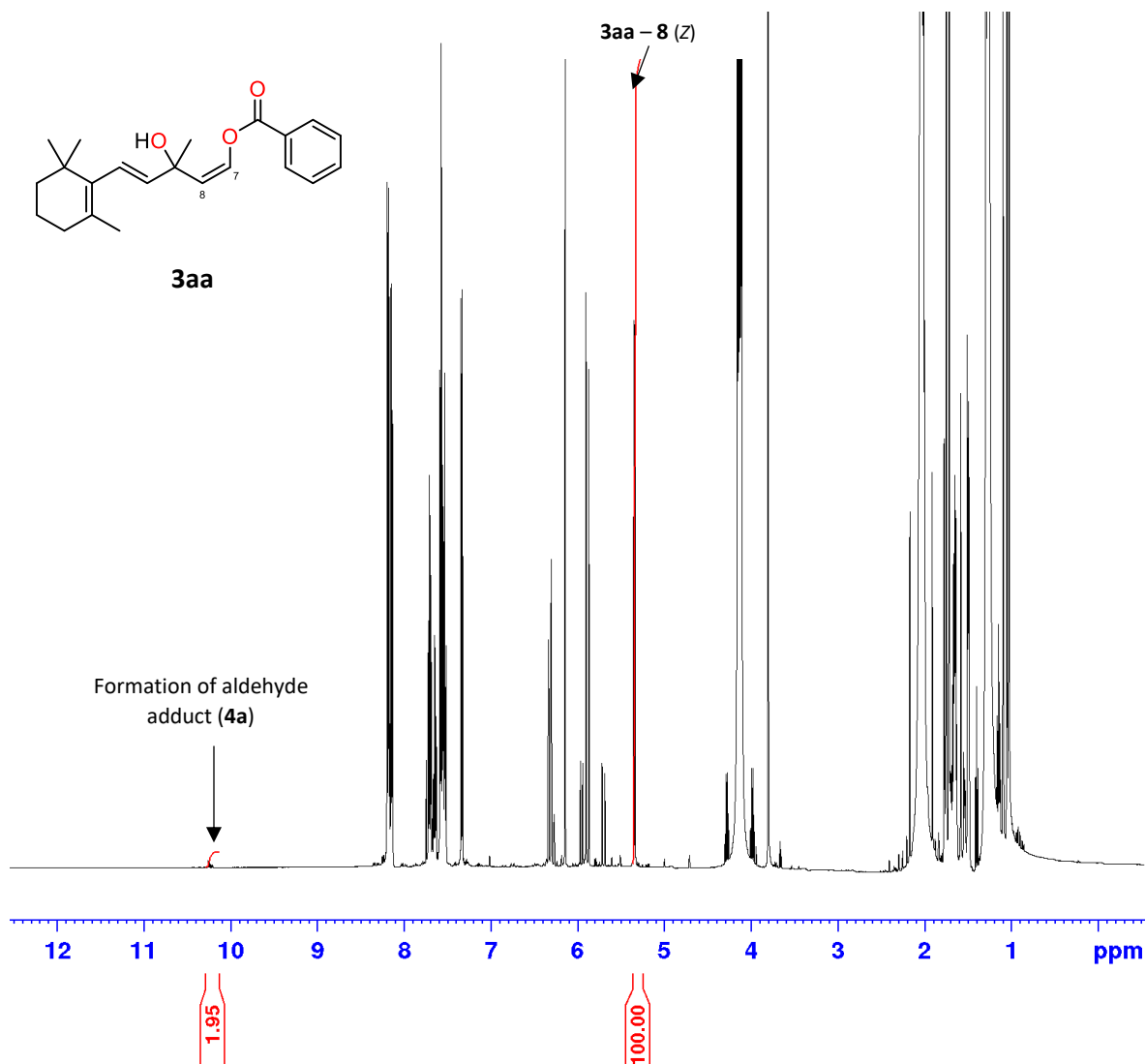
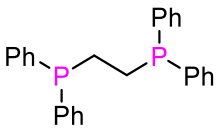
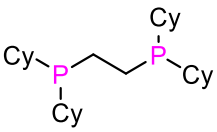
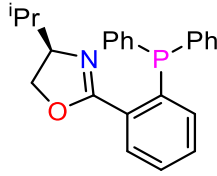
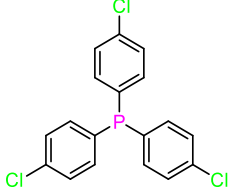
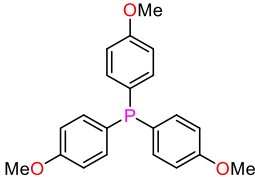
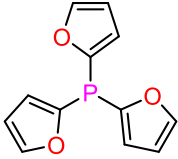
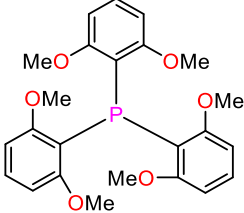
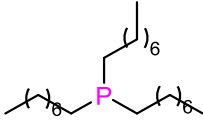
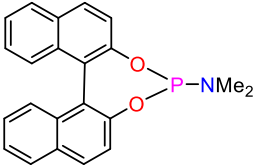
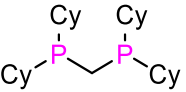
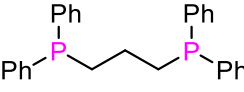
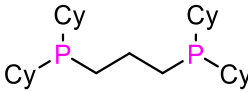
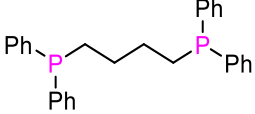
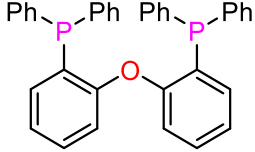
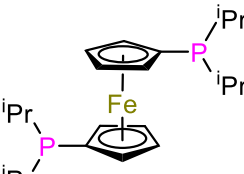
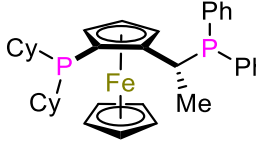
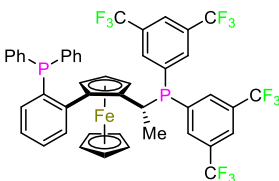
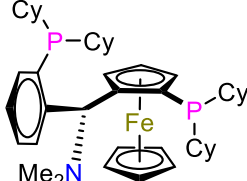
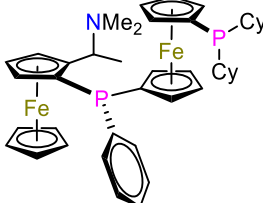
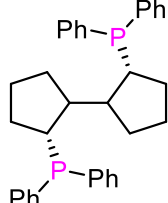


Figure S35. Example ¹H NMR spectrum showing aldehyde adduct (**4a**) formation from the Ru-mediated transformation of ethynyl- β -ionol (0.5 M) with benzoic acid (1.5 equiv.) to form **3aa** under inert atmosphere in anhydrous ethyl acetate (10 mL) at 20 °C after 24 hours.

4.3 Ligand effects

Chart S1. P, P/P and N/P ligands considered and tested in this study.

			
<p>1. 1,2-Bis(diphenylphosphino)ethane</p>	<p>2. 1,2-Bis(dicyclohexylphosphino)ethane</p>	<p>3. (R)-(+)-2-[2-(Diphenylphosphino)phenyl]-4-isopropyl-2-oxazoline</p>	<p>4. Tris(4-chlorophenyl)phosphine</p>
			
<p>5. Tris(4-methoxyphenyl)phosphine</p>	<p>6. Tri(2-furyl)phosphine</p>	<p>7. Tris(2,6-dimethoxyphenyl)phosphine</p>	<p>8. Trioctylphosphine</p>
			
<p>9. (R)-MonoPhos</p>	<p>10. Bis(dicyclohexylphosphino)methane</p>	<p>11. 1,3-Bis(diphenylphosphino)propane</p>	<p>12. 1,3-Bis(dicyclohexylphosphino)propane</p>
			
<p>13. 1,4-Bis(diphenylphosphino)butane</p>	<p>14. DPE-Phos</p>	<p>15. DiPrF</p>	<p>16. ((1R)-1-(Dicyclohexylphosphino)-2-[(1R)-1-(diphenylphosphino)ethyl]ferrocene</p>
			
<p>17. (1S)-1-[(1R)-1-[Bis(3,5-bis(trifluoromethyl)phenyl)phosphino]ethyl]-2-[2-(diphenylphosphino)phenyl]ferrocene</p>	<p>18. SL-TaniaPhos</p>	<p>19. ChenPhos</p>	<p>20. (R, R) - BICP</p>

21. (R, R)- diisopropylphospholane ethane	22. (R,R)-DIOP	23. (S, S)-NORPHOS	24. 2,2'-Bis(dicyclohexylphosphino)-1,1'-biphenyl
25. 1,2-Bis(diphenylphosphino) methane	26. (R, R)-Dipamp	27. 1,2-Bis(dimethylphosphino) ethane	28. NO ligand

Table S3. A selection of ruthenium precursors screened with 27 different P, P/P, N/P ligands for the regio- and stereo-selective anti-Markovnikov addition of pivalic acid to ethynyl- β -ionol. Reaction conditions: Substrate (0.1 mmol); catalyst (0.003 mmol; 3 mol%); monodentate ligands (0.0033 mmol) or bidentate ligands (0.0066 mmol), pivalic acid (0.15 mmol), EtOAc (1.2 mL), monitored after 19 hours.

Ru precursors	[Ru(cod)(MA) ₂]	[Ru(acac) ₃]	[Ru(H)Cl(PPh ₃) ₃]	[RuCl ₂ (DMSO) ₄]
Ligand	Yield (%)	Yield (%)	Yield (%)	Yield (%)
1	95	0	0	0
2	9	0	0	0
3	2	0	0	0
4	2	0	0	0
5	0	0	0	0
6	0	0	0	0
7	1	0	0	0
8	0	0	0	0
9	0	0	0	0
10	9	0	0	0
11	11	0	0	0
12	16	0	0	0
13	33	0	0	0
14	7	0	0	0
15	4	0	0	0
16	29	0	0	0

17	1	0	0	0
18	1	0	0	0
19	1	0	0	0
20	30	0	0	0
21	7	0	0	0
22	10	2	0	0
23	57	0	0	0
24	0	0	0	0
25	24	0	0	0
26	78	0	0	0
27	83	0	0	0
28	1	0	0	0

No Ru precursors except [Ru(cod)(me-allyl)₂] showed catalytic activity. We have identified a few ligands giving a small amount of the desired product, albeit lower than dppe (**1-4**, **7**, **10-23**, **25-27**). The ligands **13**, **16** and **20** selectively form only one isomer of the product.

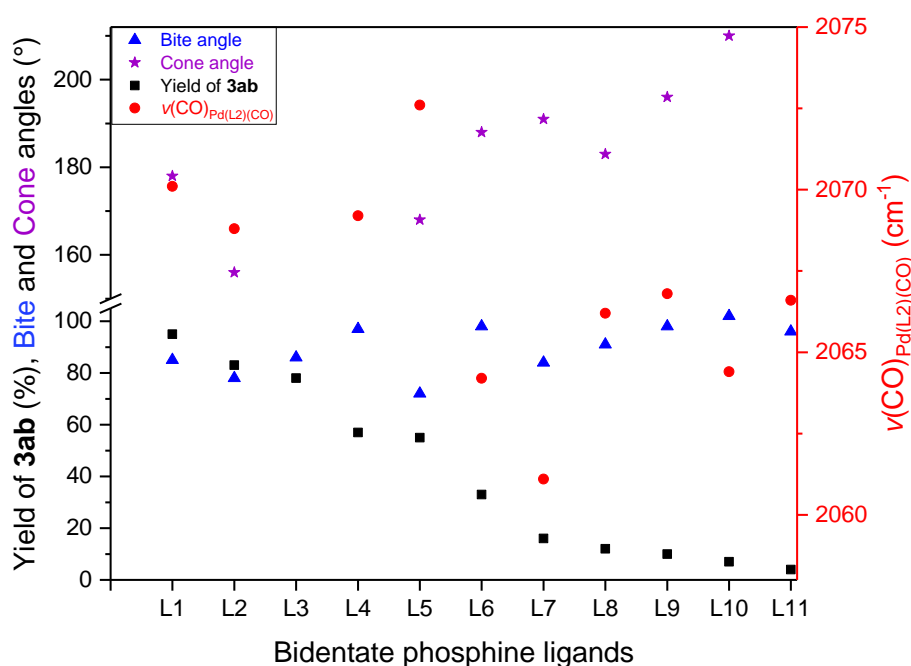


Figure S36. Steric and electronic parameters as well as reaction yields for selected chelating diphosphines used for the Ru-catalysed [(MA₂Ru(COD))] transformation of ethynyl- β -ionol (0.1 mmol) with pivalic acid (0.15 mmol) using a catalyst loading of 3 mol% to form **3ab** in anhydrous ethyl acetate (1.2 mL) at 20 °C. Yields were determined after 19 h. L1=dppe, L2=dmpe, L3=(R,R)-Dipamp, L4=(S,S)-Norphos, L5=dppm, L6=dppb, L7=dcypp, L8=dppp, L9=(R,R)-DIOP, L10=DPE-phos, L11=DⁱPrF.

4.4 TON limitation

Table S4. TONs for the ruthenium catalysed transformation of ethynyl- β -ionol (sum of Z and E adduct) to **3ab** at various catalyst loadings (0.1 – 2 mol%). In all cases the reaction was run to maximum yield. Ethynyl- β -ionol (10 mmol); pivalic acid 1.5 equiv, under inert atmosphere with anhydrous acetone (15 mL) with TMB (0.25 equiv, internal standard) was used.

[(dppe)Ru(MA) ₂] loading	Product yield at reaction completion	TON
2 mol%	99%	50
1 mol%	96%	96
0.5 mol%	57%	114
0.25 mol%	36%	144
0.1 mol%	15%	150

4.5 Substrate effects

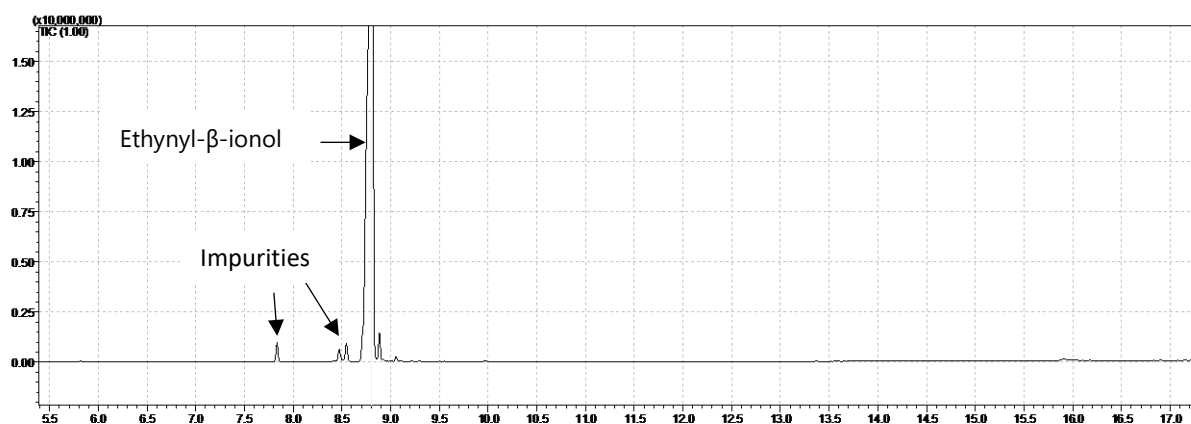


Figure S37. GC-chromatogram of distilled ethynyl- β -ionol.

Sample prepared in methanol: split ratio 10:0, column pressure = 314.2 kPa, and column flow = 3.17 mL/min. The oven temperature increased by 20 °C min⁻¹ from 40 °C to 220 °C (held at 5.5 min). The temperature program was set to 220 °C, 1 min; ramp of 5 °C min⁻¹ to 250 °C, and finally held at 280 °C for 6 min (total run time 29 min). Analyte's retention times were: methanol (2.5 min), (7.83 min), (8.47 min), (8.55 min), ethynyl- β -ionol (8.85 min), (8.88 min), (9.05 min). Impurities identified: α/β -ionone, α -ethynyl- β -ionol, ethynyl- β -ionol -oxide, ethynyl- β -ionol -dimer and dehydrated ethynyl- β -ionol.

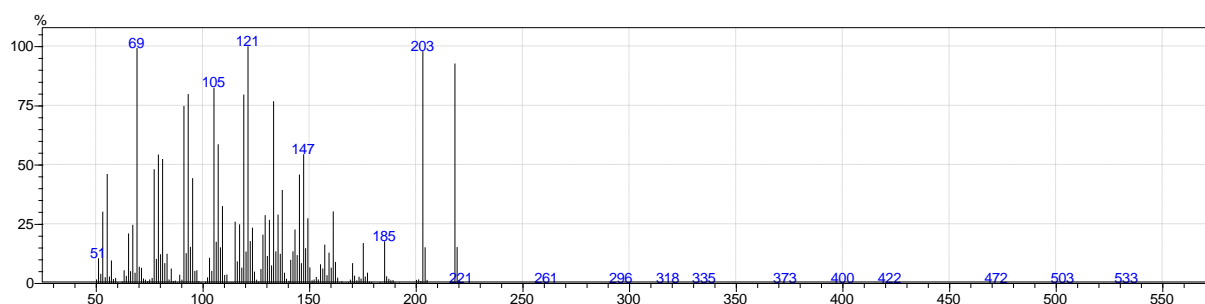


Figure S38. Mass spectrum fragmentation of ethynyl- β -ionol.

The mass spectrometry was operated in an EI positive mode, scanning mass ions in the range 10 to 550 (4–29 min) containing a helium carrier gas. The mass fragmentation spectrum of ethynyl- β -ionol ($m/z = 218$ $[M]^+$, 100%) is shown in Figure S37.

Table S5. Product yield of the Ru-mediated transformation in a range of alkynols (0.66 M) and phenylacetylene (0.66 M) under inert atmosphere in anhydrous acetone (15 mL) with pivalic acid (1 M) TMB (0.167 M), (internal standard) at room temperature after 18 hours and 40 hours

Substrate	Yield at 18 h (%)	Yield at 40 h (%)
Ethynyl- β -ionol (2a)	84%	97%
Phenylacetylene (2b)	78%	93%
Dihydroethynyl- β -ionol (2c)	87%	97%
Dehydrolinalool (DLL) (2d)	87%	96%
Dimethyloctinol (DMOI) (2e)	83%	97%
Ethynyl- β -ionol (1% β -ionone) (2a + 1)	85%	96%
Dehydrated ethynyl- β -ionol (2f)	80%	95%
2-Phenyl-3-butyne-2-ol (2g)	80%	94%

The peaks used to monitor reaction progress of **3eb** are highlighted:

Substrate (**2e**), *Z*-adduct (**3eb**), *E*-adduct (**3eb**), Internal standard

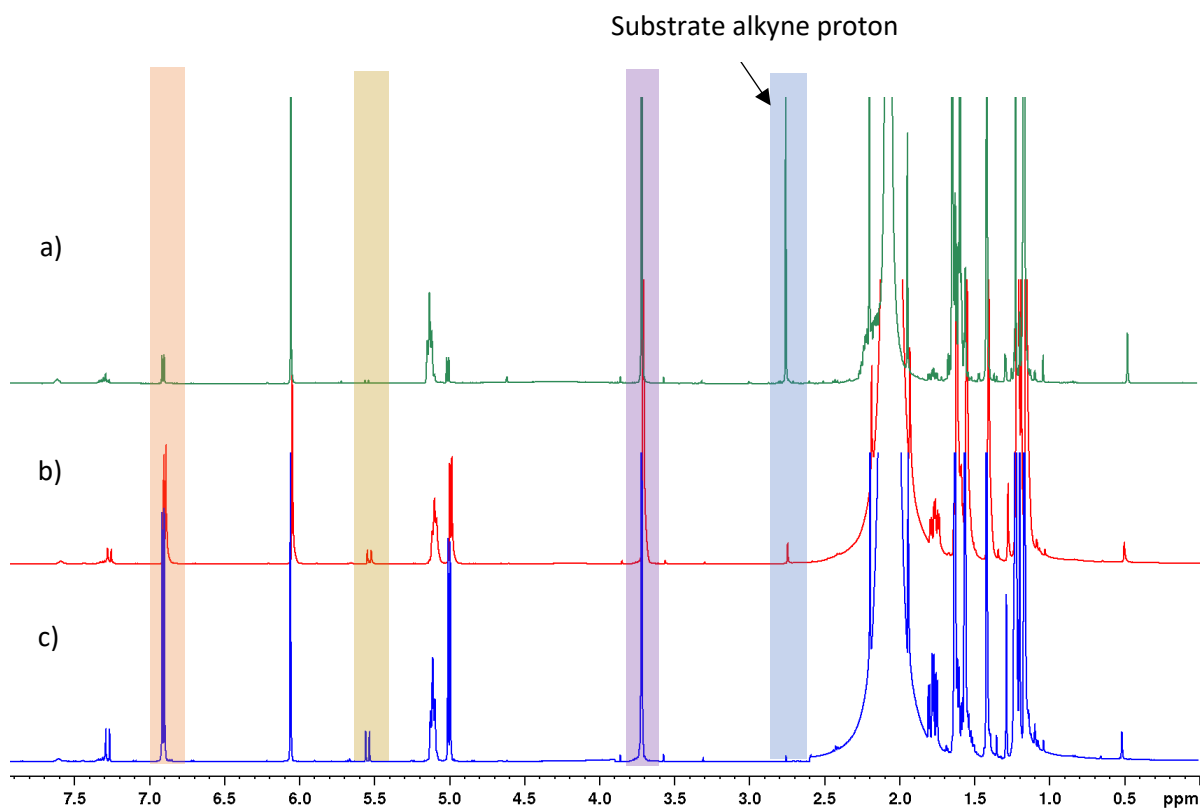


Figure S39. ¹H stacked NMR spectra of the crude product mixture of the Ru-mediated transformation (sum of *Z* and *E* adduct) of dimethyloctinol (0.667 M), pivalic acid (1 M) and [(dppe)Ru(MA)₂] (1 mol%) at room temperature under inert atmosphere in acetone after a) 1 hour b) 18 hours c) 40 hours. Illustrating reaction progression and near complete product formation of dimethyloctinol-pivalic adduct (97% yield after 40 hours).

4.6 Poisoning tests

To test for possible catalyst poisons, either present in the substrate or formed by the reaction in small amounts, the effect of different functional group additives on the Ru-mediated transformation of phenylacetylene was examined. Considering the context of ethynyl- β -ionol in vitamin A synthesis (Scheme 1), the most relevant functional groups to test included unsaturated aldehydes, unsaturated alcohols and an olefin. **1** and **2f** are minor impurities present in ethynyl- β -ionol (Figures S36-S37), and so were added to the reaction in higher amounts see if they have a negative effect on the catalysis. Other possible poisons/inhibitors tested included water and cyclooctadiene. Following the reaction progress with 0.75 mol% [(dppe)Ru(MA)₂] under optimised conditions showed that none of the tested additives caused significant levels of deactivation or inhibition of the catalysis at 10-20% loading, with all product yields falling between 79-82% after 44 hours (Figure 2).

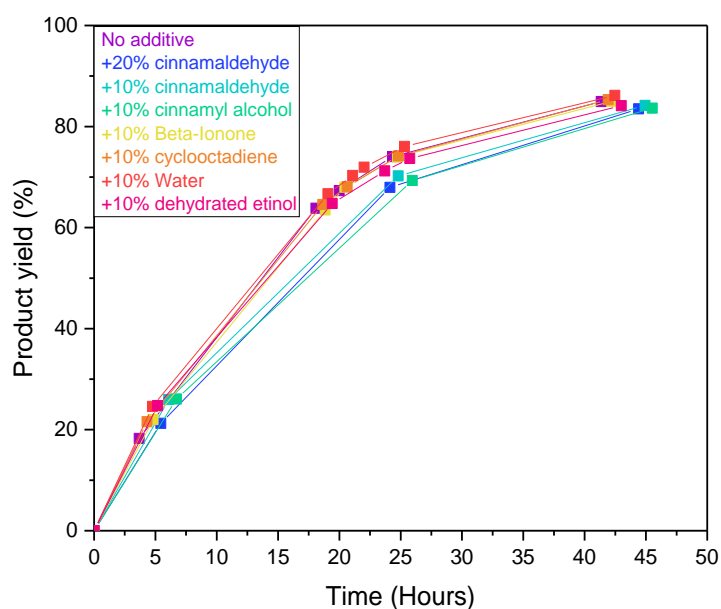


Figure S40. Product yield of the Ru-mediated transformation of phenylacetylene (0.66 M) with pivalic acid (1 M) catalysed by [(dppe)Ru(MA)₂] (0.75 mol% loading) in anhydrous acetone (15 mL) at 20 °C in the presence of various additives as detailed in the legend.

4.7 Operando ¹H FlowNMR analysis

Table S6. Selected FlowNMR experiments performed to further optimise reaction conditions for kinetic analysis of the Ru-mediated transformation of ethynyl- β -ionol (0.66 M) catalysed by [(dppe)Ru(MA)₂] at 1 mol% loading in anhydrous acetone or ethyl acetate (15 mL) at 20 °C from quantitative ¹H FlowNMR spectroscopy at 4 mL/min unless stated otherwise.

Solvent	Carboxylic acid	Additive/Comment	T [h]	Conversion [%]	TON
Ethyl acetate	Benzoic acid	-	18	78	78
Ethyl acetate	Benzoic acid	2 mol% catalyst loading	12	95	48
Ethyl acetate	acetic acid	-	18	10	10
Ethyl acetate	Pivalic acid	-	18	81	81
Acetone	Pivalic acid	-	18	79	79
Acetone	Pivalic acid	0.5 mol% catalyst loading	18	60	120
Acetone	Adamantane carboxylic acid	-	18	98	98
Ethyl acetate	Pivalic acid	H ₂ O (0.5 mol%)	18	49	49
Acetone	Pivalic acid	H ₂ O (0.5 mol%)	18	60	60
Ethyl acetate	Pivalic acid	Pivalic anhydride (2 mmol)	18	88	88
Acetone	Pivalic acid	Pivalic anhydride (2 mmol)	18	85	85

4.8 Variable Time Normalisation Analysis

4.8.1 Change in catalyst loading

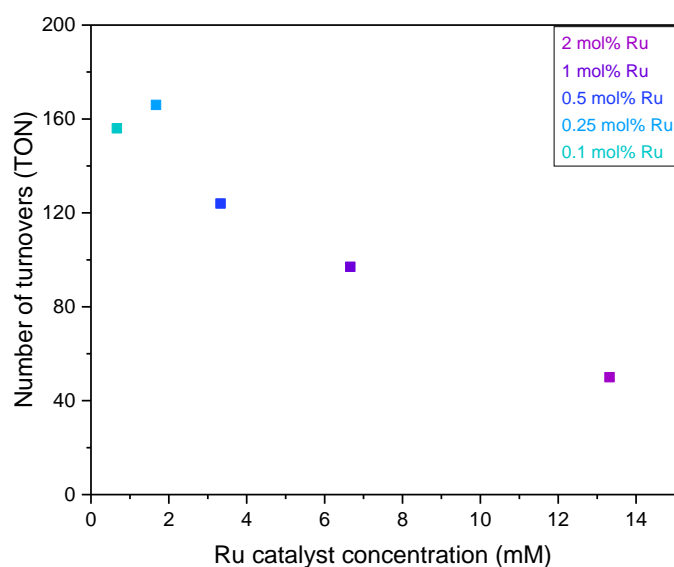


Figure S41. Maximum catalyst TONs of the Ru-mediated transformation of ethynyl- β -ionol (0.66 M) with pivalic acid (0.73 M) and pivalic anhydride (0.13 M) giving **3ab**, catalysed by various amounts of [(dppe)Ru(MA)₂] in anhydrous acetone (15 mL) at 20 °C. Determined from quantitative ¹H FlowNMR spectroscopy at 4 mL/min.

4.8.2 Change in pivalic acid loading

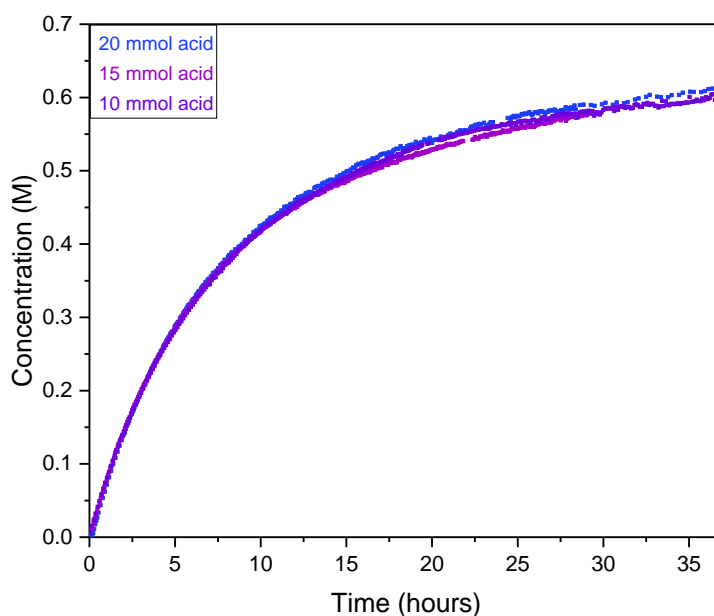


Figure S42. Product concentration profiles (sum of Z and E adduct) of the Ru-mediated transformation of ethynyl- β -ionol (0.66 M) to form **3ab**. This was catalysed with [(dppe)Ru(MA)₂] (1mol%) with various amounts of pivalic acid (10-20mmol) in anhydrous acetone (15 mL) at 20 °C. Determined from quantitative ¹H FlowNMR spectroscopy, acquired at 4 mL/min.

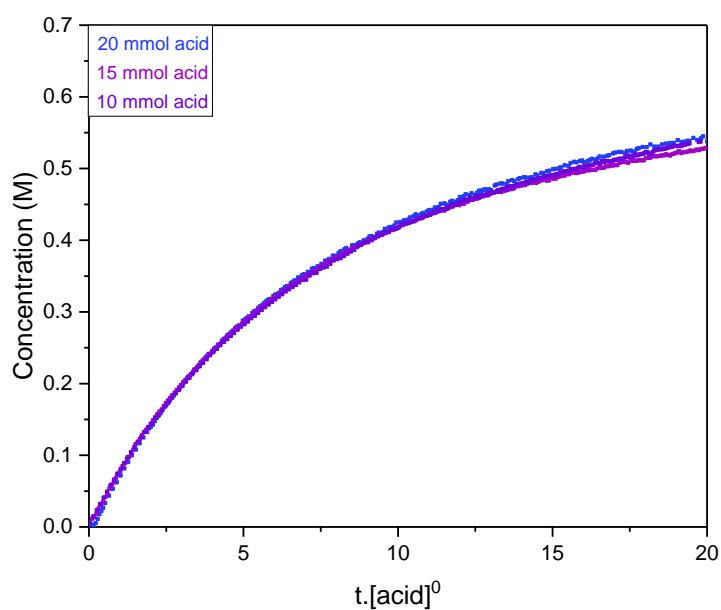


Figure S43. Time adjusted reaction progress profiles of data from **Figure S42** for a reaction order in $[\text{acid}] = 0$.

4.8.2 Change in ethynyl- β -ionol loading

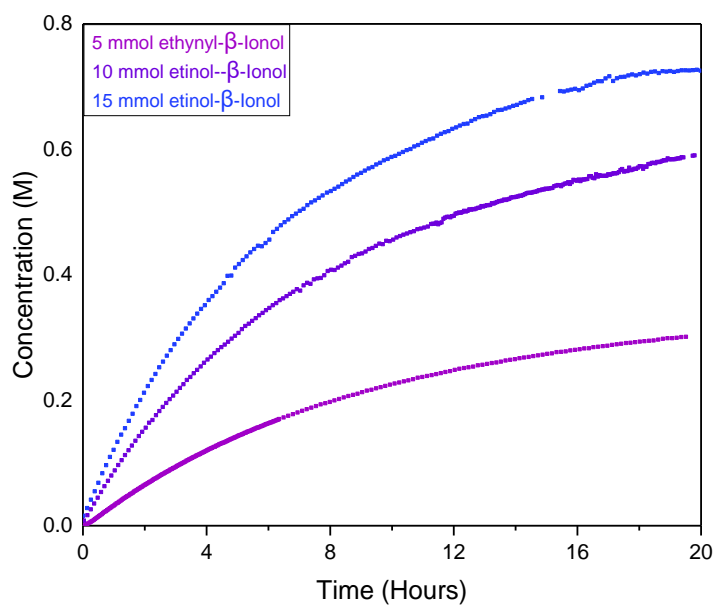


Figure S44. Product concentration profiles (sum of Z and E adduct) of the Ru-mediated transformation of ethynyl- β -ionol (at different loadings 5 - 15 mmol) with pivalic acid (0.73 M) and pivalic anhydride (0.13 M) catalysed with $[(\text{dppe})\text{Ru}(\text{MA})_2]$ (1 mol%) in anhydrous acetone (15 mL) at 20 °C from quantitative ^1H FlowNMR spectroscopy, acquired at 4 mL/min.

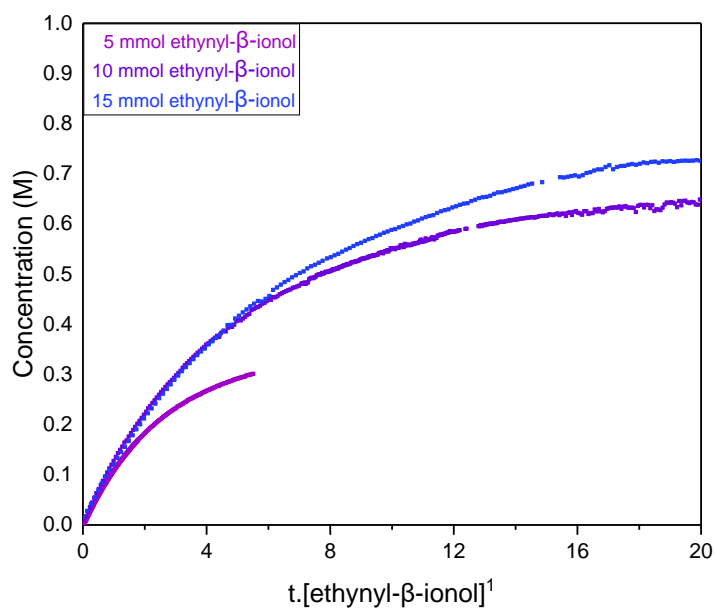


Figure S45. Time adjusted reaction progress profiles (data from **Figure S44**) for a reaction order in [Substrate] = 1.

4.8.3 Phenylacetylene concentration profile

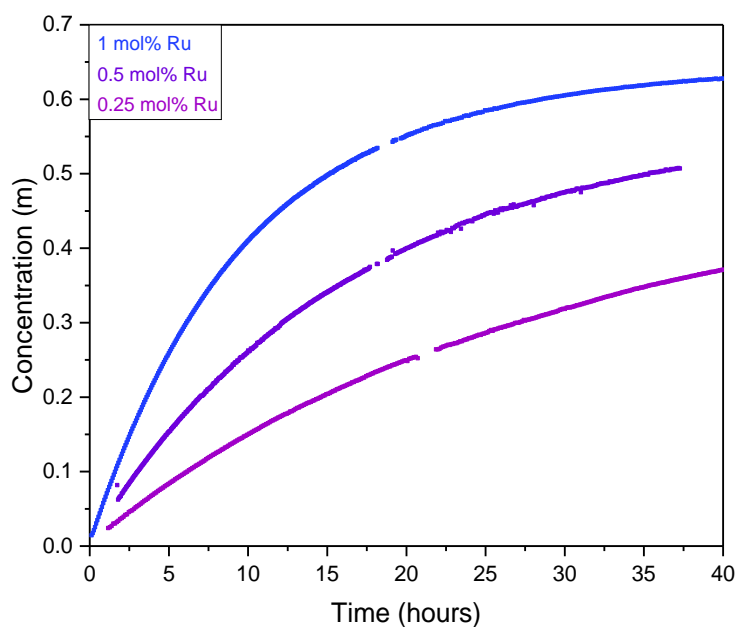


Figure S46. Product concentration profiles (sum of Z and E adduct of **3ab**) of the Ru-mediated transformation of phenylacetylene (0.66 M) with pivalic acid (0.73 M) and pivalic anhydride (0.13 M) catalysed by various amounts of [(dppe)Ru(MA)₂] in anhydrous acetone (15 mL) at 20 °C. Determined from quantitative ¹H FlowNMR spectroscopy, acquired at 4 mL/min.

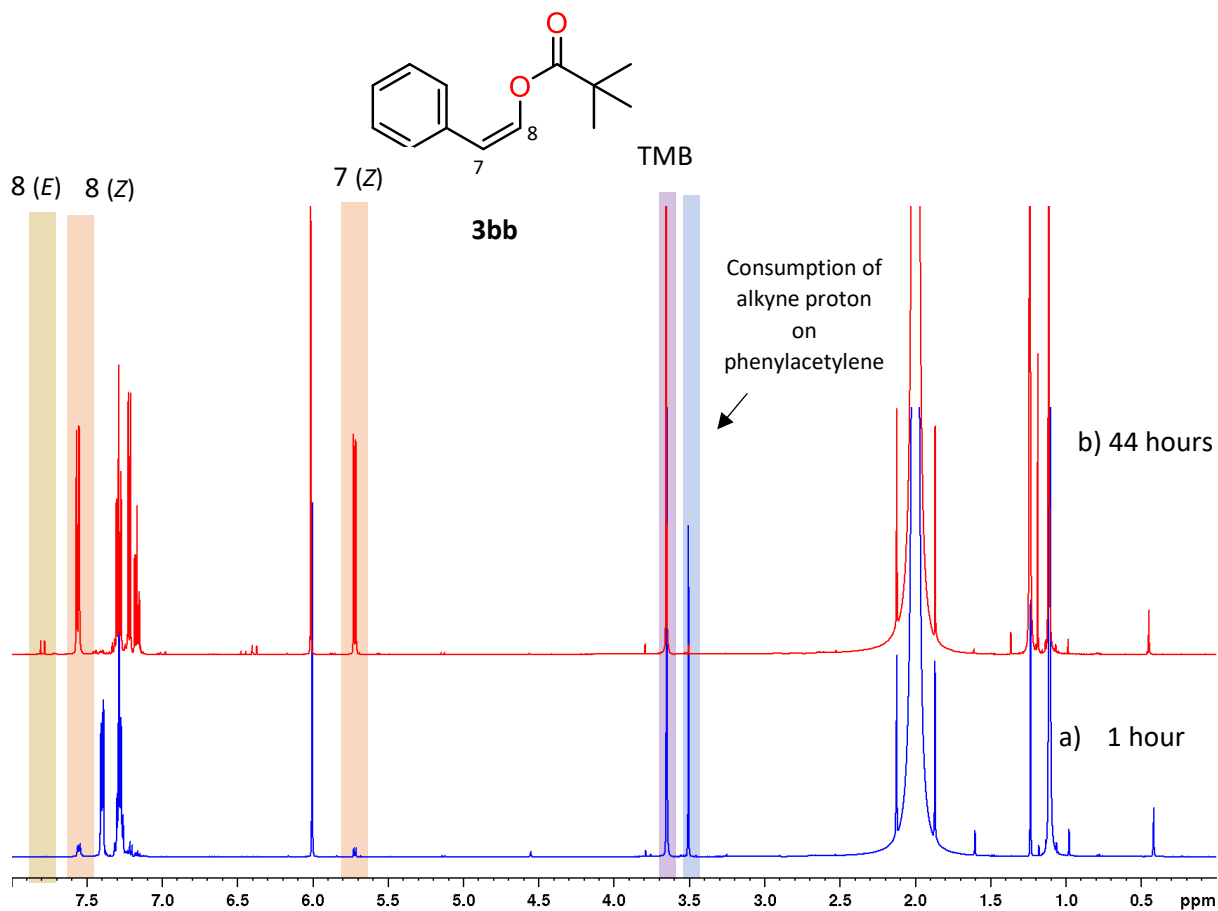
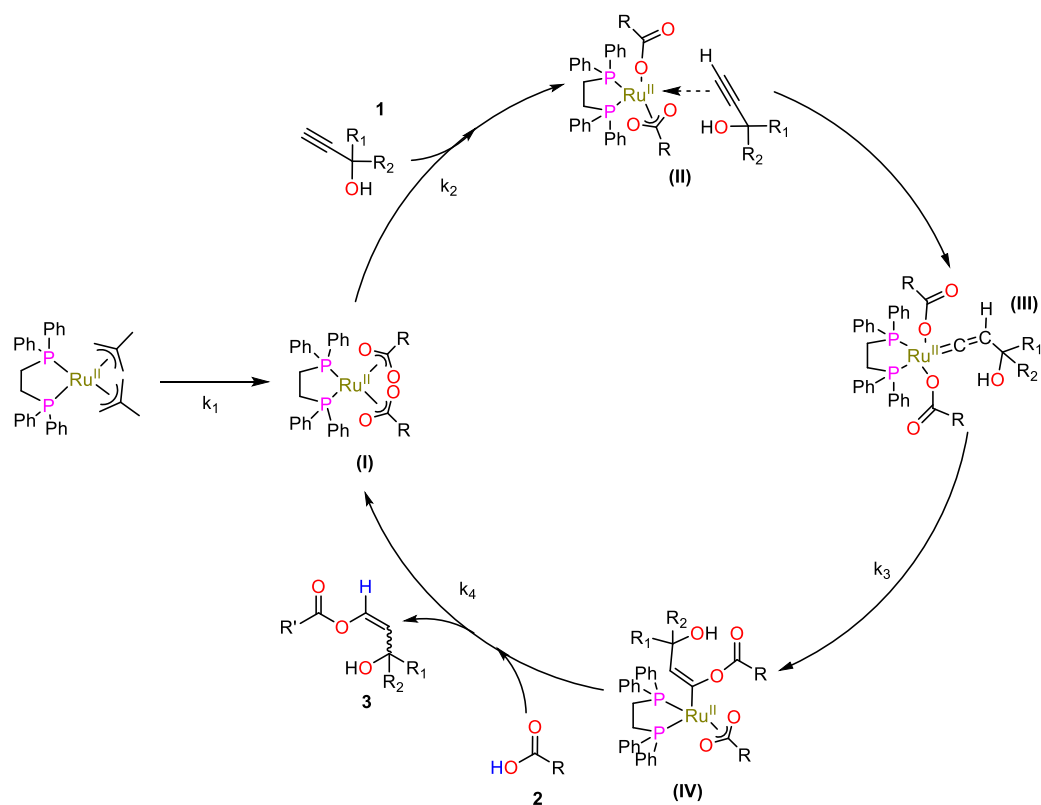


Figure S47. ^1H NMR spectra showing the crude product mixture of the Ru-mediated transformation (sum of Z and E adduct) of phenylacetylene (0.667 M), pivalic acid (1 M) and $[(\text{dppe})\text{Ru}(\text{MA})_2]$ (1 mol%) at room temperature under inert atmosphere in acetone after a) 1 hour b) 44 hours. This figure illustrates the reaction progression and near complete product formation of the phenylacetylene-pivalic adduct (97% yield after 44 hours). 7 and 8 represent the protons associated to the ester adduct, Z represents Z-ester adduct and E represents E-ester adduct (a ratio of $\sim 96/4$).

4.9 Rate law derivation

4.9.1 Irreversible literature mechanism

Proposed mechanism for the regioselective ruthenium catalysed anti-Markovnikov addition of carboxylic acids to terminal alkynes giving α,β -unsaturated carboxylates.¹¹⁻¹³



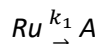
Assumptions:

- $k_1 \gg k_2, k_3, k_4$ therefore can be neglected and $[1] \approx 0$
- Steady-state Approximation

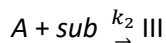
From the mechanism:

1. Ru : $[Ru(MA)_2(dppe)]$
2. A : $[Ru(\text{carboxylate})_2(dppe)]$
3. sub : Substrate (alkynol) (**1**)
4. CA : Carboxylic acid (**2**)
5. P : Product (**3**)

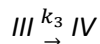
Step 1: Activation of the Ru precursor:



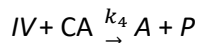
Step 2: Coordination of the substrate to **A** to form the vinylidene intermediate (**III**).



Step 3: Transformation to Intermediate (**IV**)



Step 4: Addition of carboxylic acid and product ejection / catalyst regeneration.



Equation 1 – Rate Law for Step 1: $Rate\ 1 = k_1[Ru]$

Equation 2 – Rate Law for Step 2: $Rate\ 2 = k_2[A][sub]$

Equation 3 – Rate Law for Step 3: $Rate\ 3 = k_3[III]$

Equation 4 – Rate Law for Step 4: $Rate\ 4 = k_4[IV][CA]$

Using the steady-state approximation for **III** and **IV**:

$$\text{For III: } \frac{d(III)}{dt} = Rate\ 2 - Rate\ 3 = 0$$

$$\text{Rearranging Equation (2) and Equation (3): } k_2[A][sub] = k_3[III]$$

$$\text{Equation 5} - [III] = \frac{k_2[A][sub]}{k_3}$$

$$\text{For IV: } \frac{d(IV)}{dt} = Rate\ 3 - Rate\ 4 = 0$$

$$\text{Since Rate 3 = Rate 4 - Rearranging Equation (3) and Equation (4): } k_3[III] = k_4[IV][CA]$$

$$\text{Substituting [III] into the equation for IV: } [IV] = k_3 \left(\frac{k_2[A][Sub]}{k_3} \right) = k_4[IV][CA]$$

$$\text{Equation 6} - [IV] = \left(k_2 \frac{[A][Sub]}{k_4[CA]} \right)$$

$$\text{Now, the overall rate at which the product is formed is Rate 4: } Rate_{overall} = k_4[IV][CA]$$

$$\text{Substituting [IV] from Equation (6) into Equation (4): } Rate_{overall} = k_4 \left(k_2 \frac{[A][Sub]}{k_4[CA]} \right) [CA]$$

Without assuming the rate determining step, the unbiased rate law derived from the mechanism and the steady state approximation is:

$$\text{Equation 7} - Rate_{overall} = k_2[A][Sub]$$

Applying the steady-state approximation to IV (a different intermediate prior to product formation):

The rate of formation of **IV** (from **Equation 3**):

$$\text{Equation 3 - Rate}_{\text{formation}} = \text{Rate 3} = k_3[\text{III}]$$

The rate of consumption of **IV** - Equation (4) Repeated:

$$\text{Rate}_{\text{consumption}} = \text{Rate 4} = k_4[\text{IV}][\text{CA}]$$

According to the steady-state approximation: **Equation 8** $-\frac{d(\text{IV})}{dt} = \text{Rate formation 3} - \text{Rate consumption 4} = 0$

$$k_3[\text{III}] - k_4[\text{IV}][\text{CA}] = 0 \rightarrow k_3[\text{III}] = k_4[\text{IV}][\text{CA}]$$

Now, from the steady-state approximation for **III**, we derived: $[\text{III}] = \left(k_2 \frac{[\text{A}][\text{Sub}]}{k_3}\right)$ (**Equation 5**)

Substitute this expression into the equation for **IV** from **Equation 8**:

$$\text{Equation 9: } k_3 \left(k_2 \frac{[\text{A}][\text{Sub}]}{k_3}\right) = k_4[\text{IV}][\text{CA}]$$

$$\text{This simplifies to: } k_2[\text{A}][\text{Sub}] = k_4[\text{IV}][\text{CA}] \rightarrow [\text{IV}] = k_2 \frac{[\text{A}][\text{Sub}]}{k_4[\text{CA}]}$$

The overall rate at which the product is formed is determined by Rate 4 (**Equation 4**):

$$\text{Rate}_{\text{overall}} = k_4[\text{IV}][\text{CA}]$$

Substitute our derived expression for **IV** from **Equation 9**:

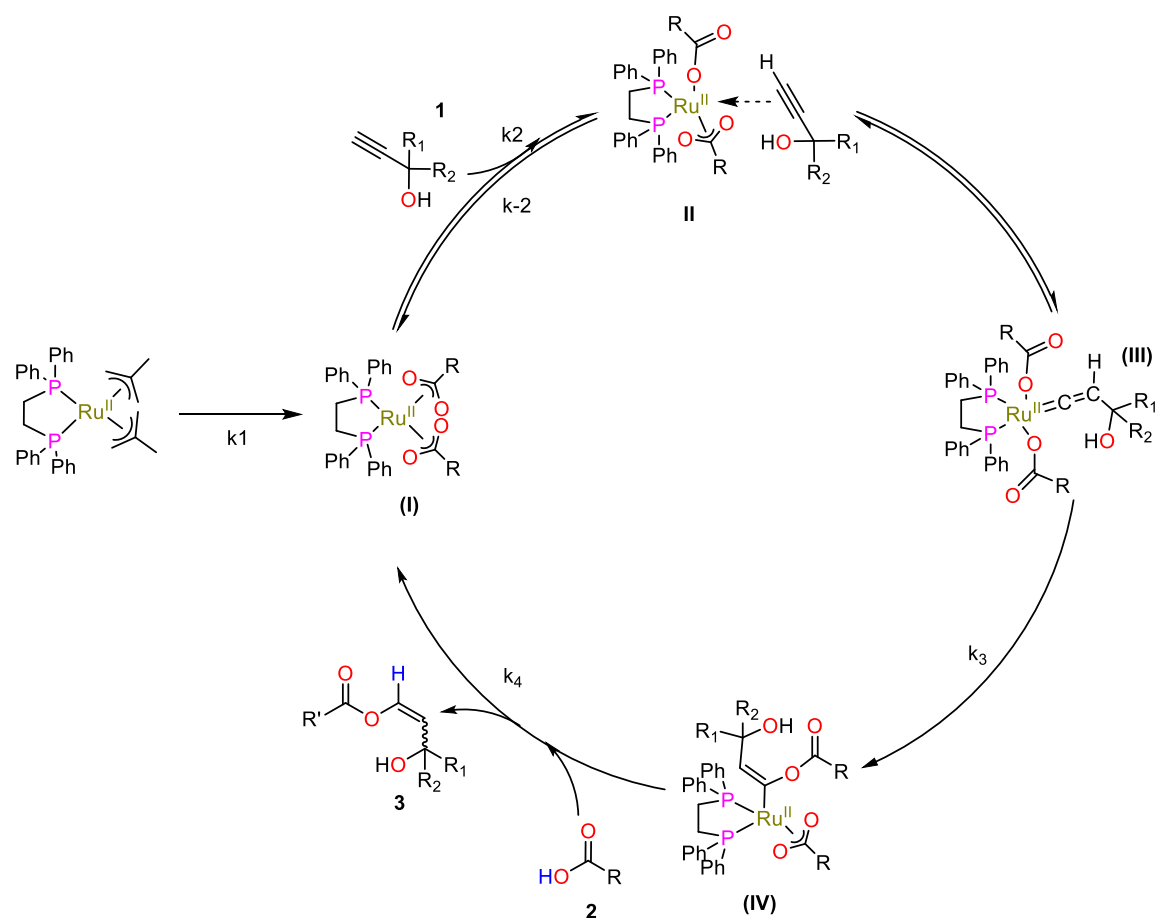
$$\text{Equation 10 - Rate}_{\text{overall}} = k_4 \left(k_2 \frac{[\text{A}][\text{Sub}]}{k_4[\text{CA}]}\right)[\text{CA}]$$

$$\text{This simplifies to: } \text{Rate}_{\text{overall}} = k_2[\text{A}][\text{Sub}]$$

This result is the same as the one we derived from the steady-state approximation for **III**. This demonstrates the internal consistency of the mechanism and shows that the rate law is robust to the choice of intermediate for which the steady-state approximation is applied.

4.9.2 Reversible literature mechanism

Revised Mechanism with reversibility for steps 2 and 3:



Step 1 (assumed irreversible): $Ru \xrightarrow{k_1} A$

Step 2 (reversible): $A + Sub \xrightleftharpoons[k_{-2}]{k_2} III$

Step 3: $III \xrightarrow{k_3} IV$

Step 4: $IV + CA \xrightarrow{k_4} A + P$

Rate Laws:

1. Rate 1 = $k_1[Ru]$ – **Equation 1** (repeated)
2. Rate 2_{formation} = $k_2[A][Sub]$ – **Equation 2** (repeated)
3. Rate 2_{dissociation} = $k_{-2}[III]$ – **Equation 11**
4. Rate 3 = $k_3[III]$ – **Equation 3** (repeated)
5. Rate 4 = $k_4[IV][CA]$ – **Equation 4** (repeated)

Steady-State Approximation for [III]: Given that the formation and consumption of **III** is in a steady state: **Equation 12** $\frac{d(\text{III})}{dt} = \text{Rate } 2_{\text{formation}} - \text{Rate } 2_{\text{dissociation}} - \text{Rate } 3 = 0$

Substituting in the rate laws: $k_2[A][\text{Sub}] - k_{-2}[\text{III}] - k_3[\text{III}] = 0$

From this equation, we can rearrange and isolate **[III]**: $[\text{III}] = k_2 \frac{[A][\text{sub}]}{k_{-2} + k_3}$

Solving for **[IV]**: **Equation 13** - $\frac{d(\text{IV})}{dt} = \text{Rate } 3 - \text{Rate } 4 = 0$

Substitute the rate laws: $k_3[\text{III}] = k_4[\text{IV}][\text{CA}]$

Substitute for **[III]** from **Equation 12**: $k_3 \left(k_2 \frac{[A][\text{sub}]}{k_{-2} + k_3} \right) = k_4[\text{IV}][\text{CA}]$

Equation 14 - Solve for **[IV]**: $k_3 \frac{k_2 k_2 [A][\text{sub}]}{(k_{-2} + k_3) k_4 [\text{CA}]}$

Overall Rate Law:

1. The overall rate is governed by Rate 4: $\text{Rate}_{\text{overall}} = k_4[\text{IV}][\text{CA}]$
2. Substitute for **[IV]** from **Equation 14**:

$$\text{Equation 15: } \text{Rate}_{\text{overall}} = k_4 \left(\frac{k_3 k_2 [A][\text{sub}]}{(k_{-2} + k_3) k_4 [\text{CA}]} \right) [\text{CA}]$$

3. Simplify: $\text{Rate}_{\text{overall}} = k_3 k_2 \frac{[A][\text{sub}]}{(k_{-2} + k_3)}$

This rate law indicates that the overall rate is dependent on the concentrations of **A** and **Sub**, as well as the forward and reverse rate constants for substrate coordination (k_2 and k_{-2}). The rate law also shows that the system's behaviour will be influenced by the relative magnitudes of k_{-2} and k_3 , with the latter not being influenced by the concentration of **CA** as it only appears in the last step.

If k_{-2} is much smaller than k_3 : This condition implies that once **III** is formed, it transforms rapidly to **IV** without significant reverse reaction back to **A + Sub**. Under this condition, the reverse rate $k_{-2}[\text{III}]$ becomes negligible compared to $k_3[\text{III}]$.

Therefore, with this approximation, $[\text{III}] \approx \left(k_2 \frac{[A][\text{sub}]}{(k_3)} \right)$

Considering Rate 4 governs the overall rate: $\text{Rate}_{\text{overall}} = k_4[\text{IV}][\text{CA}]$.

Since **IV** is formed from **III**, and assuming CA is in excess (its concentration doesn't significantly change), the rate of formation of **IV** can be approximated to be proportional to the rate at which **III** is formed, i.e., Rate 2.

Thus, under the assumption that $k_{-2} \ll k_3$ and CA is in excess, $\text{Rate}_{\text{overall}}$ simplifies to the rate of formation of **III**, which is $k_2[\text{A}][\text{Sub}]$.

The overall rate law, $\text{Rate}_{\text{overall}} \approx k_2[\text{A}][\text{Sub}]$, can be derived under the condition that the reverse reaction in step 2 is much slower than the forward reaction (i.e., k_{-2} is much smaller than k_3). Simplifying this allows us to focus on the forward reaction rates, particularly the rate of substrate coordination with **A**, as the main causes of the overall reaction rate.

4.10 Identification of reaction intermediates by $^{31}\text{P}\{^1\text{H}\}$ NMR

4.10.1 Precursor activation

a) With benzoic acid

Free acid = *

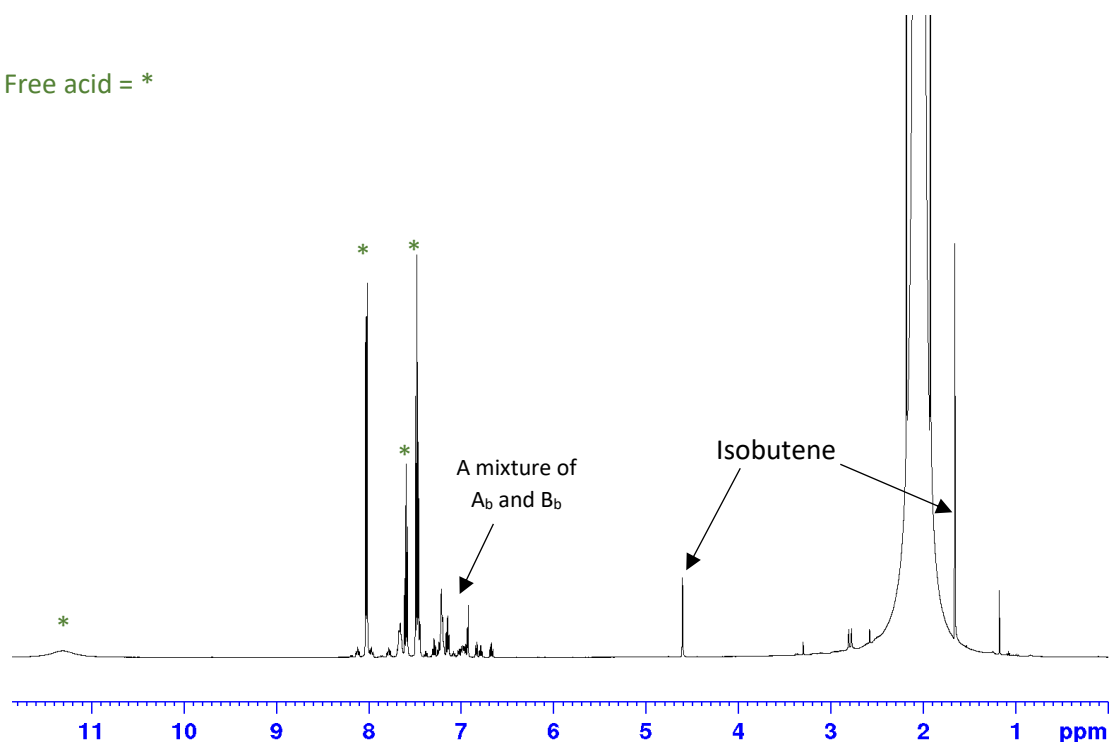


Figure S48. ^1H NMR spectrum showing a mixture of A_b , B_b , free benzoic acid and the liberation of isobutene after the addition of benzoic acid to $[(\text{dppe})\text{Ru}^{\text{II}}(\text{MA})_2]$ in acetone.

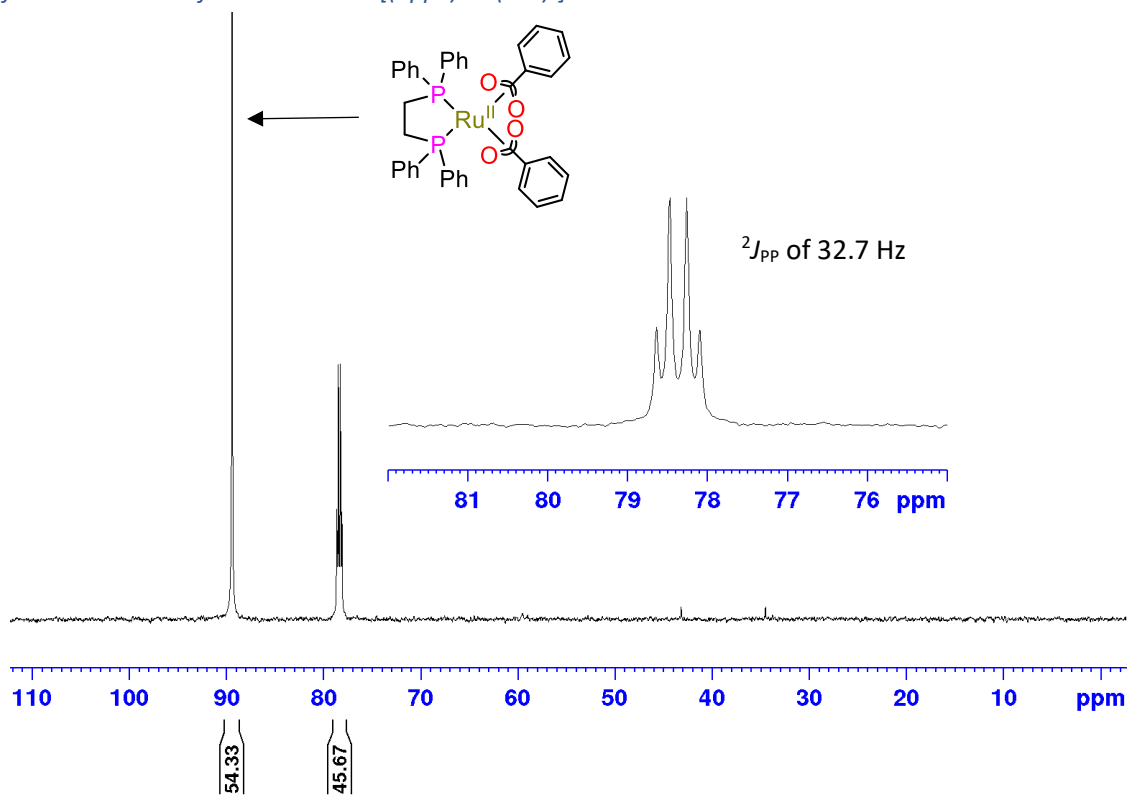


Figure S49. Quantitative $^{31}\text{P}\{^1\text{H}\}$ NMR (inverse-gated) showing a mixture of $[(\text{dppe})\text{Ru}^{\text{II}}(\eta^2\text{-O}_2\text{CPh})_2]$ (A_b) and $[(\text{dppe})\text{Ru}^{\text{II}}(\eta^2\text{-O}_2\text{CPh})(\eta^1\text{-O}_2\text{CPh})(\text{H}_2\text{O})]$ (B_b) in solution.

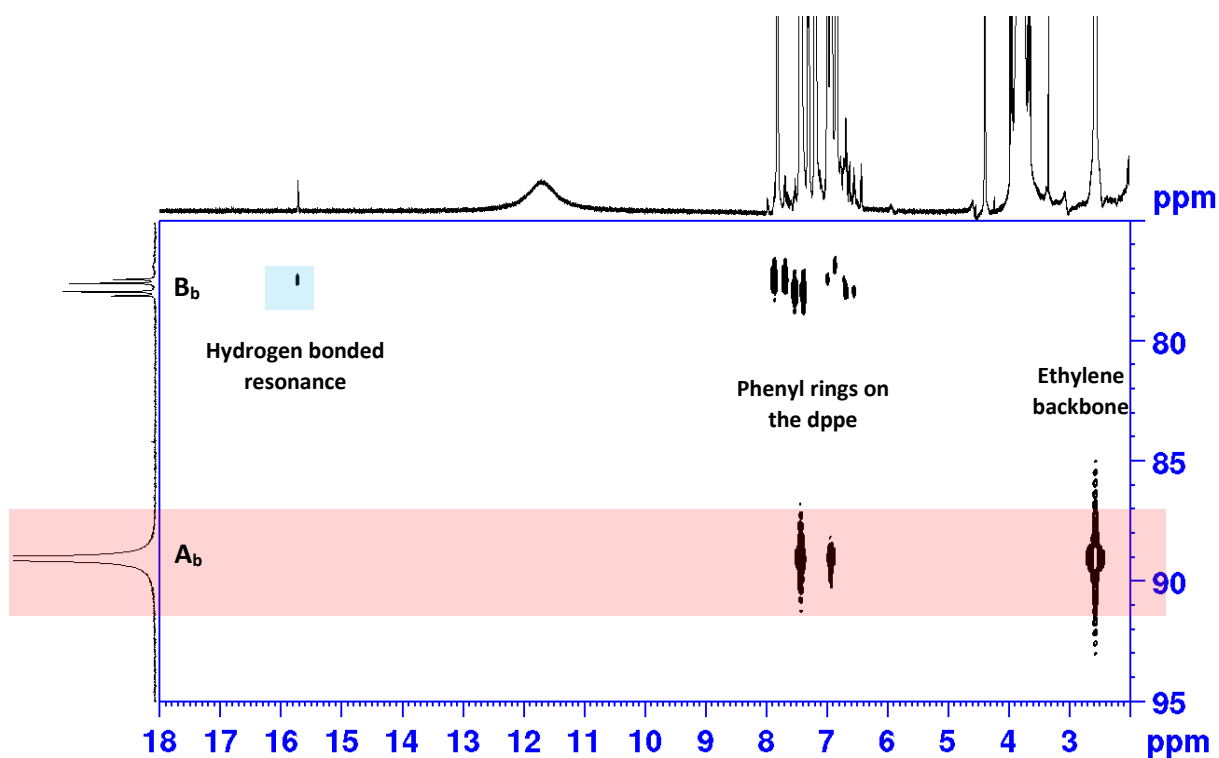


Figure S50. ^1H - ^{31}P HMBC after the addition of benzoic acid to $[(\text{dppe})\text{Ru}^{\text{II}}(\text{MA})_2]$ showing correlation assigned peaks of intermediates A_b and B_b in solution from the ^1H and $^{31}\text{P}\{^1\text{H}\}$ NMR.

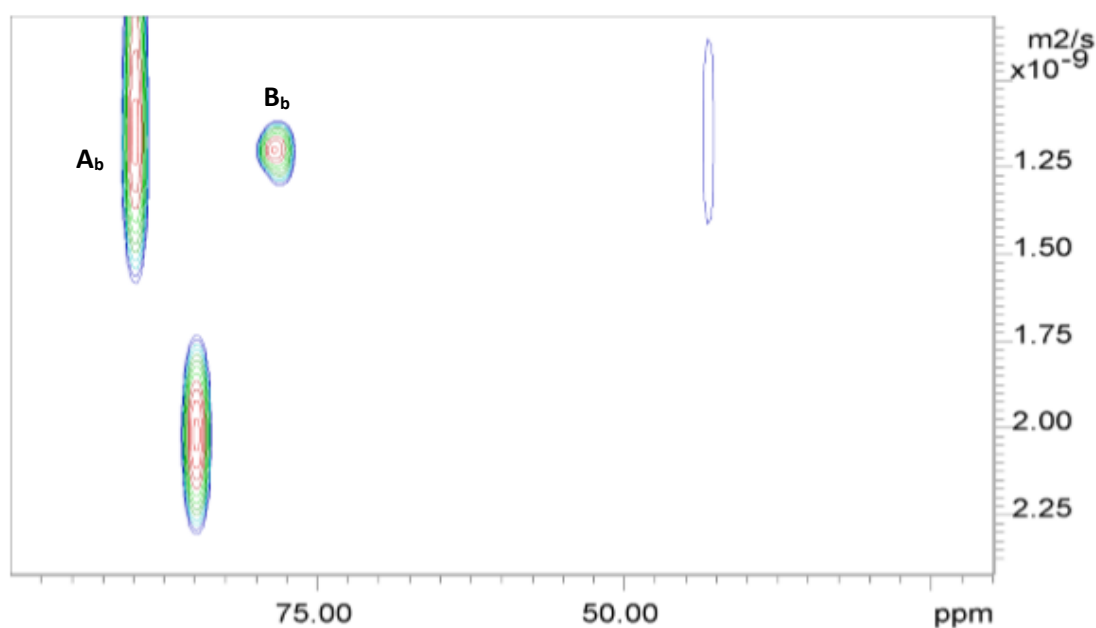


Figure S51. $^{31}\text{P}\{^1\text{H}\}$ DOSY, acquired 45 minutes after the addition of 2 eq. benzoic acid to $[(\text{dppe})\text{Ru}^{\text{II}}(\text{MA})_2]$, in ethyl acetate.

For the DOSY experiment, 64 scans were performed with a delay of 1 second and 0 dummy scans. The diffusion delay, Δ , was set to a value of 0.06 s, and the gradient pulse length, $\delta/2$, was set to 2000 μs . After acquisition, Fourier transform, phase and baseline correction in TopSpin, the diffusion data was processed in dynamics centre to obtain diffusion coefficients for $[(\text{dppe})\text{Ru}^{\text{II}}(\text{MA})_2]$, A_b and B_b .

Table S7. The effect of different amounts of moisture on the ratio of intermediate **A_b** and **B_b** in toluene once 2 equivalents of benzoic acid has been completely reacted with [(dppe)Ru^{II}(MA)₂] where the starting ratios of **A_b** and **B_b** were 98 and 2. Loading of moisture is in respect to [(dppe)Ru^{II}(MA)₂].

	2 equiv. of benzoic acid added to [(dppe)Ru ^{II} (MA) ₂]	
Loading of moisture (%)	A (%)	B (%)
0	98	2
5	73	26
10	70	30
25	60	40
50	53	47
100	27	73
1000	2	98

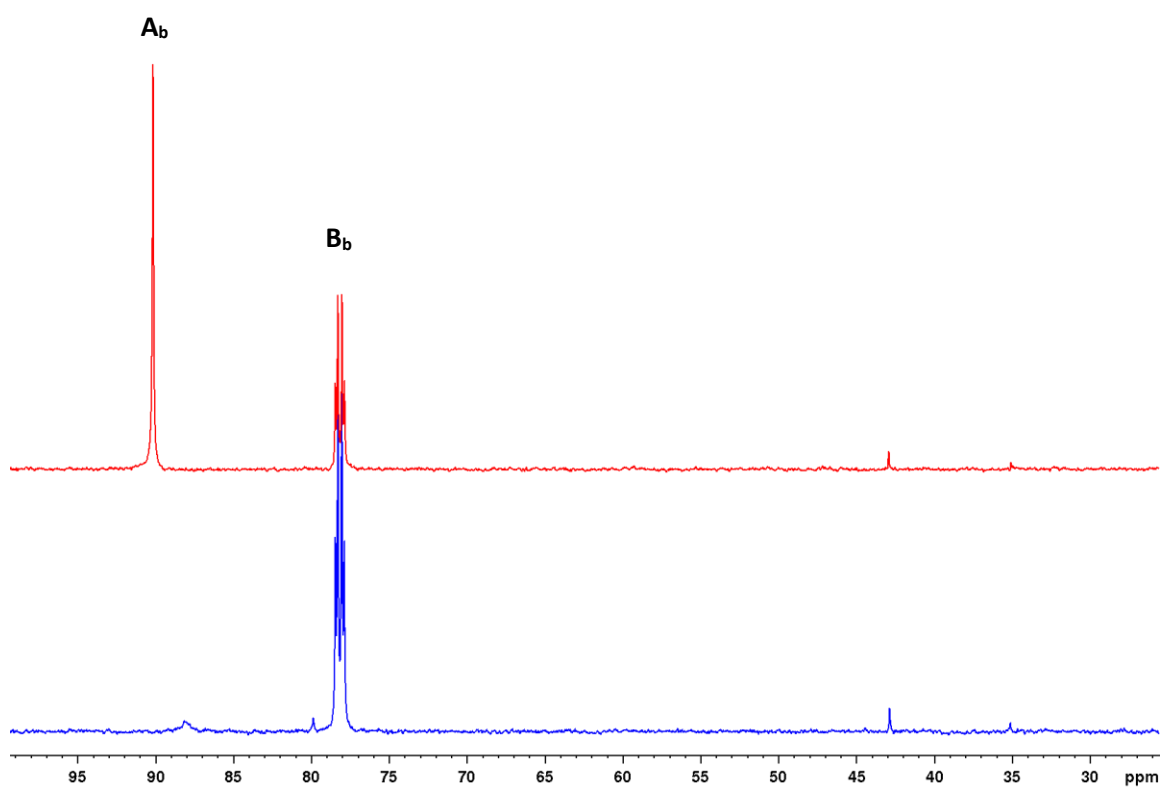


Figure S52. ³¹P{¹H} NMR showing the addition of H₂O to a ~1:1 mixture of **A_b** and **B_b** generated from [(dppe)Ru(MA)₂] and benzoic acid in acetone at room temperature resulting in the shift of distribution in favour of **B_b**

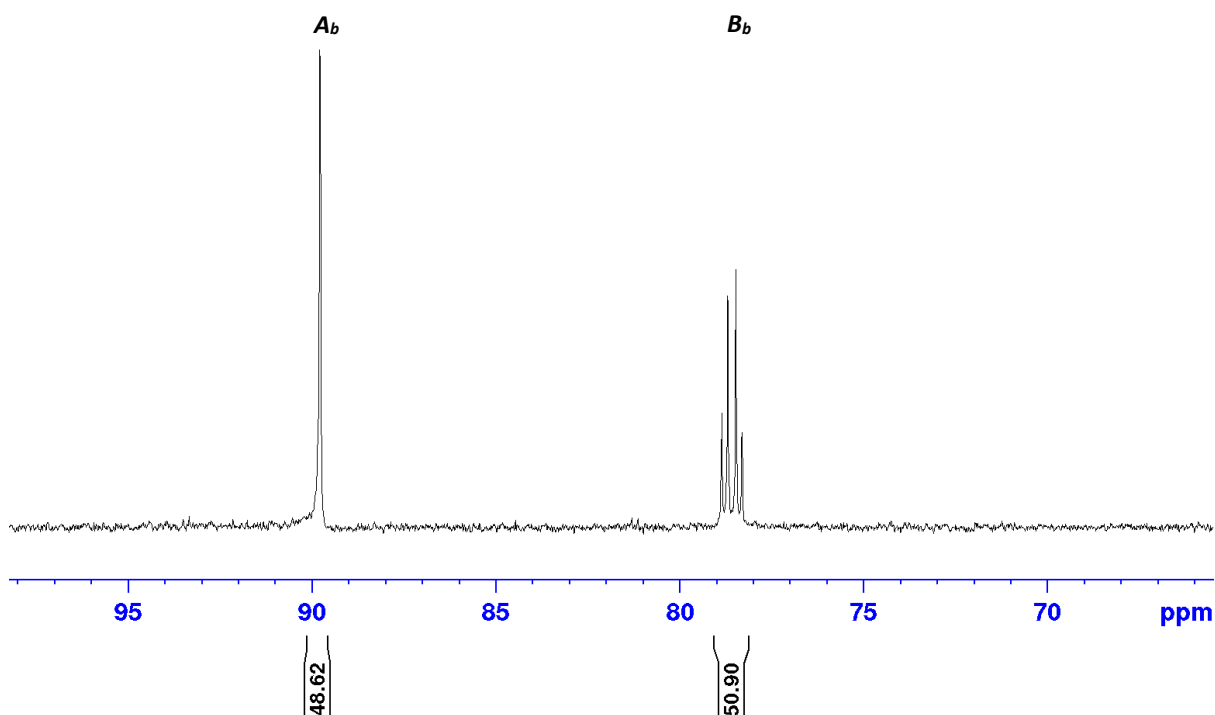


Figure S53. $^{31}\text{P}\{^1\text{H}\}$ NMR spectrum showing relative amounts of A_b $[(\text{dppe})\text{Ru}^{\text{II}}(\eta^2\text{-O}_2\text{CPh})_2]$ and B_b $[(\text{dppe})\text{Ru}^{\text{II}}(\eta^2\text{-O}_2\text{CPh})(\eta^1\text{-O}_2\text{CPh})(\text{H}_2\text{O})]$ resulting from the addition of 15 equiv of benzoic acid to $[(\text{dppe})\text{Ru}^{\text{II}}(\text{MA})_2]$.

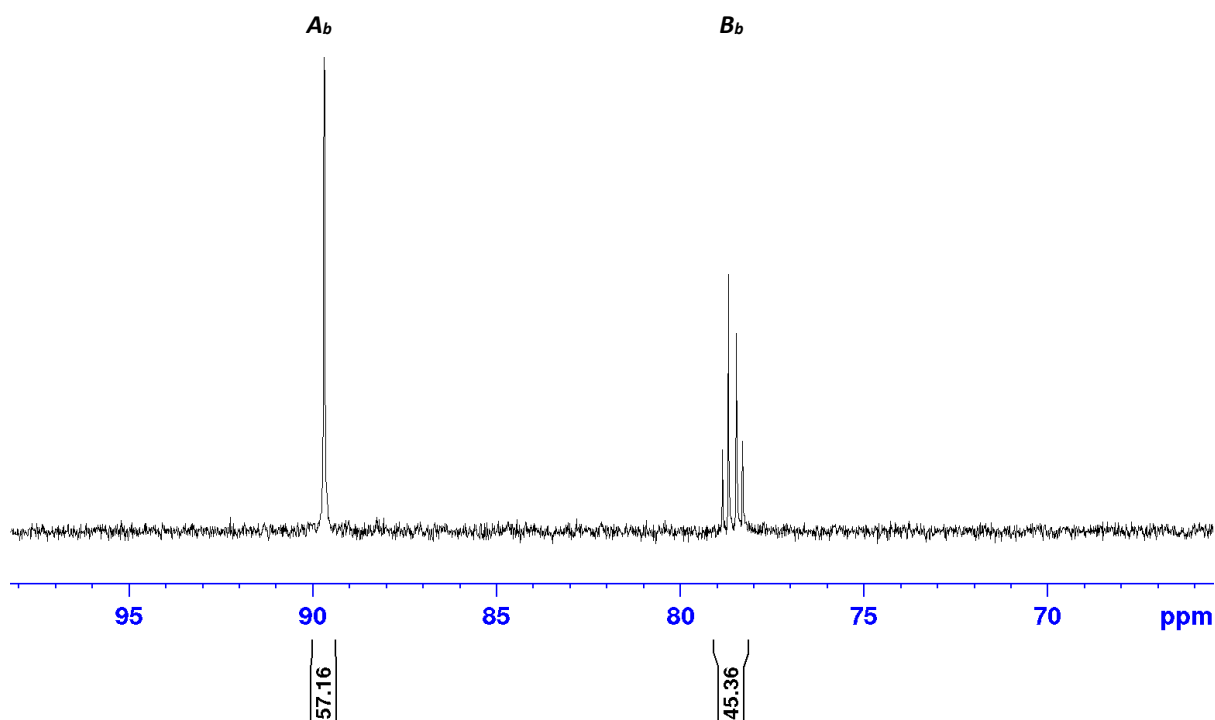


Figure S54. $^{31}\text{P}\{^1\text{H}\}$ NMR spectrum showing relative amounts of A_b $[(\text{dppe})\text{Ru}^{\text{II}}(\eta^2\text{-O}_2\text{CPh})_2]$ and B_b $[(\text{dppe})\text{Ru}^{\text{II}}(\eta^2\text{-O}_2\text{CPh})(\eta^1\text{-O}_2\text{CPh})(\text{H}_2\text{O})]$ from the addition of 11 equiv of benzoic acid and 2 equiv of benzoic anhydride to $[(\text{dppe})\text{Ru}^{\text{II}}(\text{MA})_2]$.

b) With pivalic acid and adamantane carboxylic acid

$^{31}\text{P}\{^1\text{H}\}$ T_1 of $[(\text{dppe})\text{Ru}^{\text{II}}(\text{MA})_2]$

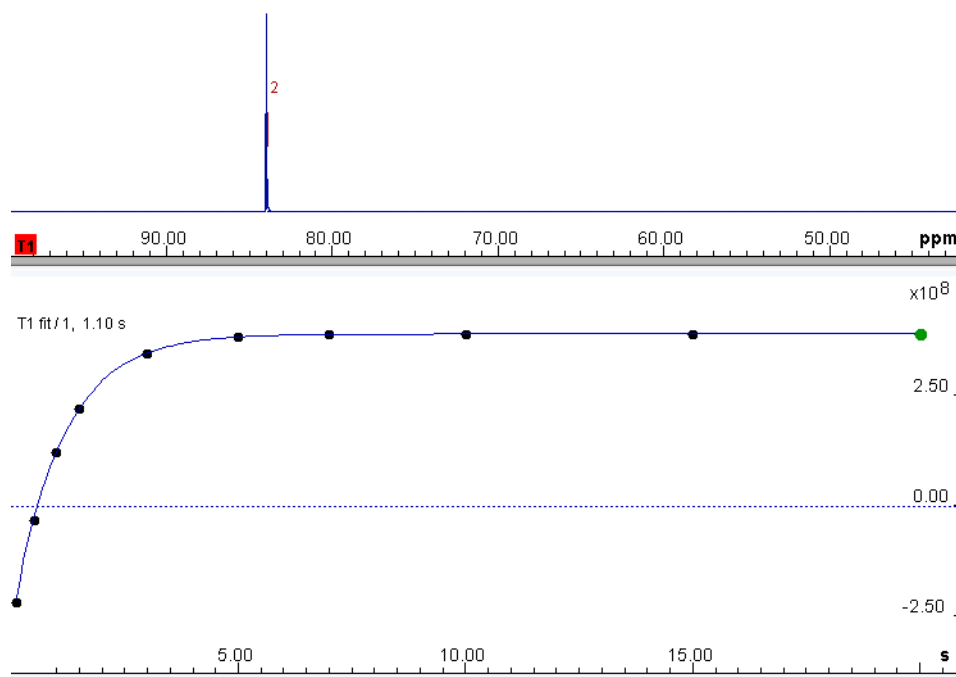


Figure S55. ^{31}P inversion recovery NMR experiment performed to obtain the T_1 value of $[(\text{dppe})\text{Ru}^{\text{II}}(\text{MA})_2]$ in acetone. Value of 1.1 s obtained.

$^{31}\text{P}\{^1\text{H}\}$ T_1 of $[(\text{dppe})\text{Ru}^{\text{II}}(\eta^2\text{-O}_2\text{C}^t\text{Bu})_2]$

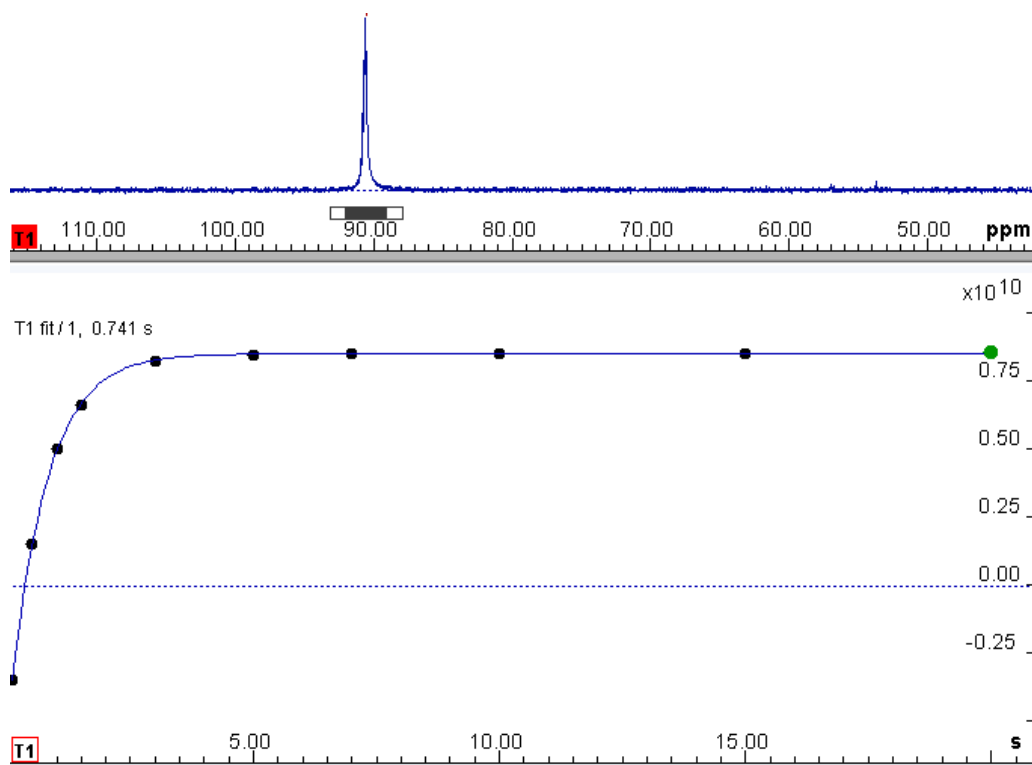


Figure S56. ^{31}P inversion recovery NMR experiment performed to obtain the T_1 value of A_p in acetone. Value of 0.74 s obtained.

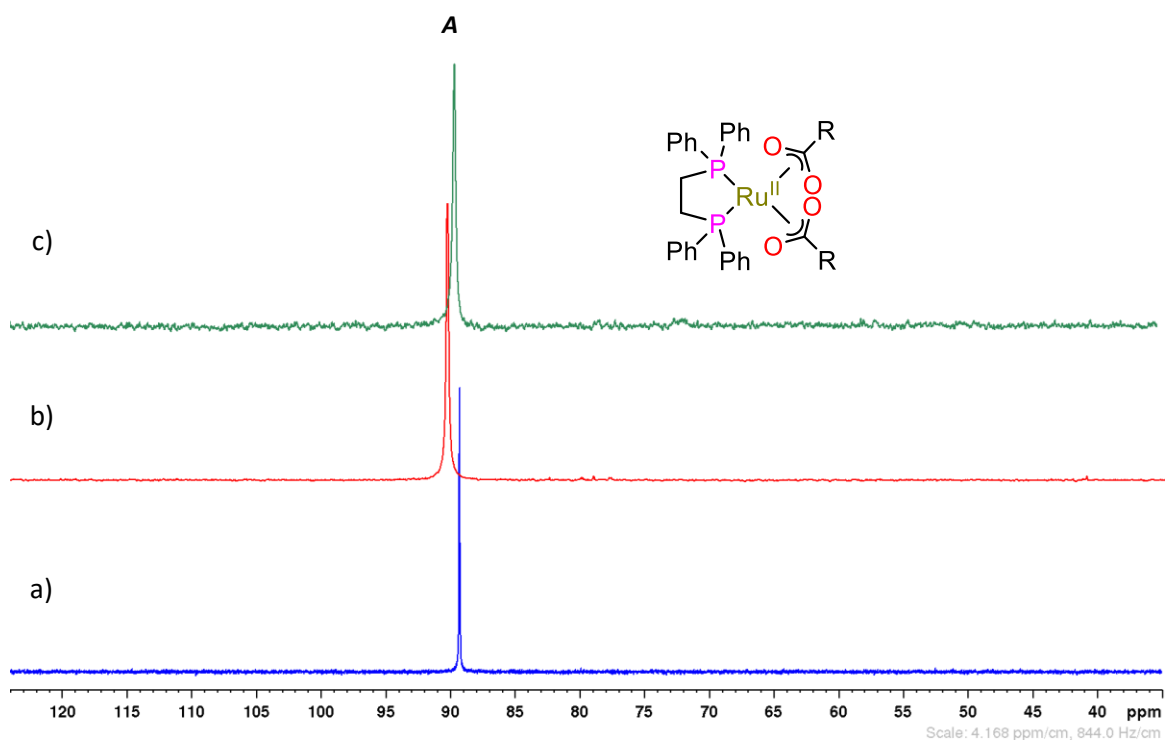


Figure S57. Stacked $^{31}\text{P}\{^1\text{H}\}$ NMR showing the formation of **A** using different carboxylic acids a) pivalic, b) acetic, c) adamantane carboxylic acids.

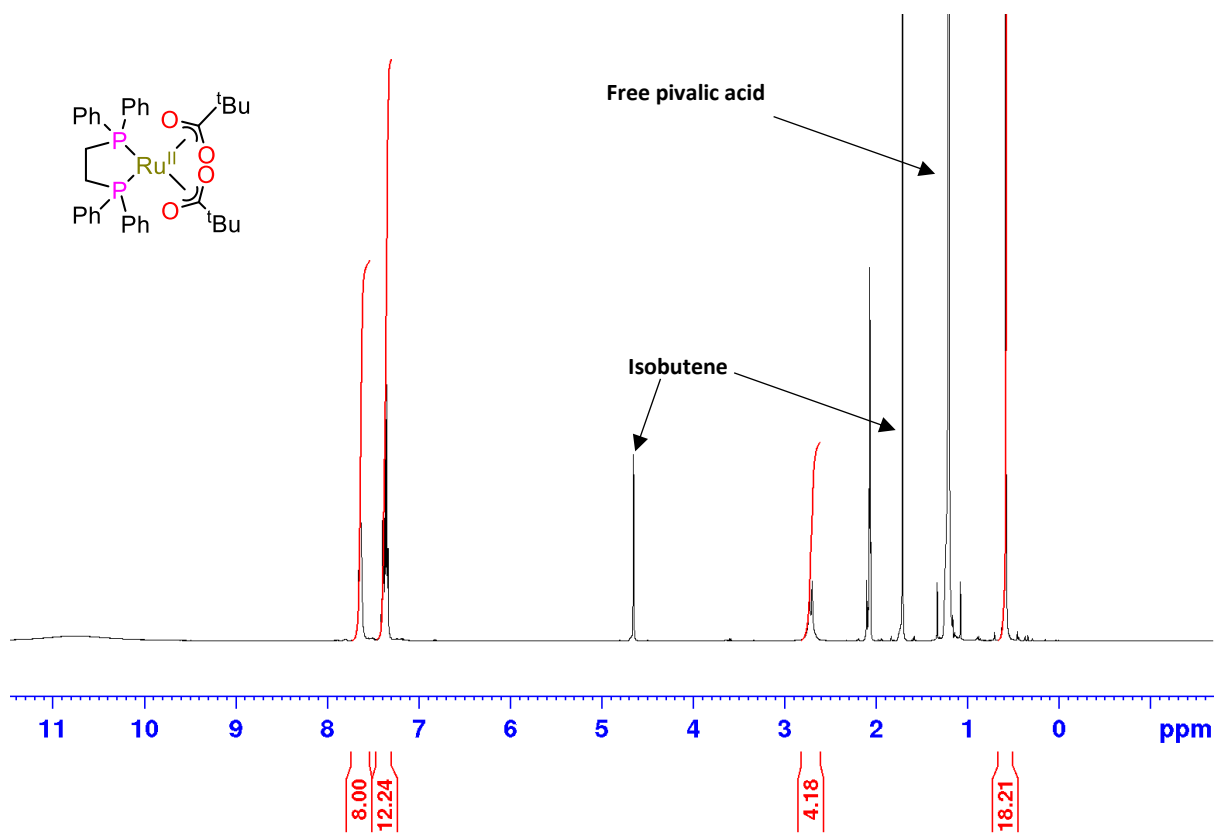


Figure S58. Exemplary ^1H NMR spectrum of the formation of A_p in $(\text{CD}_3)_2\text{CO}$.

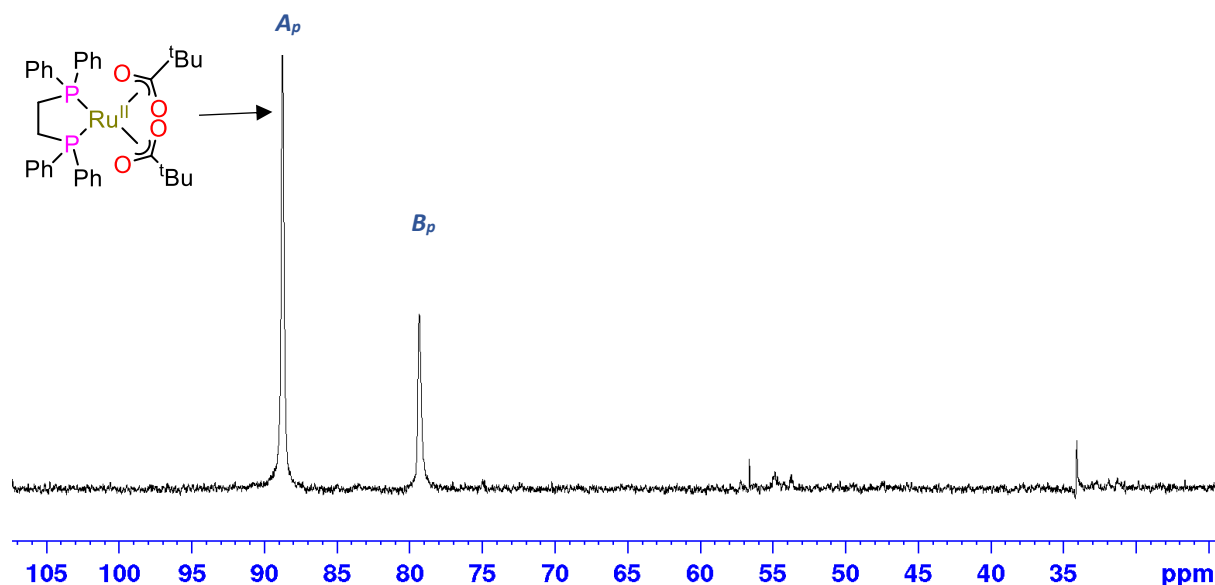


Figure S59. Exemplary $^{31}\text{P}\{^1\text{H}\}$ NMR spectrum observed after for the addition of H_2O to $[(\text{dppe})\text{Ru}^{\text{II}}(\eta^2\text{-O}_2\text{C}^t\text{Bu})_2]$ (A_p).

Table S8. A list of selected bond lengths from the crystallographic data to show how the central ruthenium atom is coordinated to the carboxylates in the various analogues of **A**, and to the methyl allyls in $[(\text{dppe})\text{Ru}(\text{MA})_2]$. Also showing selected C-O bond lengths. Refer to pages S45-S62 for corresponding labels. Similar structures for comparison angles and lengths can be found here.¹⁴

Compound	Selected bond lengths (Å):	Selected bond angles:
$[(\text{dppe})\text{Ru}(\text{MA})_2]$	Ru-P(2), 2.2941, Ru-P(1), 2.2951 Ru-C(28), 2.1794, Ru-C(32), 2.1811, Ru-C(31), 2.2158, Ru-C(27), 2.2367, Ru-C(29), 2.2422, Ru-C(33) 2.2610	P(2)-Ru-P(1), 85.684 C(28)-Ru-P(2), 108.67, C(32)-Ru-P(2), 126.40, C(31)-Ru-P(2), 93.17, C(27)-Ru-P(2), 91.26, C(29)- Ru-P(2), 88.26, C(33)-Ru-P(2), 157.72, C(28)-Ru- P(1), 128.12, C(32)-Ru-P(1), 108.05, C(31)-Ru- P(1), 90.72, C(27)-Ru-P(1), 95.33, C(29)-Ru-P(1), 159.78, C(33)-Ru-P(1), 87.85
A_p'	Ru-P, (1) 2.2336, Ru-P (2) 2.2198 Ru-O(1), 2.1021(16), Ru-O (2) 2.2438 O(1)-C(3), 1.273(3), O(2)-C(3), 1.261(3), O(3)-C(8), 1.240(3), O(4)- C(8), 1.282(3), O(5)-C(13), 1.254(3), O(6)-C(13), 1.265(3) O(4)-H(4), 0.858(19)	P(2)-Ru-P(1), 84.81, O(1)-Ru-P(1), 105.13, O(3)-Ru-P(1), 96.33, P(2)- Ru-O(2), 95.78, P(1)-Ru-O(2), 165.35
A_{ad}'	Ru-P(2), 2.2185, Ru-P(1), 2.2199 Ru-O(1A), 2.021, Ru-O(6), 2.1024, Ru-O(1), 2.1104(19), Ru-O(3), 2.1743, Ru-O(5), 2.2203,	P(2)-Ru-P(1), 85.320 O(1A)-Ru-O(6) 155.2, O(6)-Ru-O(1), 170.16, O(1A)-Ru-O(3), 87.8, O(6)-Ru-O(3), 82.25, O(1)- Ru-O(3), 94.08, O(1A)-Ru-O(5), 95.9, O(6)-Ru- O(5), 60.67, O(1)-Ru-O(5), 110.03, O(3)-Ru-O(5),

	O(3)-C(38), 1.224, O(4)-C(38), 1.289, O(5)-C(49), 1.265, O(6)-C(49), 1.276, O(1)-C(27), 1.261, O(2)-C(27), 1.255	84.92 O(1A)-Ru-P(2), 99.6, O(6)-Ru-P(2), 103.85, O(1)-Ru-P(2), 85.52, O(3)-Ru-P(2), 94.93, O(1A)-Ru-P(1), 92.7, O(6)-Ru-P(1), 97.13, O(1)-Ru-P(1), 86.52, O(3)-Ru-P(1), 179.37, P(2)-Ru-O(5), 164.44, P(1)-Ru-O(5), 94.68
B_p'	Ru-P(2), 2.2401, Ru-P(1), 2.2479 Ru-O(3), 2.0824, Ru-O(1), 2.1065 O(1)-C(27), 1.2689, O(2)-C(27), 1.2488, O(3)-C(32), 1.2571, O(4)-C(32), 1.2582 O(5)-H(5), 0.83, O(5)-H(5), 1, 0.83	O(3)-Ru-O(1), 172.79, O(3)-Ru-O(5), 90.95 O(3)-Ru-P(2), 97.70, O(1)-Ru-P(2), 88.91, O(5)-Ru-P(2), 92.78
B_{ad}'	Ru(1)-P(2), 2.234, Ru(1)-P(1), 2.249, Ru(2)-P(3), 2.240, Ru(2)-P(4), 2.246, Ru(1)-O(4), 2.076, Ru(1)-O(5), 2.100, Ru(1)-O(1), 2.177, Ru(1)-O(9), 2.208, Ru(2)-O(7), 2.082, Ru(2)-O(2), 2.083, Ru(2)-O(3), 2.164, Ru(2)-O(9), 2.197, P(1)-C(9), 1.838, P(1)-C(3), 1.839, P(1)-C(2), 1.851, P(2)-C(21), 1.830, P(2)-C(1), 1.831, P(2)-C(15), 1.847, P(3)-C(29), 1.836, O(1)-C(53), 1.217, O(2)-C(53), 1.263, O(3)-C(64), 1.256, O(4)-C(64), 1.270, O(5)-C(75), 1.262, O(6)-C(75), 1.259, O(7)-C(86), 1.264, O(8)-C(86), 1.268	P(2)-Ru(1)-P(1) O(4)-Ru(1)-O(5), 176.8, O(4)-Ru(1)-O(1), 96.2, O(5)-Ru(1)-O(1), 84.7, O(4)-Ru(1)-O(9), 91.4, O(5)-Ru(1)-O(9), 91.8, O(1)-Ru(1)-O(9), 83.9, O-Ru(2)-O(2), 177.9, O(7)-Ru(2)-O(3), 86.5, O(2)-Ru(2)-O(3), 95.0, O(7)-Ru(2)-O(9), 90.5, O(2)-Ru(2)-O(9), 91.1, O(3)-Ru(2)-O(9), 86.0 O(4)-Ru(1)-P(2), 89.04, O(5)-Ru(1)-P(2), 87.90, O(1)-Ru(1)-P(2), 89.7, O(9)-Ru(1)-P(2), 173.62, O(4)-Ru(1)-P(1), 86.47, O(5)-Ru(1)-P(1), 92.34, O(1)-Ru(1)-P(1), 173.6, O(9)-Ru(1)-P(1), 101.86, 84.52, O(7)-Ru(2)-P(3), 89.85, O(2)-Ru(2)-P(3), 88.71, O(3)-Ru(2)-P(3), 88.83, O(9)-Ru(2)-P(3), 174.83, O(7)-Ru(2)-P(4), 86.53, O(2)-Ru(2)-P(4), 91.74, O(3)-Ru(2)-P(4), 170.0, O(9)-Ru(2)-P(4), 101.25, P(3)-Ru(2)-P(4), 83.92
B_b'	Ru(1)-P(2), 2.2351, Ru(1)-P(1), 2.2466, Ru(2)-P(3), 2.2293, Ru(2)-P(4), 2.2387, Ru(1)-O(1), 2.070, Ru(1)-O(7), 2.106, Ru(1)-O(3), 2.171, Ru(1)-O(9), 2.181, Ru(2)-O(4), 2.077, Ru(2)-O(5), 2.102, Ru(2)-O(2), 2.181, Ru(2)-O(9), 2.181 O(1)-C(53), 1.260, O(2)-C(53), 1.241, O(3)-C(60), 1.251, O(4)-C(60), 1.260, O(5)-C(67), 1.263, O(6)-C(67), 1.250, O(7)-C(74), 1.269, O(8)-C(74), 1.251	P(3)-Ru(2)-P(4), 84.23, P(2)-Ru(1)-P(1), 85.04 O(1)-Ru(1)-O(7), 176.74, O(1)-Ru(1)-O(3), 88.80, O(7)-Ru(1)-O(3), 88.76, O(1)-Ru(1)-O(9), 91.18, O(7)-Ru(1)-O(9), 90.96, O(3)-Ru(1)-O(9), 89.38, O(4)-Ru(2)-O(5), 176.68, O(4)-Ru(2)-O(2), 89.26, O(5)-Ru(2)-O(2), 88.27, O(4)-Ru(2)-O(9), 91.40, O(5)-Ru(2)-O(9), 90.65, O(2)-Ru(2)-O(9), O(1)-Ru(1)-P(2), 89.75, O(7)-Ru(1)-P(2), 88.09, O(3)-Ru(1)-P(2), 90.19, O(9)-Ru(1)-P(2), 178.96,

		O(1)-Ru(1)-P(1), 93.81, O(7)-Ru(1)-P(1), 88.44, O(3)-Ru(1)-P(1), 174.55, O(9)-Ru(1)-P(1), 95.35, 86.24, O(4)-Ru(2)-P(3), 96.62, O(5)-Ru(2)-P(3), 85.68, O(2)-Ru(2)-P(3), 172.67, O(9)-Ru(2)-P(3), 97.94, O(4)-Ru(2)-P(4), 87.82, O(5)-Ru(2)-P(4), 90.04
Bif'	Ru(1)-P(2), 2.2353, Ru(1)-P(1), 2.2413, Ru(2)-P(4), 2.2423, Ru(2)-P(3), 2.2339 Ru(1)-O(6), 2.086, Ru(1)-O(5), 2.089, Ru(1)-O(3), 2.207, Ru(1)-O(1), 2.218, Ru(2)-O(2), 2.077, Ru(2)-O(8), 2.107, Ru(2)-O(4), 2.187, Ru(2)-O(1), 2.221, O(1)-H(1C), 0.87, O(1)-H(1D), 0.86	P(3)-Ru(2)-P(4), 84.54 O(6)-Ru(1)-O(5), 174.27, O(6)-Ru(1)-O(3), 82.51, O(5)-Ru(1)-O(3), 2.70, O(6)-Ru(1)-O(1), 91.99, O(5)-Ru(1)-O(1), 90.55, O(3)-Ru(1)-O(1), 83.12, (2)-Ru(2)-O(1), 86.39, O(8)-Ru(2)-O(1), 89.97, O(4)-Ru(2)-O(1), 90.05, O(2)-Ru(2)-P(3), 97.03

4.10.2 Monitoring catalyst speciation under catalytic conditions using $^{31}\text{P}\{^1\text{H}\}$ NMR

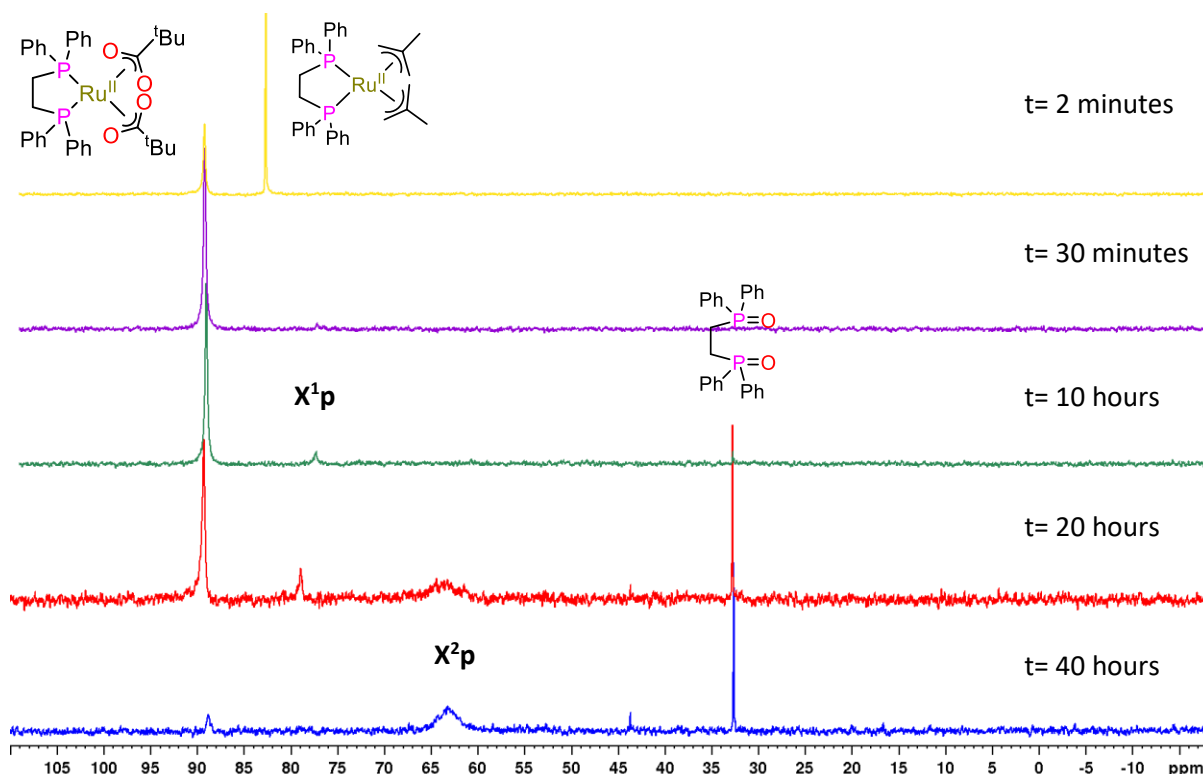


Figure S60. Exemplary $^{31}\text{P}\{^1\text{H}\}$ FlowNMR spectra showing the reaction progress of the Ru-mediated transformation of ethynyl- β -ionol (0.66 M) with pivalic acid (0.73 M) and pivalic anhydride (0.14 M) forming **3ab** catalysed by $[(\text{dppe})\text{Ru}(\text{MA})_2]$ (1 mol%) in anhydrous acetone (15 mL) at 20 °C. Clearly depicting the consumption of A_p over time and the formation of other reaction species. Determined from $^{31}\text{P}\{^1\text{H}\}$ FlowNMR spectroscopy, acquired at 4 mL/min.

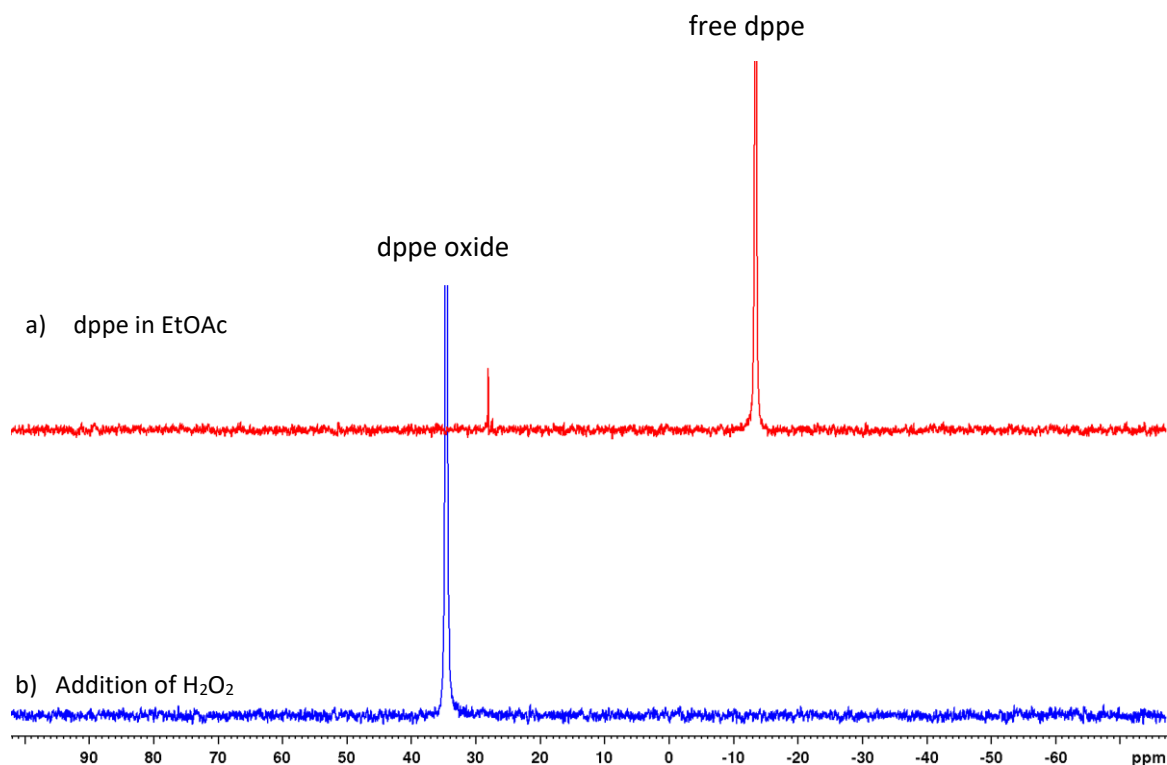


Figure S61. Stacked $^{31}\text{P}\{^1\text{H}\}$ NMR showing a) dppe in EtOAc and b) after addition of H_2O_2 to form dppe oxide.

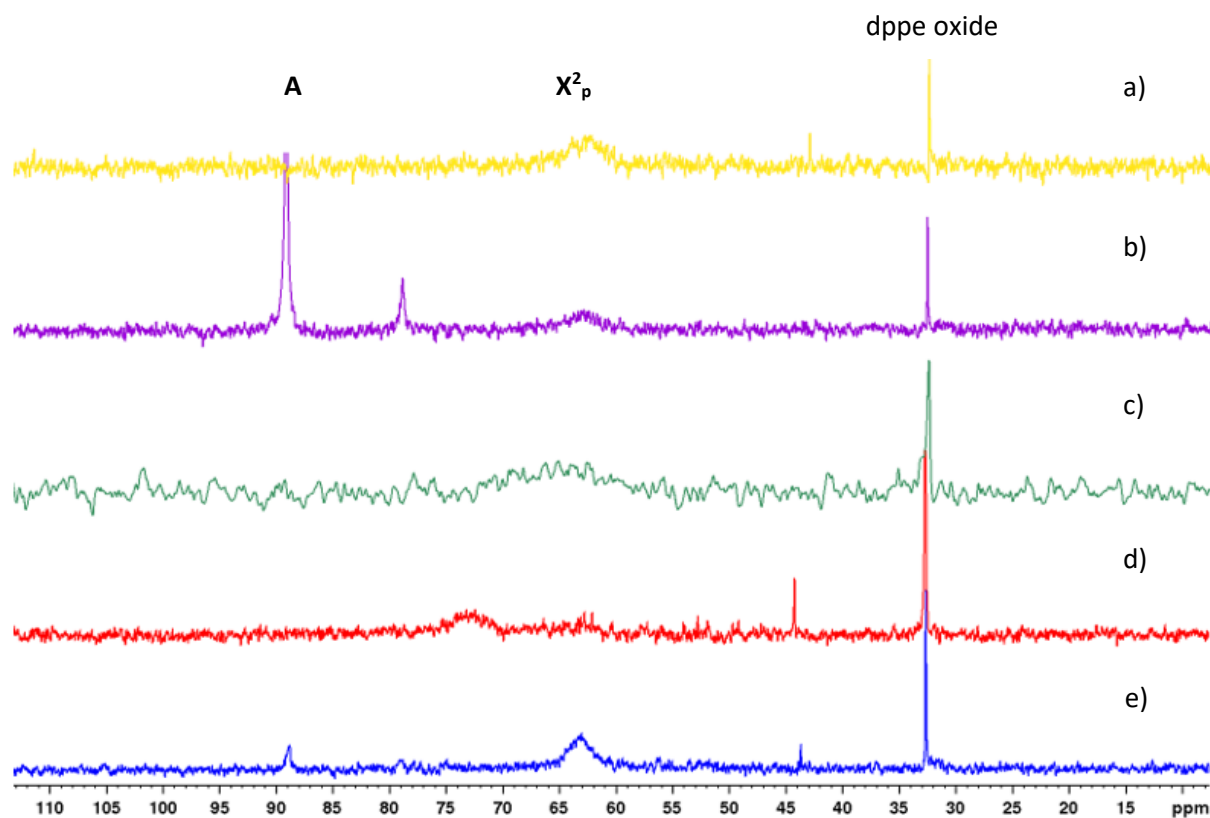


Figure S62. Stacked $^{31}\text{P}\{^1\text{H}\}$ NMR showing the reaction progress of the Ru-mediated transformation of ethynyl- β -ionol (0.66 M) using pivalic acid under different conditions, recorded at 30 h under inert atmosphere at rt unless stated: a) in acetone with pivalic acid (1 M) at 1 mol% catalyst, b) with phenylacetylene in acetone with pivalic acid (0.66 M) and pivalic anhydride (0.17 M) at 1 mol% catalyst, c) in acetone with pivalic acid (1 M) at 0.5 mol% catalyst, d) in ethyl acetate with pivalic acid (1 M) at 1 mol% catalyst, e) in acetone with pivalic acid (0.66 M) and pivalic anhydride (0.17 M) at 0.5 mol% catalyst. Determined from $^{31}\text{P}\{^1\text{H}\}$ FlowNMR, acquired at 4 mL/min.

4.10.3 Deactivation pathways

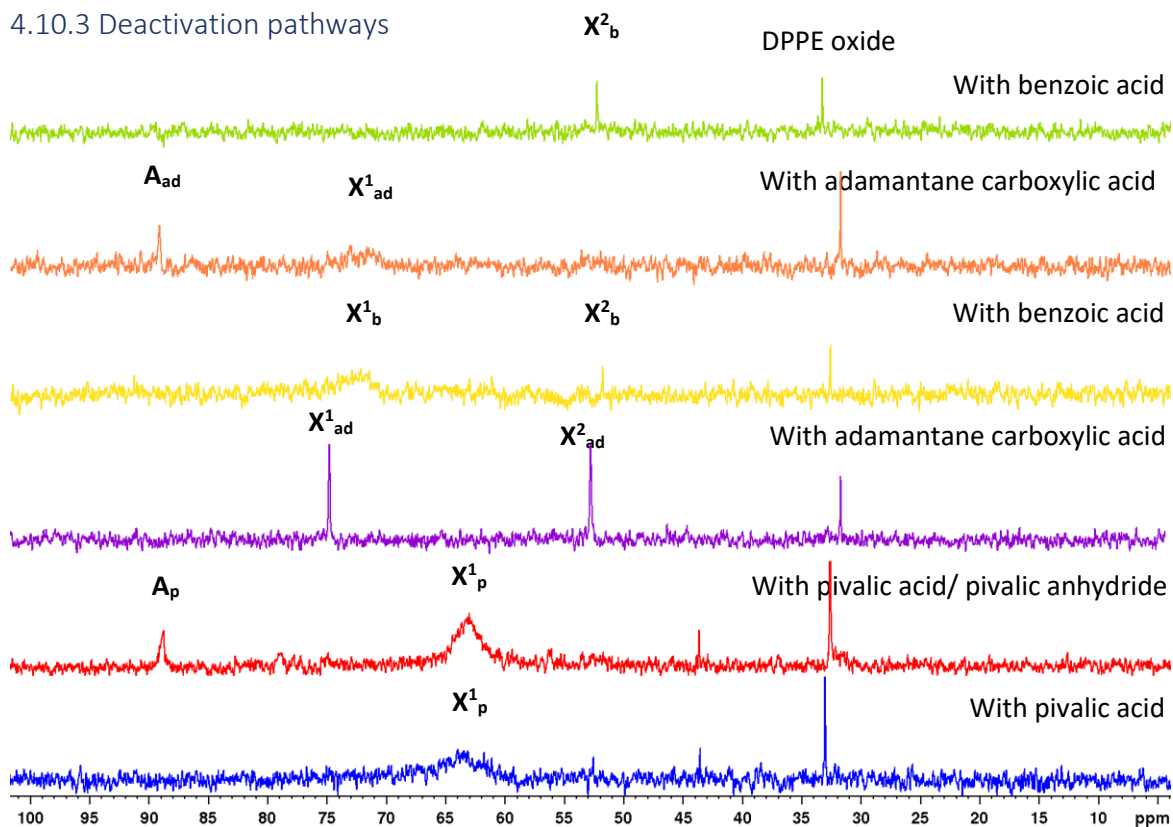


Figure S63. Stacked $^{31}\text{P}\{^1\text{H}\}$ NMR showing the reaction progress of the Ru-mediated transformation of ethynyl- β -ionol (0.66 M) with various carboxylic acids catalysed by $[(\text{dppe})\text{Ru}(\text{MA})_2]$ in anhydrous acetone (15 mL) at 20 °C after 40 hours. Determined from $^{31}\text{P}\{^1\text{H}\}$ FlowNMR spectroscopy, acquired at 4 mL/min.

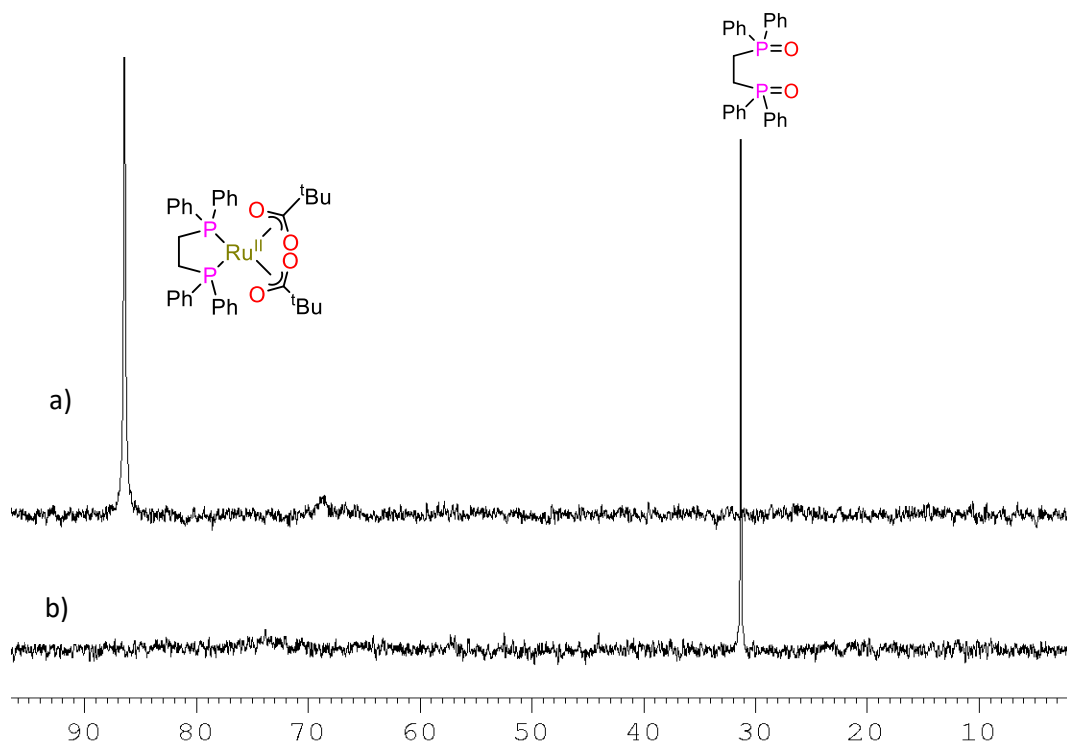


Figure S64. $^{31}\text{P}\{^1\text{H}\}$ NMR stack plot showing a) A_{p} under inert atmosphere b) A_{p} opened to air after 48 hours.

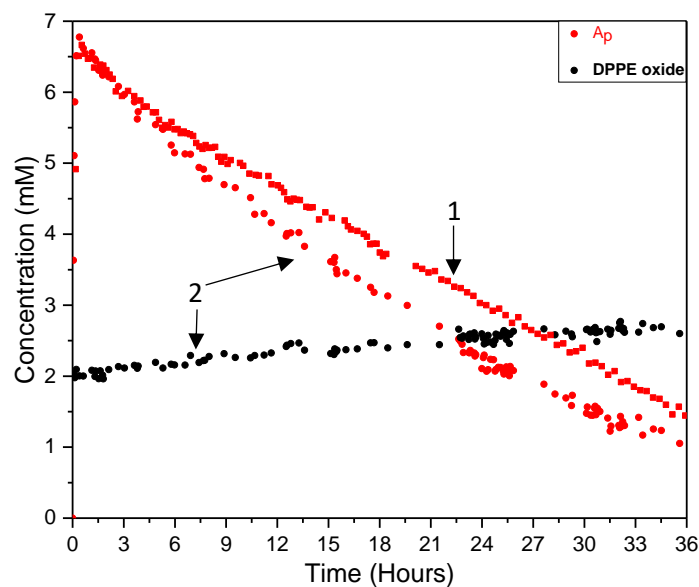


Figure S65. $^{31}\text{P}\{^1\text{H}\}$ NMR concentration profiles showing the comparison of the consumption of A_p with the addition of 2 mM of DPPE oxide at the start of the reaction (1) and without (2) to a reaction solution of ethynyl- β -ionol (0.66 M) with pivalic acid (0.73 M) and pivalic anhydride (0.13 M) catalysed by $[(\text{dppe})\text{Ru}(\text{MA})_2]$ (1 mol%) in anhydrous acetone (15 mL) at 20 °C. Determined by quantitative $^{31}\text{P}\{^1\text{H}\}$ FlowNMR spectroscopy at 4 mL/min.

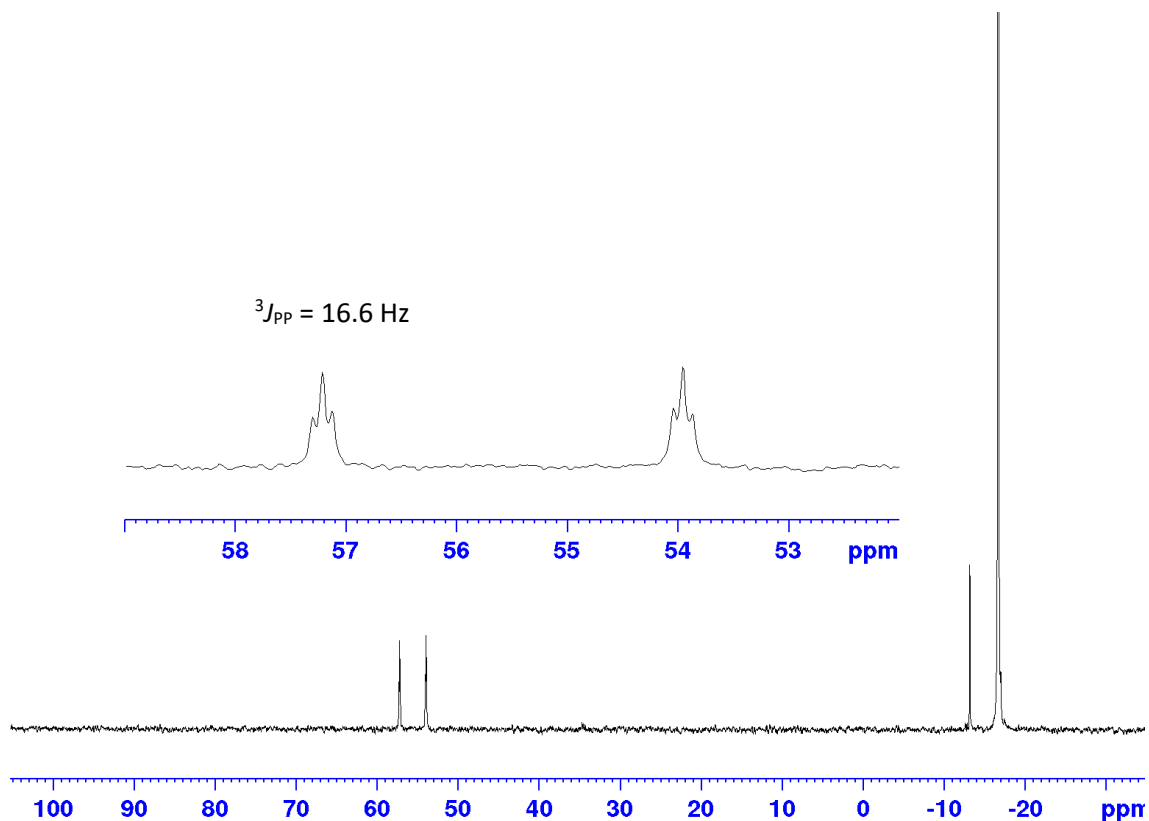


Figure S66. $^{31}\text{P}\{^1\text{H}\}$ NMR spectrum showing the formation of two mutually coupling triplets at 54.0 ppm and 57.2 ppm in the Ru-mediated transformation of ethynyl- β -ionol (0.66 M) with pivalic acid (0.1 M) catalysed by $[(\text{dppe})\text{Ru}(\text{MA})_2]$ (0.5 mol%) in anhydrous acetone (15 mL) at 20 °C with at 0.5 equiv. of DPPE added at the start of the reaction, resulting in no product yield observed. Peak at -13 ppm shows free dppe present and tri-*o*-tolyl phosphate at -16 ppm.

Table S9. Comparison of the crystallographic data of selected bond lengths of $[(dppe)Ru^{II}(\eta^2-O_2CPh)_2(CO)(H_2O)]$ and $[(dppe)Ru^{II}(\eta^2-O_2CPh)_2(CO)_2]$. Refer to pages S45-S62 for corresponding labels.¹¹

Compound	Selected bond lengths:	Selected bond angles:
$X^2_b \cdot H_2O$	Ru-C(41) 1.839, Ru-O(3) 2.1226, Ru-O(1) 2.1436, Ru-O(6) 2.1820, O(6)-H(6A) 0.82, O(6)-H(6B) 0.95 Ru-P(1) 2.2799, Ru-P(2) 2.2856,	C(41)-Ru-O(3) 174.22, C(41)-Ru-O(1), C(41)-Ru-O(6) 95.88 O(3)-Ru-O(1) 87.13, O(3)-Ru-O(6) 89.51, O(1)-Ru-O(6) 87.42 C(41)-Ru-P(1) 94.07, C(41)-Ru-P(2) 85.99 O(3)-Ru-P(1) 83.55, O(1)-Ru-P(1) 170.67, O(6)-Ru-P(1) 92.95, O(3)-Ru-P(2) 88.57, O(1)-Ru-P(2) 93.83, O(6)-Ru-P(2) 177.66 P(1)-Ru-P(2) 85.49
X^2_b	Ru-C(21) 1.919(2), Ru-C(21) 1.919(2) Ru-O(1) 2.0750, Ru-O(1) 2.0751, Ru-P 2.3988, Ru-P 2.3988, O(1)-C(14) 1.293, O(2)-C(14) 1.227, O(3)-C(21) 1.136	C(21)-Ru-C(21) 91.02(14), C(21)-Ru-O(1) 93.40(11), C(21)-Ru-O(1) 95.12(11), C(21)-Ru-O(1) 95.13(11), C(21)-Ru-O(1) 93.40 (11), O(1)-Ru-O(1) 167.82(9), O(1)-Ru-P 84.58(5), O(1)-Ru-P 86.29(5) C(21)-Ru-P 93.09(7), C(21)-Ru-P 175.89(7), C(21)-Ru-P 175.89(7), C(21)-Ru-P#1 93.09(7), O(1)-Ru-P#1 86.29(5), O(1)#1-Ru-P#1 84.58(5) P-Ru-P#1 82.81(3), C(2)-P-Ru 119.72, C(8)-P-Ru 115.09, C(1)-P-Ru 106.57 C(14)-O(1)-Ru 122.63

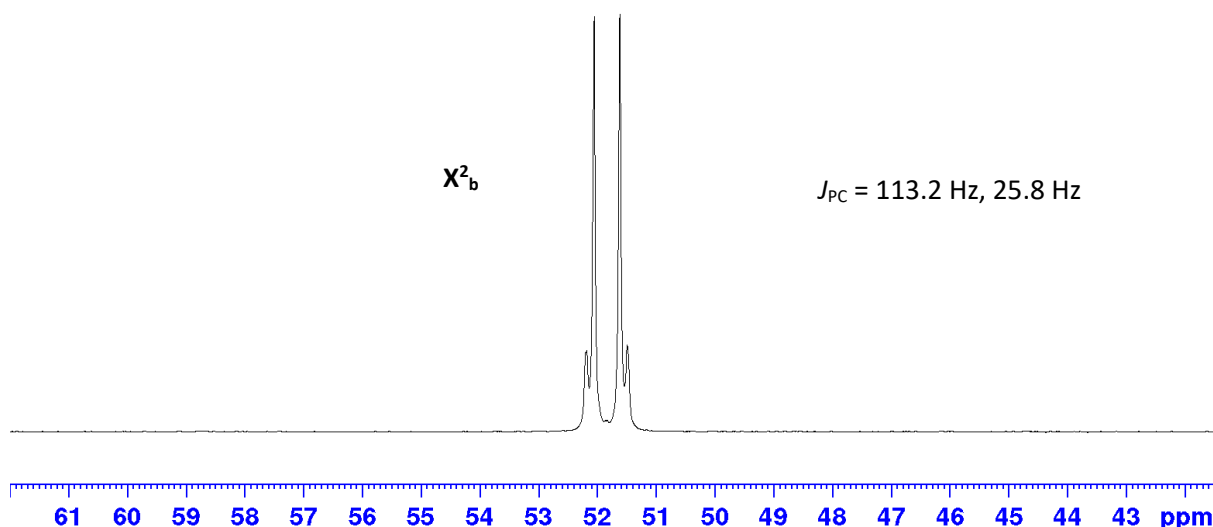


Figure S67. $^{31}P\{^1H\}$ NMR spectrum showing the isolated $[(dppe)Ru^{II}(^{13}CO)_2(\eta^2-O_2CPh)_2]$ in $CDCl_3$.

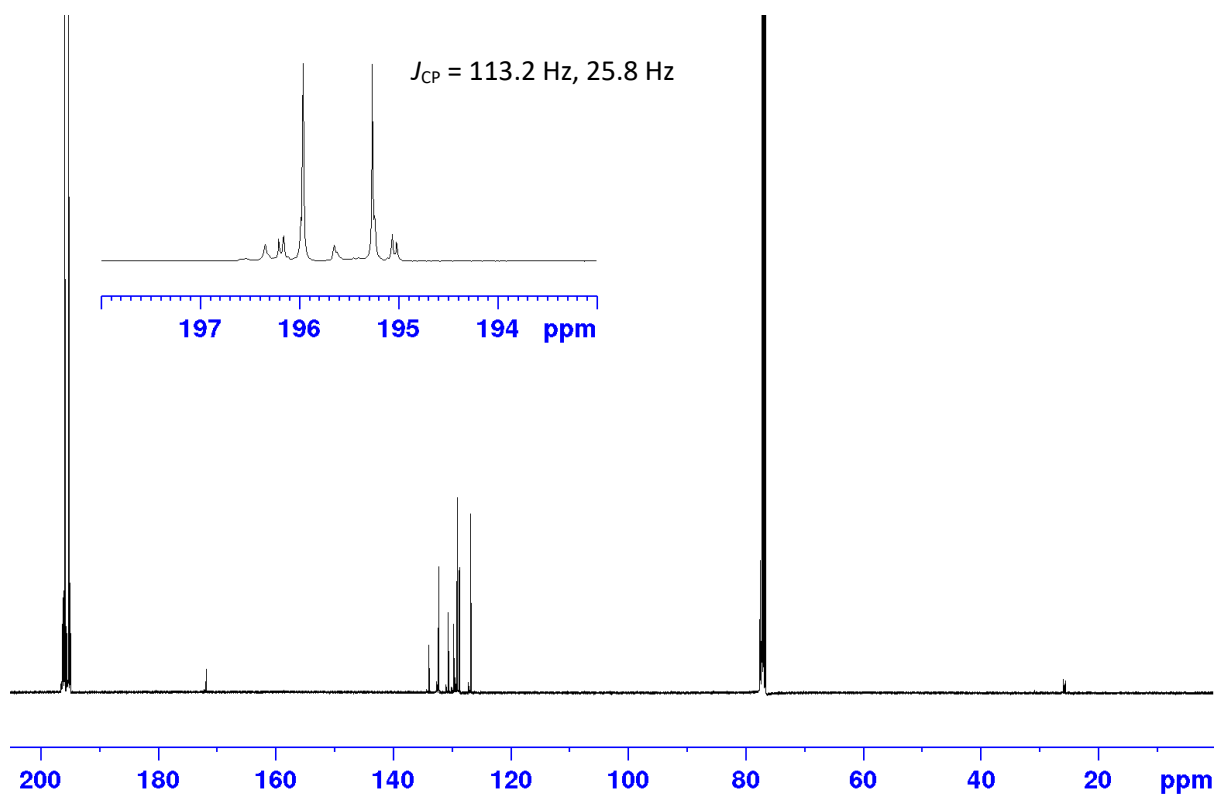
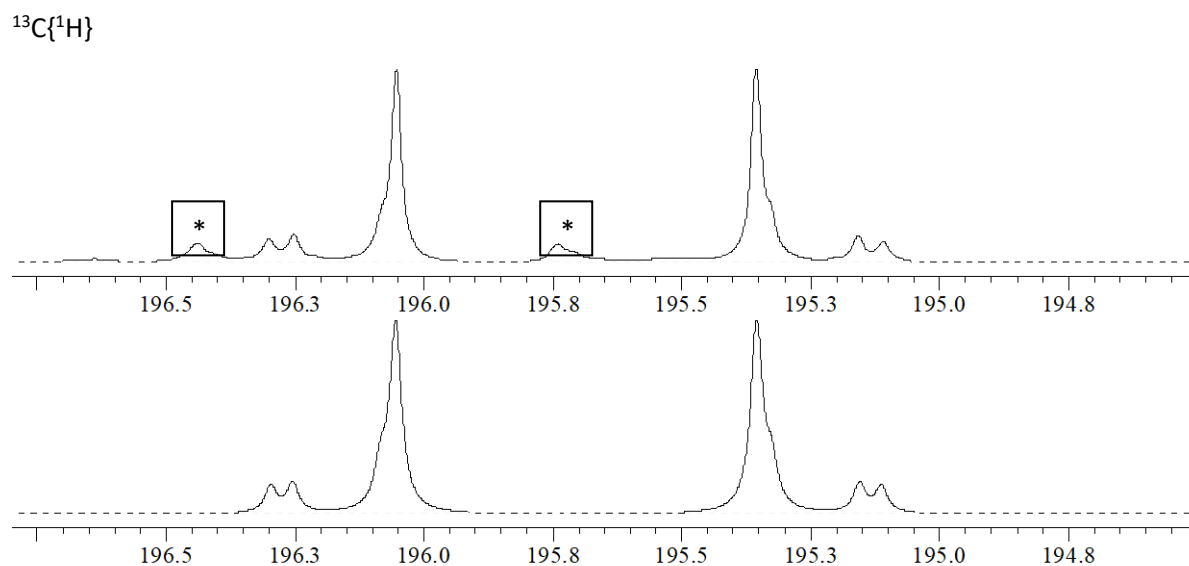


Figure S68. $^{13}\text{C}\{^1\text{H}\}$ NMR spectrum showing the isolated $[(\text{dppe})\text{Ru}^{\text{II}}(^{13}\text{CO})_2(\eta^2\text{-O}_2\text{CPh})_2]$ in CDCl_3 .



$^{31}\text{P}\{^1\text{H}\}$

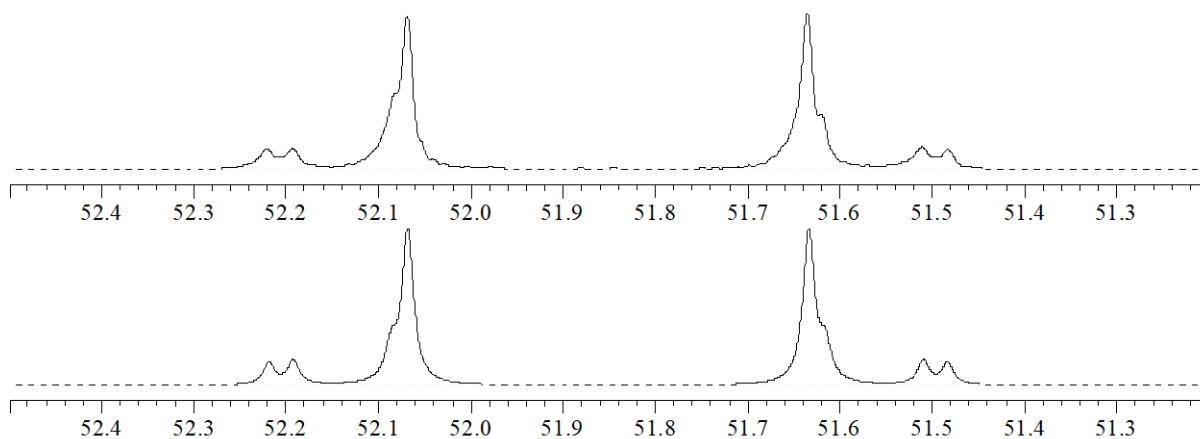


Figure S69. $^{13}\text{C}\{^1\text{H}\}$ (top) and $^{31}\text{P}\{^1\text{H}\}$ (bottom) simulations of $[(\text{dppe})\text{Ru}^{\text{II}}(^{13}\text{CO})_2(\eta^2\text{-O}_2\text{CPh})_2]$. In each case the real spectrum is on top, simulated is on the bottom. Impurity peaks are marked with an asterisk. Only the relevant carbonyl region is shown in the $^{13}\text{C}\{^1\text{H}\}$ spectrum, and impurity peaks are marked with an asterisk. Simulations were carried out using gNMR (IvorySoft) version 5.0.6.0. Simulations were achieved with $J_{\text{CC}} = 4.36$; $J_{\text{PP}} = -25.84$; $J_{\text{PC}} = 113.24$ (E) and -13.45 (Z).

$^{13}\text{C}\{^1\text{H}\}$

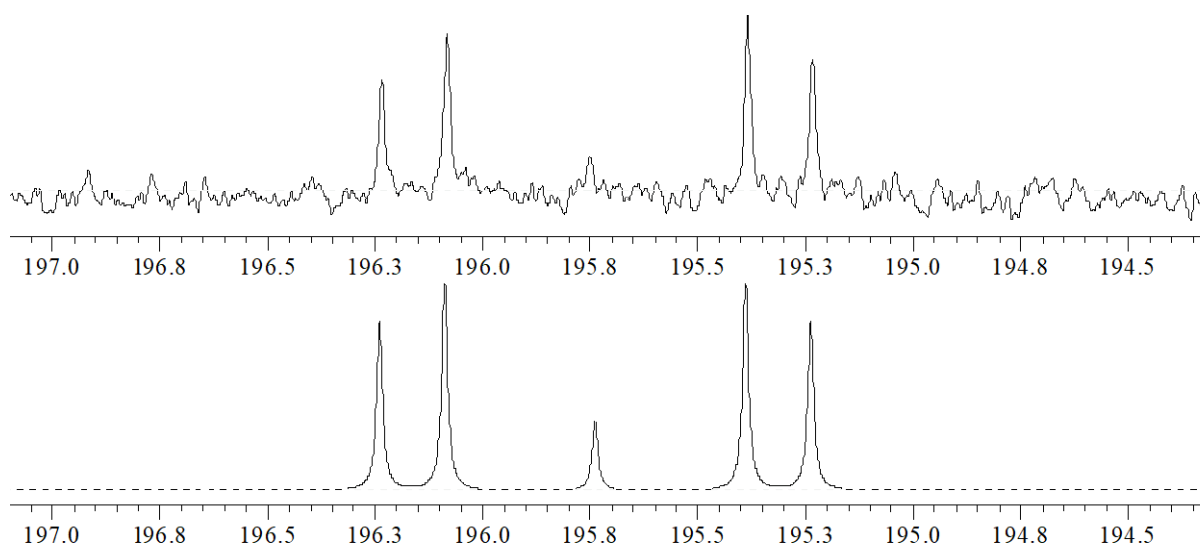


Figure S70. $^{13}\text{C}\{^1\text{H}\}$ of $[(\text{dppe})\text{Ru}^{\text{II}}(\text{CO})_2(\eta^2\text{-O}_2\text{CPh})_2]$. The real spectrum is on top, simulated is on the bottom. Only the carbonyl region is shown. Simulations were carried out using gNMR (IvorySoft) version 5.0.6.0. Simulations were achieved with the same coupling constants as in **Figure S69**.

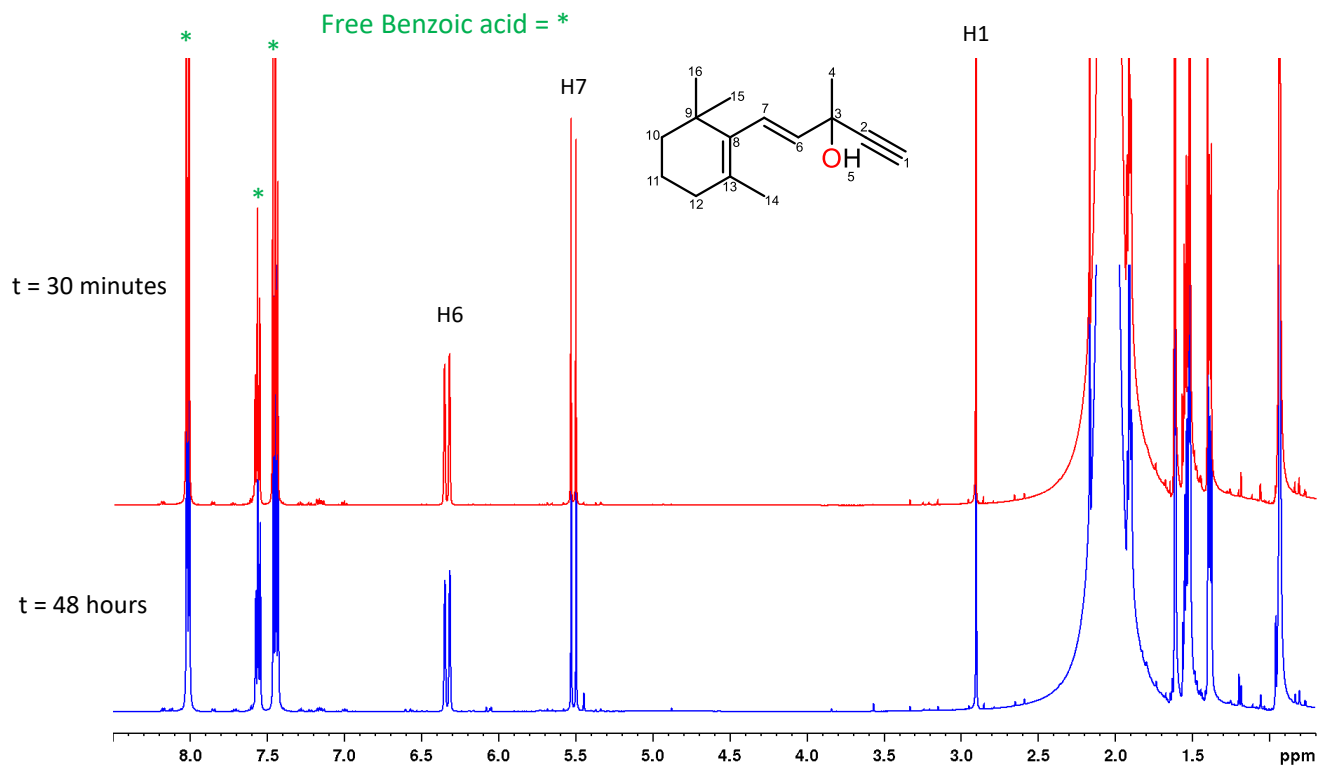


Figure S71. ^1H NMR showing no reaction progress of the Ru-mediated transformation of ethynyl- β -ionol (0.66 M) with benzoic acid (1 M) and $[(\text{dppe})\text{Ru}^{\text{II}}(\text{CO})(\text{OH}_2)(\eta^2\text{-O}_2\text{CPh})_2]$ ($\mathbf{X}^2\mathbf{b}$, 1 mol%) in anhydrous acetone (15 mL) at 20 °C at a) $t = 30$ minutes b) $t = 48$ hours. No product formation was observed in this time.

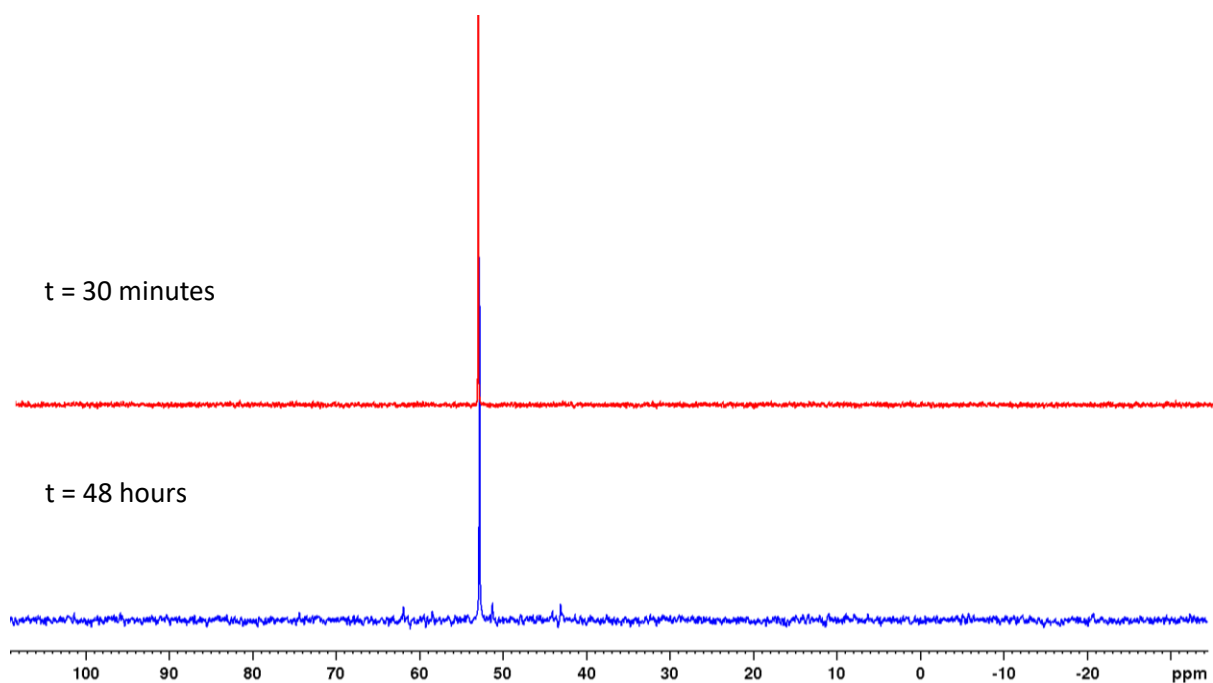


Figure S72. $^{31}\text{P}\{^1\text{H}\}$ NMR showing no change in the chemical shift of $\mathbf{X}^2\mathbf{b}$ in the Ru-mediated transformation of ethynyl- β -ionol (0.66 M) with benzoic acid (1 M) and $[(\text{dppe})\text{Ru}^{\text{II}}(\text{CO})(\text{OH}_2)(\eta^2\text{-O}_2\text{CPh})_2]$ ($\mathbf{X}^2\mathbf{b}$, 1 mol%) in anhydrous acetone (15 mL) at 20 °C at a) $t = 30$ minutes b) $t = 48$ hours.

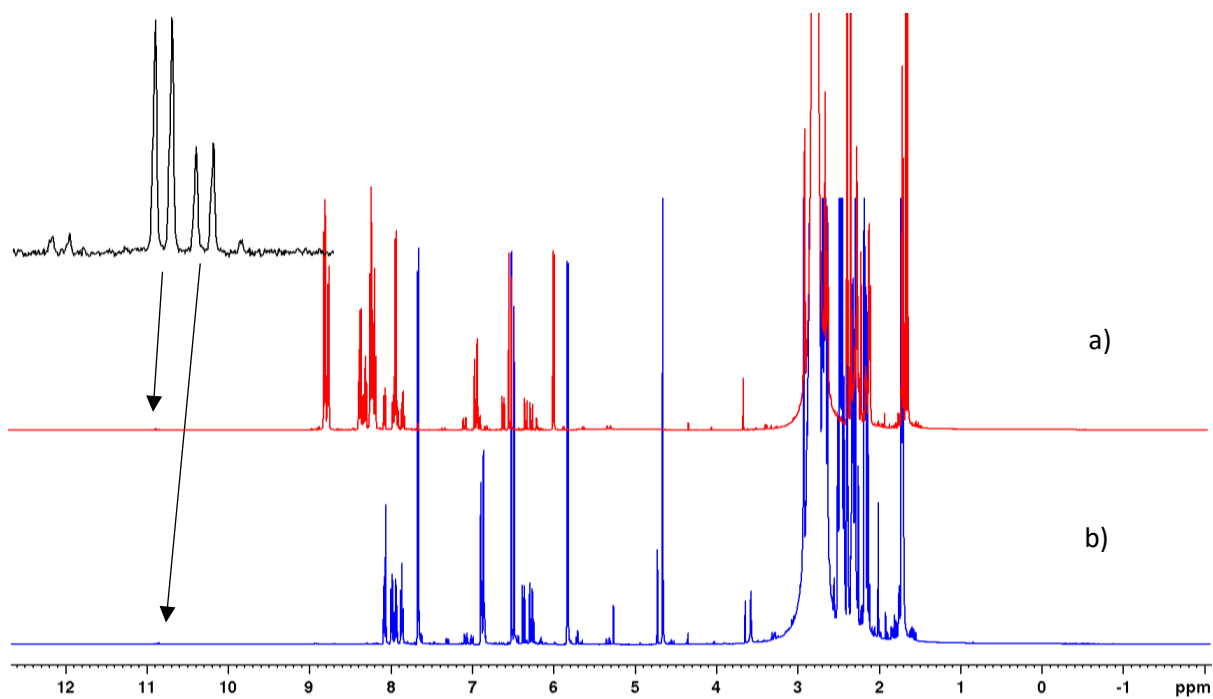


Figure S73. ¹H NMR spectra showing the post reaction mixture of the Ru-mediated transformation of ethynyl-β-ionol (0.66 M) with a) benzoic acid to form **3aa** b) adamantane carboxylic acid to form **3ae**, catalysed by [(dppe)Ru(MA)₂] (1 mol%) in anhydrous acetone (15 mL) at 20 °C, identifying the characteristic shift for the formation of the aldehyde adduct.

4.11 Mechanistic relevance of $[(dppe)Ru^{II}(\eta^2-O_2CR)_2]$

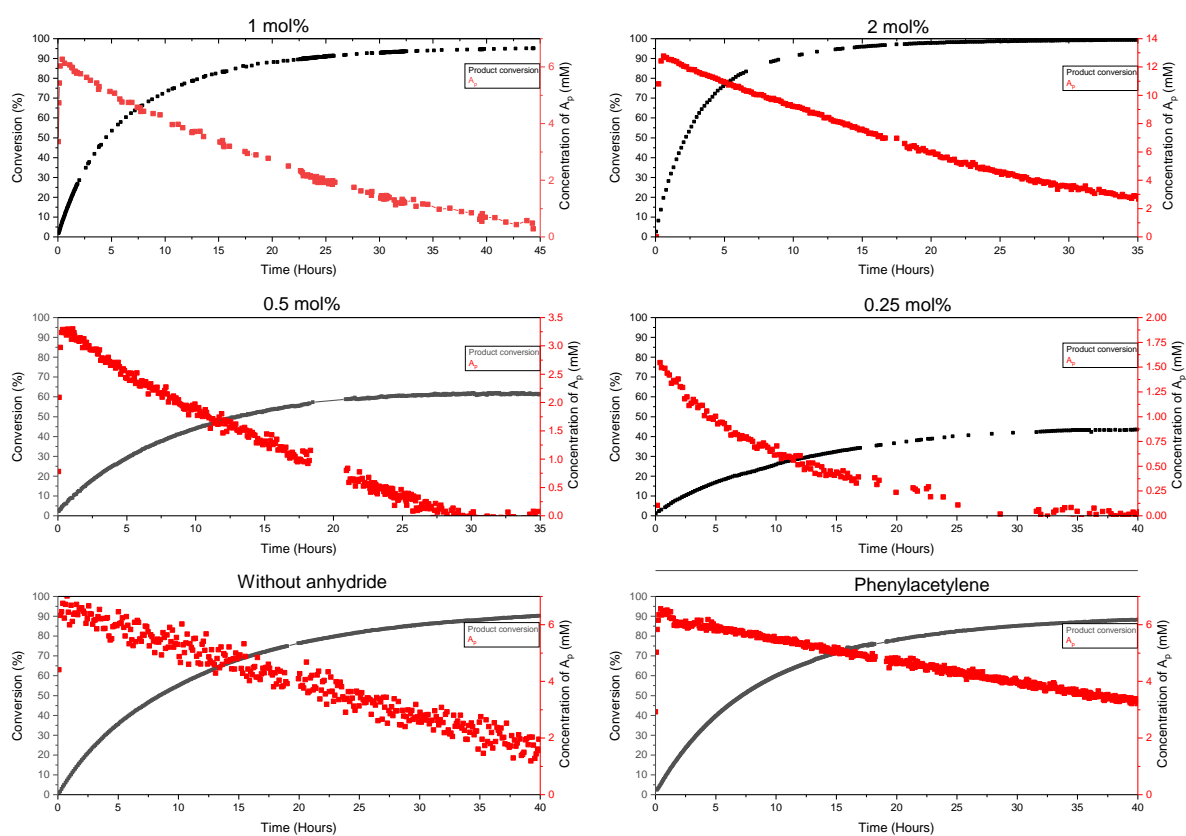


Figure S74. Product concentration profiles (sum of Z and E adduct) overlaid with deactivation of A showing the Ru-mediated transformation of ethynyl- β -ionol (0.66 M) or phenylacetylene (0.66 M) with pivalic acid (0.73 M) and pivalic anhydride (0.13 M) catalysed by $[(dppe)Ru(MA)_2]$ at various loadings in anhydrous acetone (15 mL) at 20 °C from quantitative 1H and $^{31}P\{^1H\}$ FlowNMR spectroscopy at 4 mL/min.

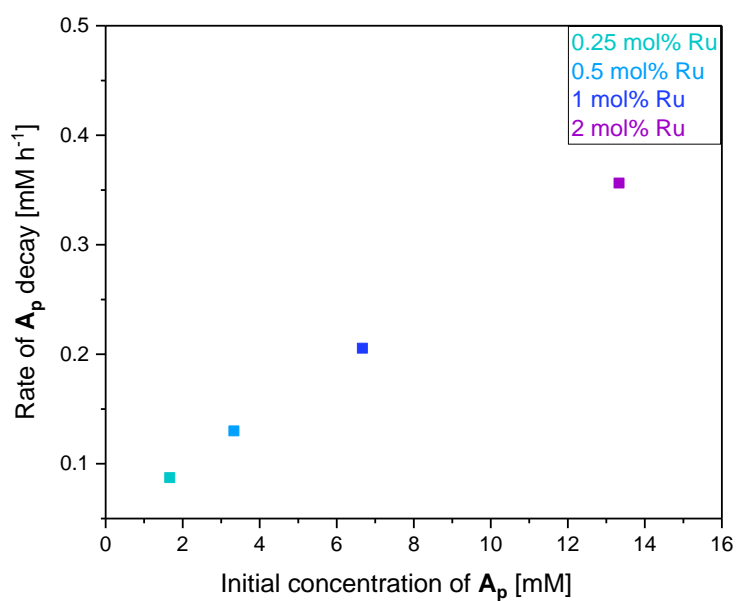


Figure S75. Initial rates of $[A_p]$ decay against the total initial concentration of A_p for the Ru-mediated transformation of ethynyl- β -ionol (0.66 M) with pivalic acid (0.73 M) and pivalic anhydride (0.13 M) catalysed by various amounts of $[(dppe)Ru(MA)_2]$ (0.25 - 2 mol%) in anhydrous acetone (15 mL) at room temperature.

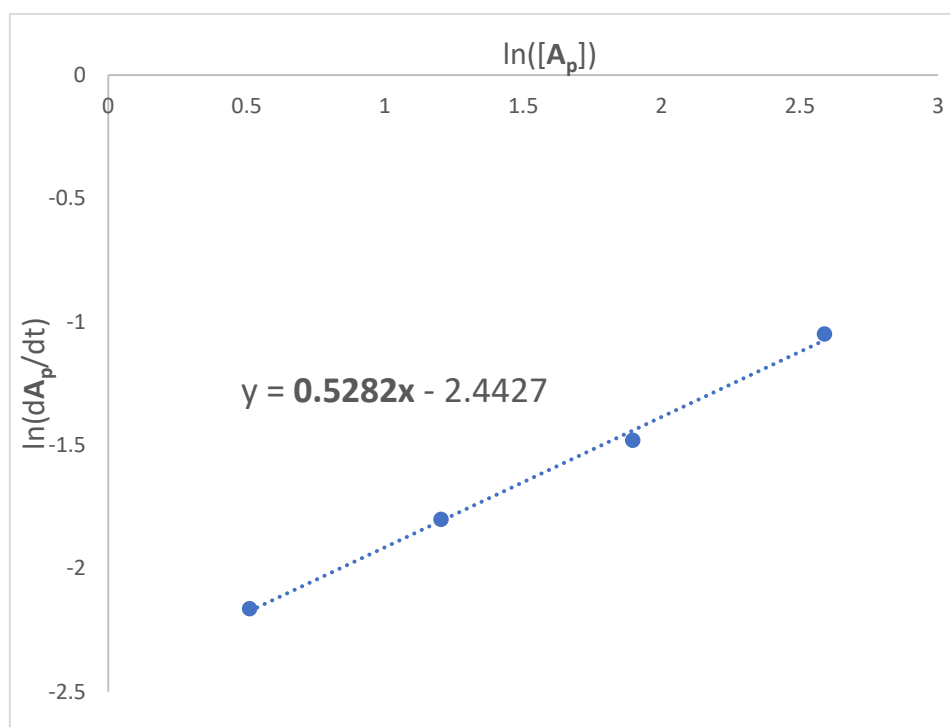


Figure S76. $\ln([A_p])$ vs $\ln(dA_p/dt)$ showing catalyst deactivation to be half order in $[A]$ through the gradient.

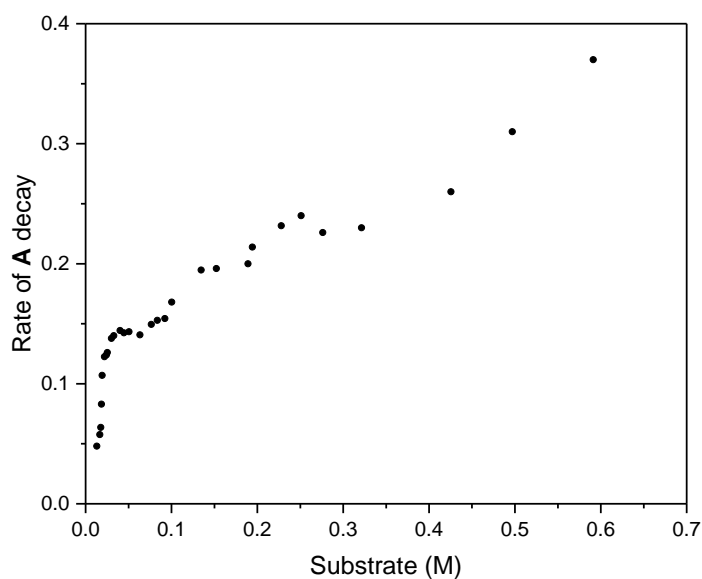


Figure S77. Rate of decay of **A** against substrate consumption in the Ru-mediated transformation of ethynyl- β -ionol (0.66 M) with pivalic acid (0.73 M) and pivalic anhydride (0.13 M) to form **3ab**, catalysed by $[(dppe)Ru(MA)_2]$ (1 mol%) in anhydrous acetone (15 mL) at room temperature.

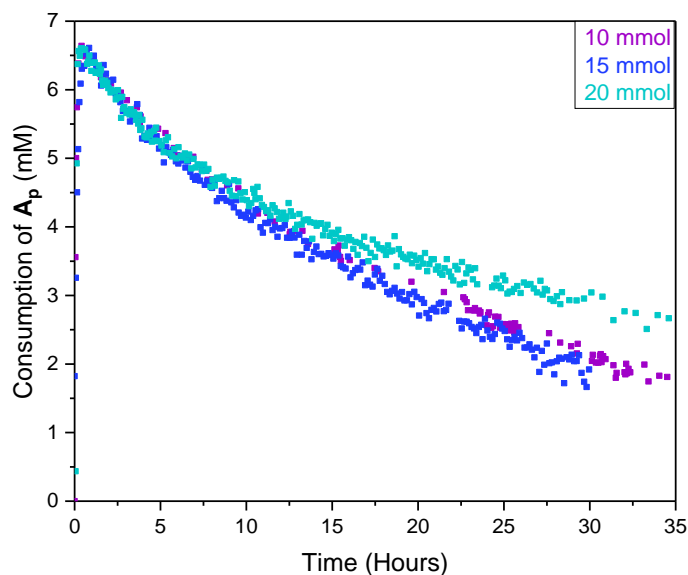


Figure S78. Concentration profiles showing the consumption of **A_p** for the Ru-mediated transformation of ethynyl- β -ionol at three different loadings (0.33 M, 0.66 M, 1 M) with pivalic acid (0.73 M) and pivalic anhydride (0.13 M) to form **3ab**, catalysed by $[(dppe)Ru(MA)_2]$ (6.66mM) in anhydrous acetone (15 mL) at 20 °C. Determined from quantitative $^{31}P\{^1H\}$ FlowNMR spectroscopy at 4 mL/min.

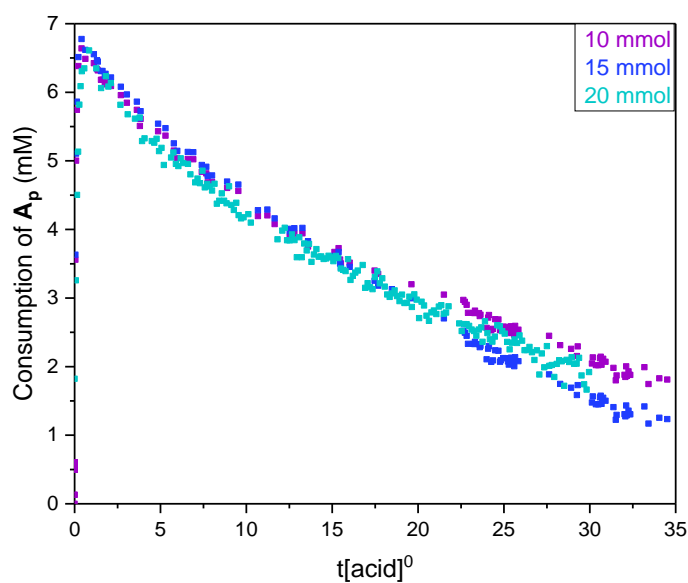


Figure S79. Time adjusted reaction progress profiles (from **Figure S78**) for the deactivation rate as a function of $[Acid] = 0$

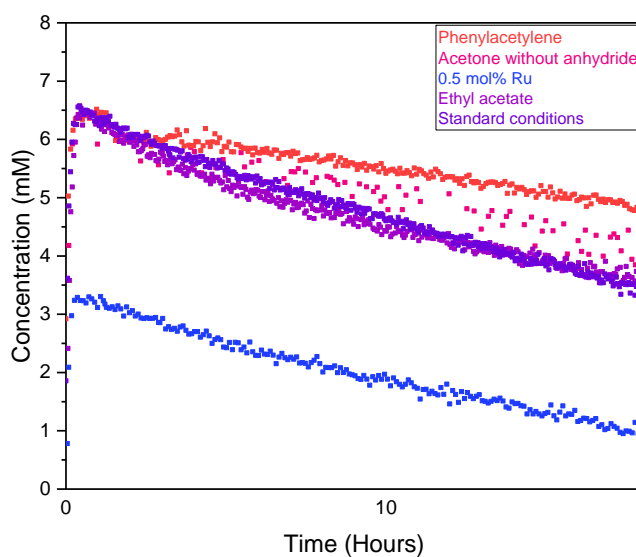


Figure S80. Overlay of the decline of A_p over time under different catalytic conditions at room temperature: a) phenylacetylene (0.66 M) with pivalic acid (0.73 M) and pivalic anhydride (0.13 M) with $[(dppe)Ru(MA)_2]$ (1 mol%) in anhydrous acetone, b) ethynyl- β -ionol (0.66 M) with pivalic acid (1 M) with $[(dppe)Ru(MA)_2]$ (1 mol%), c) ethynyl- β -ionol (0.66 M) with pivalic acid (0.73 M) and pivalic anhydride (0.13 M) with $[(dppe)Ru(MA)_2]$ (0.5 mol%) in anhydrous acetone, d) ethynyl- β -ionol (0.66 M) with pivalic acid (0.73 M) and pivalic anhydride (0.13 M) with $[(dppe)Ru(MA)_2]$ (1 mol%) in anhydrous ethyl acetate, e) ethynyl- β -ionol (0.66 M) with pivalic acid (0.73 M) with $[(dppe)Ru(MA)_2]$ (1 mol%) in anhydrous acetone. Determined from quantitative $^{31}P\{^1H\}$ FlowNMR spectroscopy at 4 mL/min.

4.12 Maximising catalyst productivity

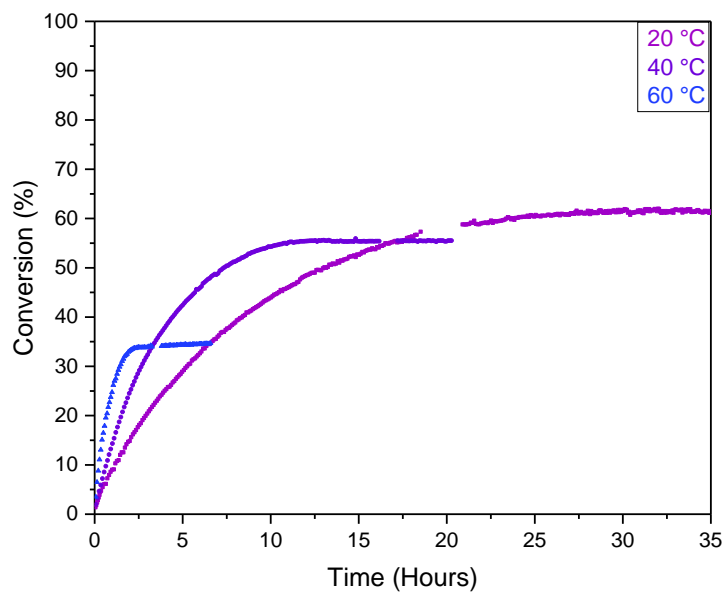


Figure S81. Conversion profiles from ^1H FlowNMR data of the Ru-mediated transformation of ethynyl- β -ionol (0.66 M) with pivalic acid (0.73 M) and pivalic anhydride (0.13 M) catalysed by 0.5 mol% $[(\text{dppe})\text{Ru}(\text{MA})_2]$ in anhydrous acetone (15 mL) at different temperatures.

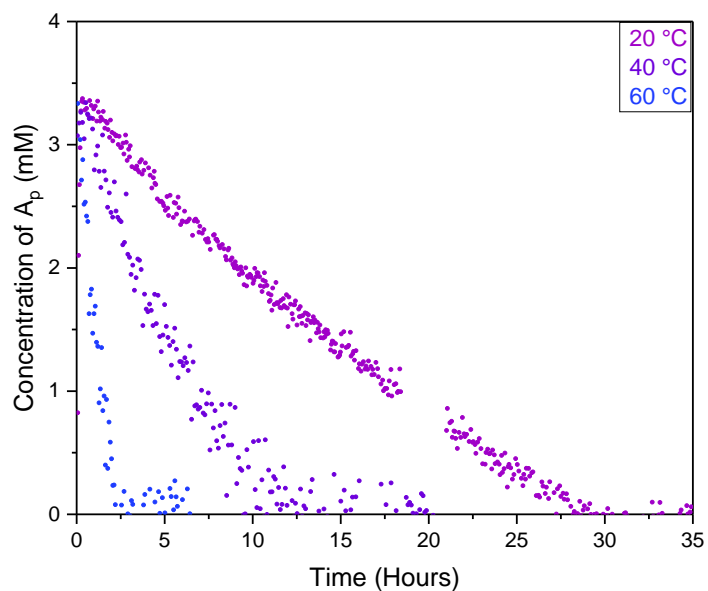


Figure S82. Decline of **A** from $^{31}\text{P}\{^1\text{H}\}$ FlowNMR data of the Ru-mediated transformation of ethynyl- β -ionol (0.66 M) with pivalic acid (0.73 M) and pivalic anhydride (0.13 M) catalysed by 0.5 mol% $[(\text{dppe})\text{Ru}(\text{MA})_2]$ in anhydrous acetone (15 mL) at different temperatures.

The peaks used to monitor reaction progress of **3ae** are highlighted:

Substrate (**2a**), *Z*-adduct (**3ae**), *E*-adduct (**3ae**), Internal standard

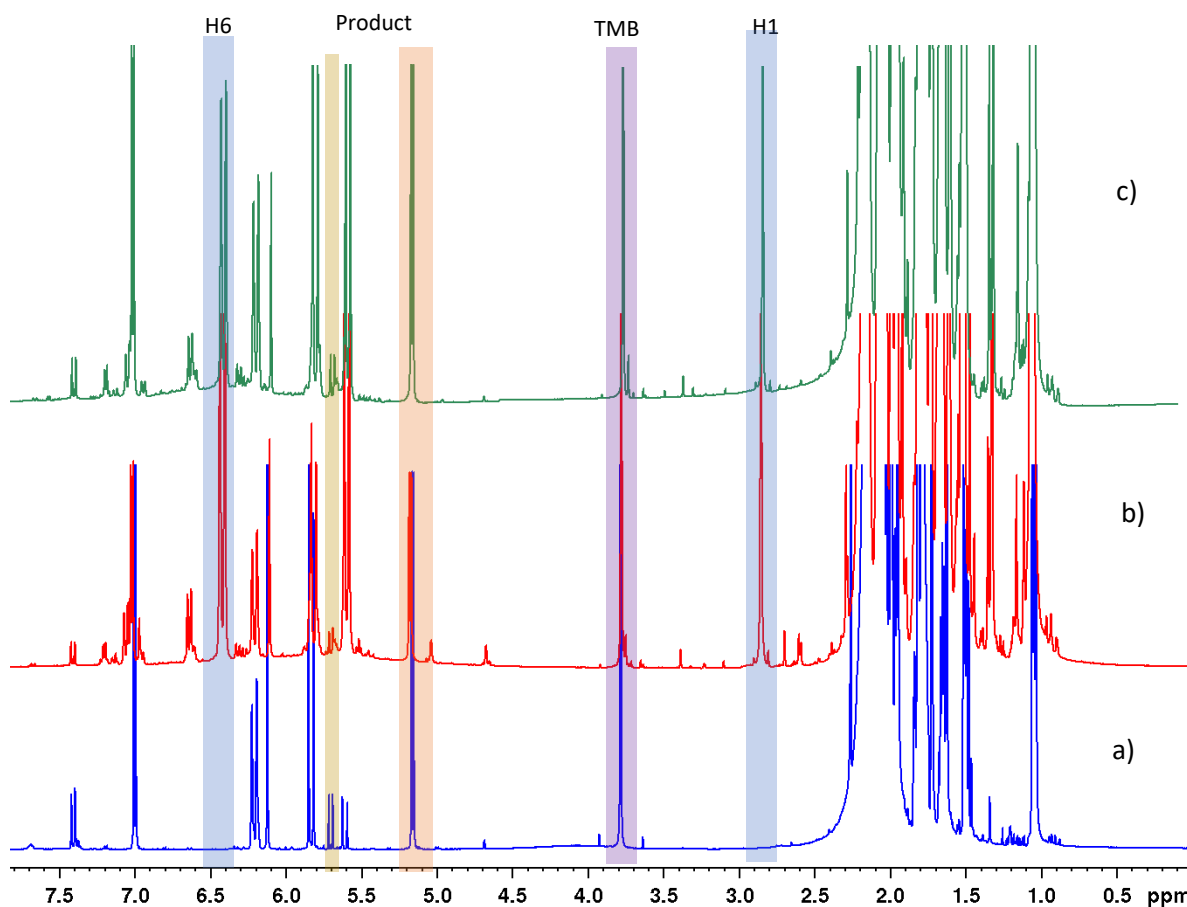


Figure S83. The Ru-mediated transformation of ethynyl- β -ionol with adamantane carboxylic acid and $[(dppe)Ru(MA)_2]$ in anhydrous acetone under inert atmosphere (final product yields after 45 hours obtained from quantitative ex-situ 1H NMR spectroscopy against trimethoxybenzene as internal standard) at: a) 2 M substrate loading and 6.67 mM Ru loading b) 5.23 M substrate loading with 3.34 mM Ru loading c) 5.23 M substrate loading with 6.67 mM Ru loading at 40 °C. With example substrate and product peak highlight for quantification.

Table S10. The Ru-mediated transformation of phenylacetylene with adamantane carboxylic acid with $[(dppe)Ru(MA)_2]$ in anhydrous acetone under inert atmosphere (final product yields after 60 hours obtained from quantitative ex-situ 1H NMR spectroscopy against trimethoxybenzene as an internal standard).

Entry	Substrate	Catalyst	Catalyst loading	Acid (M)	Temperature (°C)	Conversion (%)	TON
1	1.333 M	6.67 mM	0.5%	1.8	20	100	200
2	5.23 M	6.67 mM	0.125%	5.5	20	100	800
3	10.46 M	6.67 mM	0.0625%	11	20	98	1568
4	20.98 M	6.67 mM	0.03125%	22	20	66.8	2138

5.0 References

1. H. Doucet, B. Martin-Vaca, C. Bruneau and P. H. Dixneuf, *J. Org. Chem.*, 1995, **60**, 7247-7255.
2. F. Aquino, W. Bonrath, F. Pace, P. Ruckstuhl and K. Witzgall, WO2020025512A1, 2020.
3. J. G. Malecki and A. Maroń, *Transit. Met. Chem.*, 2012, **37**, 727-734.
4. M. S. Quinby and R. D. Feltham, *Inorg. Chem.*, 1972, **11**, 2468-2476.
5. A. Hall, PhD Thesis, University of Bath, 2019.
6. CrysAlisPro 1.171.42.49 (Rigaku Oxford Diffraction, **2022**).
7. G. M. Sheldrick, *Acta Cryst.*, 2015, C71, 3-8.
8. C. B. Hübschle, G. M. Sheldrick and B. Dittrich, *J. Appl. Cryst.*, 2001, **44**, 1281-1284.
9. C. F. Macrae, P. R. Edgington, P. McCabe, E. Pidcock, G. P. Shields, R. Taylor, M. Towler and M. van der Streek, *J. Appl. Crystallogr.*, 2006, **39**, 453-457.
10. D. A. Engel and G. B. Dudley, *Org. Biomol. Chem.*, 2009, **7**, 4149-4158
11. M. Picquet, C. Bruneau and P. H. Dixneuf, *Chem. Commun.*, 1997, **1997**, 1201-1202.
12. H. Doucet, B. Martin-Vaca, C. Bruneau and P. H. Dixneuf, *J. Org. Chem.*, 1995, **60**, 7247-7255.
13. M. Picquet, A. Fernández, C. Bruneau and P. H. Dixneuf, *Eur. J. Org. Chem.*, 2000, **2000**, 2361-2366.
14. X. L. Lu, S. Y. Ng, J. J. Vittal, G. K. Tan, L. Y. Goh and T. S. A. Hor, *J. Organomet. Chem.*, 2003, **688**, 100-111.